Towards High Bandwidth Communication Systems: From Multi-Gbit/s over SI-POF in Home Scenarios to 5G Cellular Networks over SMF

by

Fahad Mohammed Abdulhussein Al-Zubaidi

A dissertation submitted in partial fulfillment of the requirements for the degree of Doctor of Philosophy in

Electrical Engineering, Electronic and Automation

Universidad Carlos III de Madrid

Advisors:

Prof. María Carmen Vázquez García

Prof. David Ricardo Sánchez Montero

Tutor:

Prof. María Carmen Vázquez García

May 2021

ACKNOWLEDGEMENTS

First and Foremost, praises and many thanks to God for his continuous blessings during all the times of my research.

I would like to express my sincere gratitude and heartfelt thanks to my thesis directors, Prof. Carmen Vázquez and Prof. David Sánchez Montero for their unlimited support, motivation and patience. Their guidance and availability during all times of research and thesis writing are valuable and unforgettable. They were always there to support me in many challenges that I have faced during my stay in Spain. I am so grateful for the chance they gave me to work with challenging and interesting research topics.

I am extremely thankful to my colleague and friend J.D Lopez Cardona whom with I shared the same office and lab for almost four years. His collaboration in the lab is appreciated. His other supports made my resident and life in Spain more and more easier. I would also like to thank Dr. P. J. Pinzón for his collaboration in the lab.

I would also like to thank all the members of Group of Display and Photonics Applications (GDAF) for their collaborations.

I also must acknowledge my family and especially my parents (Mohammed and Khadeeja) for their daily engorgement and support during all the time that I have spent abroad for this research. Special thanks also to my uncle Khaled and my Aunt Huda for their support. Last and not least many thanks to my friend Haider for his support

PUBLISHED AND SUBMITTED CONTENT

Papers in international Journals

- **Fahad M. A. Al-Zubaidi**, Juan D. López-Cardona, D. Sánchez Montero and C. Vázquez, "Optically powered Radio-over-Fiber Systems in Support of 5G Cellular Networks and IoT," Submitted in Journal of Lightwave Technology,
- **Fahad M. A. Al-Zubaidi**, D. Sánchez Montero and C. Vázquez, "SI-POF Supporting Power-over-Fiber in Multi-Gbit/s Transmission for In-Home Networks," in Journal of Lightwave Technology, vol. 39, no.2, pp. 112-121, doi: 10.1109/JLT.2020.3025444.
- C. Vázquez Juan D. López-Cardona, P. C. Lallana , D. S. Montero , **Fahad M. A. Al-Zubaidi**, S. Pérez-Prieto, and I. Pérez-Garcilópez, "Multicore Fiber Scenarios Supporting Power Over Fiber in Radio Over Fiber Systems," in IEEE Access, vol. 7, pp. 158409-158418, 2019, doi: 10.1109/ACCESS.2019.2950599.

Contributions in International Conferences

- **Fahad M. A. Al-Zubaidi**, D. S. Montero, A. Lopez, J. Zubia and C. Vázquez, "Investigation of power over fiber impact on gigabit data transmission in SI-POF" in Proc. of International Conference on Plastic Optical Fiber, Yokohama, Japan, 2019.

- C. Vázquez, **Fahad M. A. Al-Zubaidi**, D. S. Montero, P. C. Lallana, P. J. Pinzón, J. Mateo and J. Zubia, " Characterization for simultaneous Gigabit data transmission and energy delivery in Large core Plastic Optical Fibers" in Proc. of International Conference on Plastic Optical Fiber, USA, 2018.

- C. Vázquez, D. S. Montero, **Fahad M. A. Al-Zubaidi** and J. D. López-Cardona, "Experiments on Shared- and Dedicated- Power over Fiber Scenarios in Multi-core Fibers," 2019 European Conference on Networks and Communications (EuCNC), Valencia, Spain, 2019, pp. 412-415, doi: 10.1109/EuCNC.2019.8802042.

- C. Vázquez, J. D. López-Cardona, D. S. Montero, I. Pérez, P. C. Lallana and **Fahad M. A. Al-Zubaidi**, "Power over Fiber in Radio over Fiber Systems in 5G Scenarios," 2019 21st International Conference on Transparent Optical Networks (ICTON), Angers, France, 2019, pp. 1-4, doi: 10.1109/ICTON.2019.8840168.
- D. S. Montero, J. D. López-Cardona, **F. M. A. Al-Zubaidi**, I. Pérez, P. C. Lallana and C. Vázquez, "The Role of Power-over-Fiber in C-RAN Fronthauling Towards 5G," *2020 22nd International Conference on Transparent Optical Networks (ICTON)*, Bari, Italy, 2020, pp. 1-4, doi: 10.1109/ICTON51198.2020.9203531.

Contributions in National Conferences

- Fahad M. A. Al-Zubaidi, D. S. Montero, C. Vázquez and P. J. Pinzón, "Noise analysis and Multi-Gbit/s transmission in PoF scenarios over SIPOF" in Proc.of XI Spanish Optoelectronics Meeting (OPTOEL), Zaragoza, Spain, 2019

Contents

List of Figures

List of Tables

List of Abbreviations

Abbreviation	Phrase
A_{eff}	Effective Area
APD	Avalanche Photodiode
ARoF	Analog Radio over Fiber
ASE	Amplified Spontaneous Emission
B2B	Back to Back
BBU	Base Band Units
BER	Bit Error Rate
CO	Central Office
CP-OFDM	Cyclic-Prefix Orthogonally frequency Division Multiplexing
CPRI	Common Public Radio Interface
C-RAN	Centralized Radio Access Network
CT	Crosstalk
CU	Central Unit
D	Chromatic Dispersion
D-RoF	Digitized Radio over Fiber
DSB	Double Sideband Modulation
EDFA	Erbium-Doped Fiber Amplifier
eMBB	Enhanced Mobile Broadband
EMI	Electromagnetic Interface
EVM	Error Vector Magnitude
FBG	Fiber Bragg Grating
FI	Fan-In
FO	Fan-Out
FTTH	Fiber to the Home
GI	Graded-Index
HPL	High Power Laser
IoT	Internet of Things
LED	Light Emitting Diode
LO	Local Oscillator

LTE	Long Term Evolution
MC	Media Converter
MCF	Multi-core Fiber
MFD	Mode Field Diameter
MFH	Mobile-Fronthaul
MIMO	Multi-Input-Multi-Output
MMF	Multimode Fiber
MMTC	Massive Machine Type Communication
MZM	Mach-Zehnder Modulator
NA	Numerical Aperture
NLSE	Non-linear Schrödinger equation
NR	New Radio
NZDSF	Non-zero Dispersion Shifted Fiber
OLT	Optical Line Terminal
ONU	Optical Network Unit
PAM	Pulse Amplitude Modulation
PMD	Polarization Mode Dispersion
PMMA	Poly (Methyl methacrylate)
PoF	Power over Fiber
PON	Passive Optical Network
PV	Photovoltaic Cell
QoS	Quality of Service
RAN	Radio Access Network
RF	Radio Frequency
RIN	Relative Intensity Noise
RN	Remote Node
RoF	Radio over Fiber
RRU	Radio Remote Unit
SBS	Stimulated Brillouin Scattering
SDM	Space Division Multiplexing
SDN	Software-Defined Networking

SEE	System Energy Efficiency
SI-POF	Step-index Plastic Optical Fiber
SMF	Single Mode Fiber
SNR	Signal to Noise Ratio
SOA	Semiconductor Amplifier
SPM	Self-Phase Modulation
SRS	Stimulated Raman Scattering
V_2X	Vehicle to Everything
VLC	Visible Light Communication
VOA	Variable Optical Attenuator
VoD	Video on Demand
WAN	Wide Area Network
WDM	Wavelength Division Multiplexing
WSN	Wireless Sensor Network
XPM	Cross Phase Modulation
3GPP	3rd Generation Partnership project

Chapter 1:

Introduction

1.1 Motivation

The rapid increase in the global mobile traffic boosts the demand of developing high data rates systems. This will require high bandwidth channels with the possibility of gigabit speed data transmission, especially for short/medium range networks like in home or automated industry scenarios. The 5G technology is designed to meet this requirement and to support different new services like Internet of Things (IoT) applications [1] and vehicle to everything (V2X) [2] with frequency bands from 1 GHz to 100 GHz [3] to be used. Many networks operators are also proposing the use of small cell technology for 5G coverage. This means the use of small antennas with low power consumption, small coverage areas per antenna but massive deployments of the latter, and high data rate handling capability to replace the classical base stations. Fig. 1.1 shows the different services tiers that 5G expects to support in near future. The expected data traffic demands in the distribution network leads to the optical fiber as the infrastructure network solution.

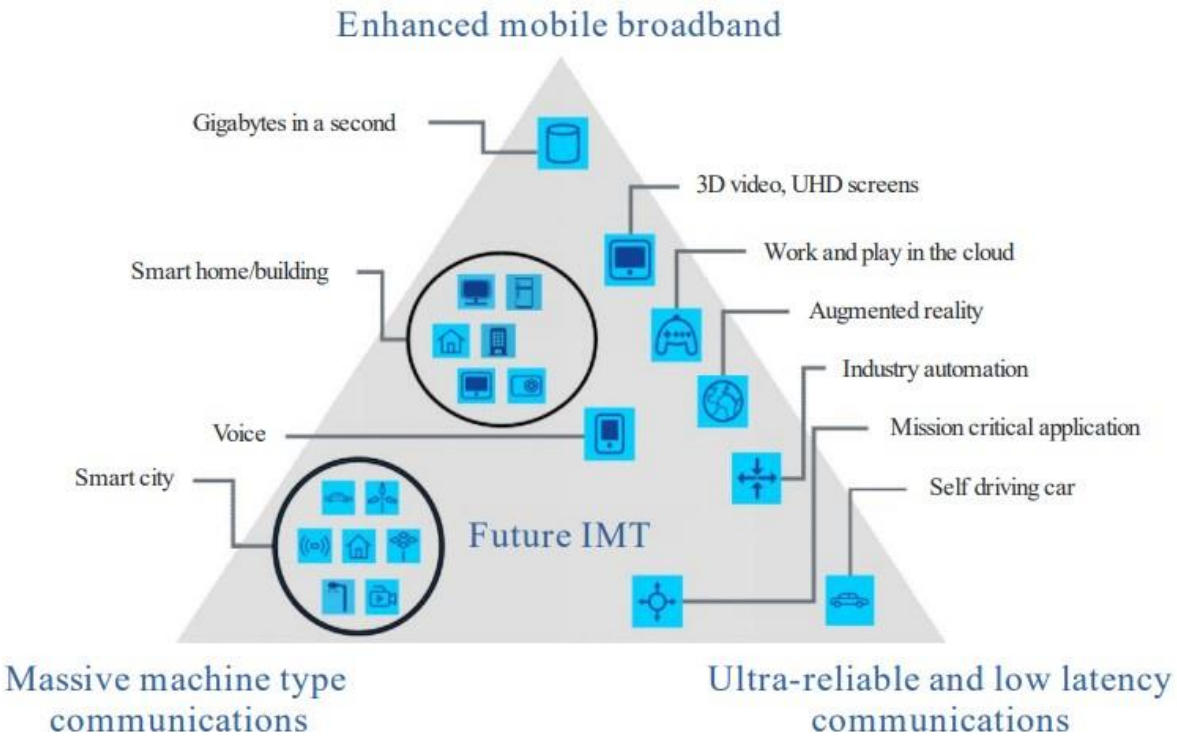

Fig.1.1: 5G services [4].

On the other hand, high speed telecommunications applications for within home networks are gaining a lot of interest year by year due to the huge amount of data transmitted because of the different services like Video on Demand (VoD), High-Definition (HD) TV, smart phones and many other services which increase the number of connected devices as shown

in Fig. 1.2 [5]. And large core step index (SI) plastic optical fiber (POF) is considered to be very useful in many applications related with home networking due to many advantages such as its low cost, light weight, easy to handle and high transmission capacity.

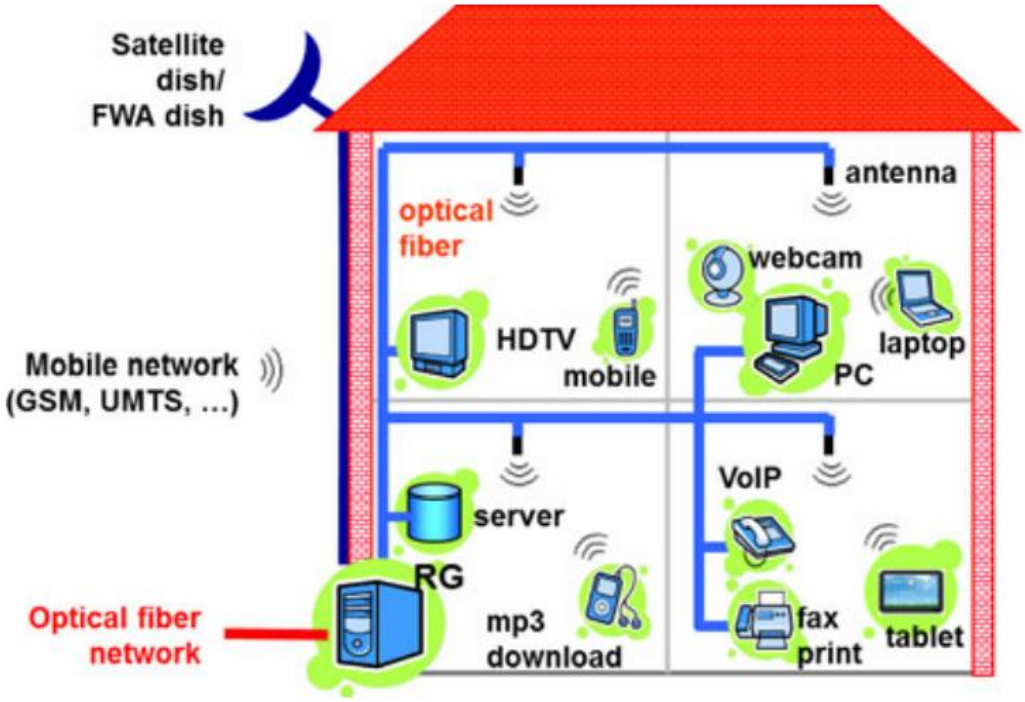

Fig. 1.2: Home network with fiber backbone. © 2013 [5].

For the access network systems concept, the currently installed infrastructure consists mainly of single mode fiber (SMF). Many research groups have proposed different technologies to support the future 5G access networks by exploiting the optical fiber technology [6-8]. Among these technologies Radio over Fiber (RoF) seems one of the most promising technologies for the future for radio signal transmission due to the many advantages like low transmission loss and high capacity [9]. The Radio Access Network (RAN) is composed of two main elements: central office (CO) and Remote Radio Units (RRU), also named Remote Radio Heads (RRH). Due to the current challenges especially in the crowded and large cities, the centralized-RAN (C-RAN) is chosen as a solution where the processing of data is done in a centralized way in the CO [10] thus reducing the cost and the complexity of the network structure and maintenance. The deployment of C-RAN networks opens the door to develop novel optical front-haul solutions. RoF is used to connect multiple RRUs at the remote site with the Baseband Units (BBUs) at the CO [11]. And, particularly, Analog RoF (ARoF) based C-RAN will bring the benefit of the bandwidth requirements and cost saving thus allowing the possibility to integrate simple RRU solutions. Fig. 1.3 shows the next generation

access networks where the fiber can be utilized for the end-to-end transport between different Wide Area Networks (WAN) [12].

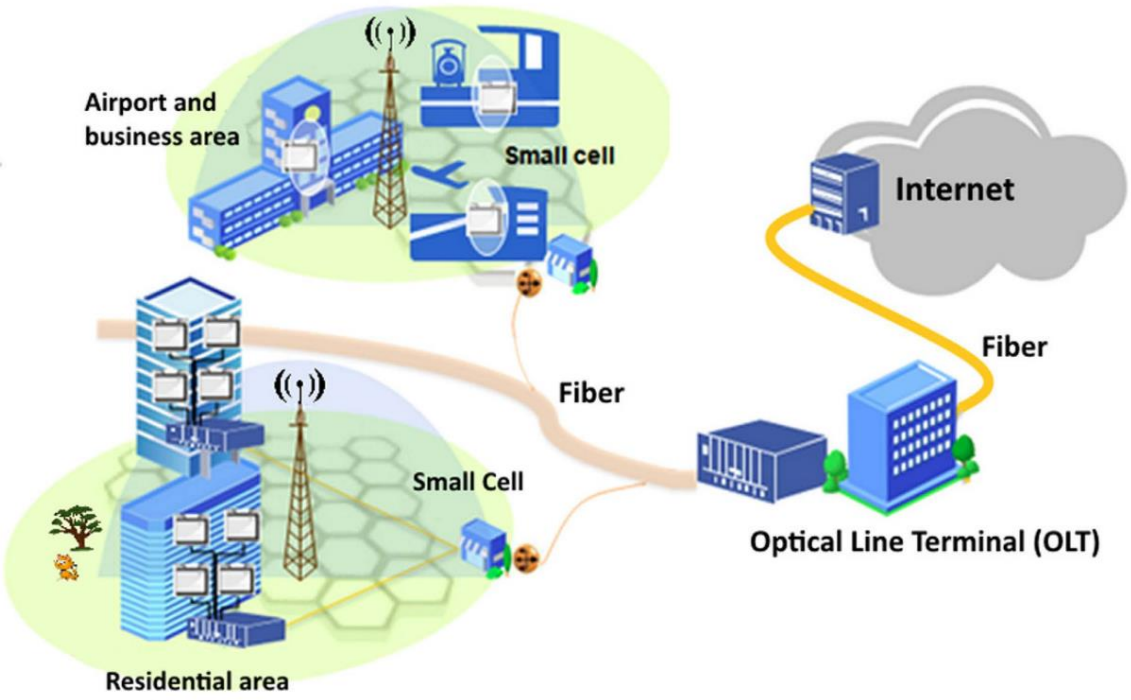

Fig. 1.3: Access network with different services [12].

The huge increment in the data traffic brings the need to develop flexible and energy efficient optical access networks serving as front-haul to support future 5G cellular networks. Utilizing the current optical infrastructure based on SMF can be a cost-effective solution where even adding SMF fiber bundles can increase the transmission capacity.

On the other hand, energy consumption is now also considered as one of the primary requirements in the design of the access networks. There are different research aspects that can support the reduction of the power consumption of the networks like improving the energy efficiency of the hardware components in the transmission system, the reduction of the cell size that leads to the use of low power antennas, sleep mode operation for some devices or finding new energy sources [13]. Power-over-Fiber (PoF), i.e. the remote electrical power delivery via an optical fiber, is one of the most promising technologies that can have its chance in the future to optically powering different components using the optical distribution network. This technology has great advantages compared to copper wiring with lighter weight and being immune to electromagnetic interference thus offering reliable and secure powering so that it can fulfill the requirements in some fields for powering purposes.

Direct application niches can be hazardous areas like laboratories, storage gas tanks or any fields with flammable atmosphere [14] with extension to communication networks. In general, the PoF system in its simplest form consists of a high-power light source, an optical fiber and a photovoltaic cell (PV) at reception. It also has some challenges and limitations, as some examples the limited efficiency of the commercially available PV cells and the fiber damage in a high optical power level operation.

In this framework, the aim of this work is to design and develop optical communication systems in different scenarios, based on different fiber types and network topologies, able to support the high bandwidth and data rates demands with the integration of optimized PoF solutions at the same time. The first part of the work, comprising chapter two, exploits the potential of SI-POF for high data transmission rates with PoF energy delivery in the in-home network scenario with sets of experimental validations and theoretical studies. The second part, comprising chapter three, focuses on the analysis of the impact of fiber impairments due to non-linear effects in the access networks with legacy SMFs. The work presents extensive simulation studies with additional experimental testbeds to support this analysis. The final part, comprising chapter four and five, focuses on the development of RoF systems with the transmission of 5G NR (New Radio) signals and the integration of PoF techniques in these systems. These last two chapters present an extensive simulation analysis with specific experimental testbed developments to address the main design parameters and limiting factors in these RoF systems as well as the impact of simultaneous PoF transmission on the latter. The possible application scenario that can benefit from the designed systems in this work is also detailed. A case study is proposed to integrate the potential of PoF in RoF transmission systems.

1.2 Objectives

The main objective of the thesis is to study high bandwidth communication systems for different network architectures from the end user at the in-home scenario to the service provider through the mobile cellular front-haul network. This is in parallel with the integration of power over fiber (PoF) technology in these systems.

From all these issues, the research has the following specific objectives:

- **Objective 1**: To test prototypes for in-home applications with potential to transmit multi-Gbit/s at tens of meters using SI-POF.

- **Objective 2**: To integrate the functionality of remote powering based on light transmission with data channels for home networks and analyze the impact of that on the data signals quality.

- **Objective 3**: To analyze the influence of non-linear effects on SMF and its impact on the energy delivery efficiency.

- **Objective 4:** To study specific Radio over Fiber (RoF) links following 5G New Radio signals numerology in SMFs, and address the main design parameters and their limitations with and without the integration of PoF in the transmission. Including the analysis of its potential use in different applications.

1.3 Content of the Work

The remaining parts and the structure of the document is described as follows:

Chapter 2 presents the implementation of a real time Gbit/s system over SI-POF for in-home networks with wavelength-division-multiplexing (WDM) integration. The system is compared in detail with reported state-of-the-art works in terms of bandwidth, signal quality and energy efficiency. The performance of the different link components is tested. The PoF technology is integrated with different scenarios with POF communication links. The scalability analysis of the designed PoF system shows the system capability of powering different sensor nodes in specific applications. The experimental analysis also shows no impact on data signal quality because of the PoF transmission.

Chapter 3 includes simulation and some experimental results to integrate the functionality of PoF technology in different kinds of fibers to support future access networks. A series of simulations based on Virtual Photonic Instrumentation (VPI) software tool are performed in this chapter to study the transmission of C-band data channels with PoF signals in different scenarios. The impact of nonlinear effects, including Stimulated Raman Scattering (SRS) and Stimulated Brillouin Scattering (SBS), are analyzed for different fibers including Singlemode fibers (SMF) and Multi-core fibers (MCF). The chapter also discusses the potential impact of optical crosstalk (CT) between cores in MCFs on data signal quality, due to PoF. Some experimental results are provided in this chapter in collaboration with PhD student J. D. López-Cardona to examine the PoF technology performance and its impact on data signal quality. The chapter also discusses the PoF integration in Space Division Multiplexing (SDM) fiber solutions as part of future 5G networks. A scalability analysis is also provided for different powering scenarios to show the powering capability and the number of elements/equipment required in each scenario.

Chapter 4, focuses on the design and development of Analog Radio over Fiber (ARoF) systems following 5G NR numerology. The chapter briefly discusses the state of the art of C-RAN and the integration of RoF in this network architecture. The fiber channel impairments like chromatic dispersion and the impact of different design parameters are analyzed in detail. The chapter includes extensive simulation studies to design RoF over SMF for different link lengths and modulation formats. The work uses metrics such as the Error Vector Magnitude (EVM) and the constellation diagram to evaluate the system performance. Both metrics are compared with the requirements indicated by the standard.

Chapter 5, integrates the functionality of PoF technology in RoF systems. It presents novel optically powered designed systems utilizing currently installed front-haul solutions and discuss different possible powering scenarios. The impact of PoF on the transmission of 5G NR signals in different types of optical fibers is detailed. The chapter includes extensive simulations which can help to decide the design parameters for future power-by-light systems in the 5G cellular networks. Some experimental results are also provided in collaboration with PhD student J D López-Cardona. Different examples of low power consumption devices including small radio cells, amplifiers, photodiodes etc, are provided. A use-case study is presented to show the potential of PoF in such systems. The characteristics of the high-power lasers used as PoF sources are briefly discussed.

Chapter 6 contains the main conclusions of the work and the future research lines proposed.

1.4 Acknowledgements

The present work received funds from the following Spanish and international projects:

- Spanish Ministerio de Ciencia, Innovación y Universidades, “Tecnologías avanzadas inteligentes basadas en fibras ópticas/Advanced SMART technologies based on Optical Fibers (SMART-OF)”, grant no. RTI2018-094669-B-C32, within the coordinated project “Polymer Optical Fiber Disruptive Technologies (POFTECH)”.

- Spanish Ministerio de Ciencia, Innovación y Universidades “LAboratorio de montaje, medida y CAracterización de antenas y dispositivos integrados fotónicos para comunicaciones 5G y de espacio en milimétricas, submilimétricas y THz (hasta 320 GHz) (LACA5G))”, grant no. EQC2018-005152-P.

- Comunidad de Madrid “TElealimentación FotovoLtaica por fibra Óptica para medida y coNtrol en entornos extremos (TEFLON-CM)”, grant no. Y2018/EMT-4892.

- Comunidad de Madrid “Sensores e Instrumentación en Tecnologías Fotónicas 2 (SINFOTON-2)”, grant no. P2018/NMT-4326, coordinated project with UC3M-UPM-UAH-URCJ-CSIC.

- H2020 European Union programme Bluespace project “Building the Use of Spatial Multiplexing 5G Networks Infrastructures and Showcasing Advanced Technologies and Networking Capabilities” grant nº.762055.

1.5 References

[1] L. Chettri and R. Bera, "A Comprehensive Survey on Internet of Things (IoT) Toward 5G Wireless Systems," *IEEE Internet of Things Journal*, vol. 7, no. 1, pp. 16-32, Jan. 2020.

[2] R. Lu, L. Zhang, J. Ni and Y. Fang, "5G Vehicle-to-Everything Services: Gearing Up for Security and Privacy," in *Proc. of the IEEE*, vol. 108, no. 2, pp. 373-389, Feb. 2020.

[3] A. Zaidi, R. Baldemair, V. Moles-Cases, N. He, K. Werner and A. Cedergren, "OFDM Numerology Design for 5G New Radio to Support IoT, eMBB, and MBSFN," *IEEE Communications Standards Magazine*, vol. 2, no. 2, pp. 78-83, June 2018.

[4] International Telecommunication Union (ITU) Standard, Recommendation ITU-R M.2083: IMT Vision "Framework and overall objectives of the future development of IMT for 2020 and beyond," Available Online, Accessed on Jan. 2021: https://www.itu.int/dms_pubrec/itu-r/rec/m/R-REC-M.2083-0-201509-I!!PDF-E.pdf

[5] M. J. Koonen and E. Tangdiongga, "Photonic Home Area Networks," *Journal of Lightwave Technology*, vol. 32, no. 4, pp. 591-604, Feb.15, 2014.

[6] P. Chanclou, L. A. Neto, G. Simon, A. E. Ankouri, S. Barthomeuf and F. Saliou, "FTTH and 5G Xhaul Synergies for the Present and Future," in *Proc. 21st International Conference on Transparent Optical Networks (ICTON)*, pp. 1-4, Angers, France, 2019.

[7] J. Kani, J. Terada, K. Suzuki and A. Otaka, "Solutions for Future Mobile Front-haul and Access-Network Convergence," *Journal of Lightwave Technology*, vol. 35, no. 3, pp. 527-534, 1 Feb.1, 2017.

[8] T. R. Raddo, S. Rommel, B. Cimoli and I. T. Monroy, "The Optical Fiber and mmWave Wireless Convergence for 5G Front-haul Networks," in *Proc. IEEE 2nd 5G World Forum (5GWF)*, pp. 607-612, Dresden, Germany, 2019.

[9] D. Konstantinou, A. Morales, S. Rommel, T. R. Raddo, U. Johannsen and I. T. Monroy, "Analog Radio Over Fiber Front-haul for High Bandwidth 5G Millimeter-Wave Carrier Aggregated OFDM," in *Proc. 21st International Conference on Transparent Optical Networks (ICTON)*, pp. 1-4, Angers, France, 2019.

[10] M. A. Habibi, M. Nasimi, B. Han and H. D. Schotten, "A Comprehensive Survey of RAN Architectures Toward 5G Mobile Communication System," *IEEE Access*, vol. 7, pp. 70371-70421, 2019.

[11] S. Rommel *et al*., "Towards a scalable 5G Front-haul: Analog Radio-over-Fiber and Space Division Multiplexing," *Journal of Lightwave Technology*, vol. 38, no. 19, pp. 5412-5422, 2020.

[12] Alavi, S., Soltanian, M., Amiri, *et al.* "Towards 5G: A Photonic Based Millimeter Wave Signal Generation for Applying in 5G Access Front-haul" *Scientific reports*, vol. 6**,** 19891, 2016.

[13] J. Wu, Y. Zhang, M. Zukerman, and E. K.-N. Yung, ‘‘Energy-efficient base-stations sleep-mode techniques in green cellular networks: A survey,’’ *IEEE Communication Surveys Tutorials,* vol. 17, no. 2, pp. 803–826, 2015.

[14] J. D. López-Cardona, C. Vázquez, D. S. Montero and P. C. Lallana, "Remote Optical Powering Using Fiber Optics in Hazardous Environments," *Journal of Lightwave Technology*, vol. 36, no. 3, pp. 748-754, 1 Feb.1, 2018.

Chapter 2:

Multi-Gbit/s transmission in In-Home Networks and Power-over-Fiber Integration

This chapter proposes the integration of power over fiber (PoF) for in-home networks with simultaneous multi-Gbit/s data transmission based on wavelength-division-multiplexing (WDM) in step-index plastic optical fibers (SI-POF). Different remote powering architectures are described. The efficiencies of the different components are discussed to address the maximum remote energy that can be delivered. A detailed comparison to the state of the art of POF-based home networks is presented. Experimental results show the ability of the system to deliver several mW of optical power with negligible data signal quality degradation and with BER of 1×10^{-10}. The potential of utilizing PoF in combination with low-loss WDM-POF to optically powering multiple devices for specific in-home applications and IoT ecosystems is also discussed. A PoF scalability analysis is detailed as well.

2.1 Introduction

Large core step-index (SI) plastic optical fiber (POF) has been recognized as a strong candidate for in-home networking [1] due to many advantages such as inexpensive, easy installation and high bending tolerance in comparison with multimode silica fibers [2-3]. Due to its large core this kind of fiber is easy to adapt or change even by final user (do-it-yourself approach) [4]. SI-POF also shows its feasibility to implement communication systems with bit rates up to 1 Gbit/s where it starts to take its chances in the market since 2008 [5-6]. Nowadays there is an increasing demand on operators to develop a home network that guarantees gigabit speeds to the customer due to the growth of different multimedia end-user services like high definition TV, IPTV, Video on demand, ultra HDTV format such as 4K or any Internet-based service [4,7]. Current home networks are predominantly a mixture of different network technologies, each originally optimized to carry a particular kind of communication service. Moreover, the booming amount of heterogeneous services supported by wireless devices may cause congestion in the radio-frequency (RF) spectrum as well as coverage and throughput issues thus hampering a reliable communication. Trends are becoming visible to make a transition to simplified pico- and/or femtocells which cover smaller areas suitable for the in-home scenario, generally based on a single access point (AP) in each room, and thus reduce potential interference and congestion issues [8-10]. Less transmitted power from antenna is then required but at the cost of requiring more APs. Another approach that is recently receiving growing attention is visible light communication (VLC) transmission, generally based on light emitting diodes (LEDs), which can be directly modulated and used as wireless transmitters [11]. Both approaches require a dedicated indoor fiber backbone network providing bandwidth enough to distribute the broadband signals to each wireless transmitter site, that may include wavelength-division-multiplexing (WDM) capabilities [12,13]. And plastic optical fibers are one of the most promising candidates for the in-home distribution optical network. However, POF has some disadvantages like its high attenuation losses being the best figure of merit around 150 dB/km for Polymethylmethacrylate (PMMA) at the visible range (550 nm) compared to silica fibers where these losses can be as low as 0.2 dB/km at 1550 nm. This is the main reason behind utilizing POF for short reach networks up to few hundreds of meters including home scenarios [2]. The other main disadvantage for POFs is their limited bandwidth-length products compared to silica fibers [3].

Different bandwidth-efficient modulation schemes have been proposed in the literature to overcome the limited bandwidth of POF of around 200 MHz × 50 m, mainly due to intermodal dispersion, and to meet the expectation for the data rates required within the in-home scenario [14,15]. Recently, many proposals report the capability of increased transmission capacity in terms of Multi Gbit/s, and particularly over SI-POF. 10 Gbit/s of data rate (R) over 10 m-long single SI-POF link with BER of 1×10^{-2} is achieved based on 32-PAM modulation and a multilayer perceptron-based equalizer utilizing a red LD [16].

POF large core diameter also attracts the use of light emitting diodes (LED) to achieve low cost links with the additional advantages of less eye damage risk for indoor free-space optics. In [17], 10 Gbit/s is achieved over 10 m with BER < 1×10^{-3} using two µLED and Avalanche Photodiode (APD) receivers. Violet, green and blue µLEDs are employed with PAM modulation in combination with WDM free-space components to achieve 11 Gbit/s over 10 m with BER < 1×10^{-3} [18]. In [19] a cyan LED with 47 µm active diameter is used with achieved data rates of 5.5 Gbit/s and 5.8 Gbit/s with BER of 1×10^{-3} over 1m-long SI-POF and employing NRZ and 4-PAM modulations formats, respectively. The design of µLED-based arrays that can be used for VLC-POF links is also reported in [20]. Moreover, SI-POF links based on laser diodes (LD) with higher output powers and WDM technology are also proposed to extent the transmission distance up to 100 m with data rates of 10.7 Gbit/s and BER of 1×10^{-3} [21]. In [22] low-insertion loss multiplexer/demultiplexer devices are developed thus allowing the implementation of visible WDM links over SI-POF with low power penalty [22]. These Gbit/s communication speed experimental trials demonstrate the feasibility of using large core SI-POFs as the wired solution for indoor optical communication in the near future to meet end users' data rate demands. For example, Fig. 2.1 shows different application areas with short reach that can utilize POF for communication.

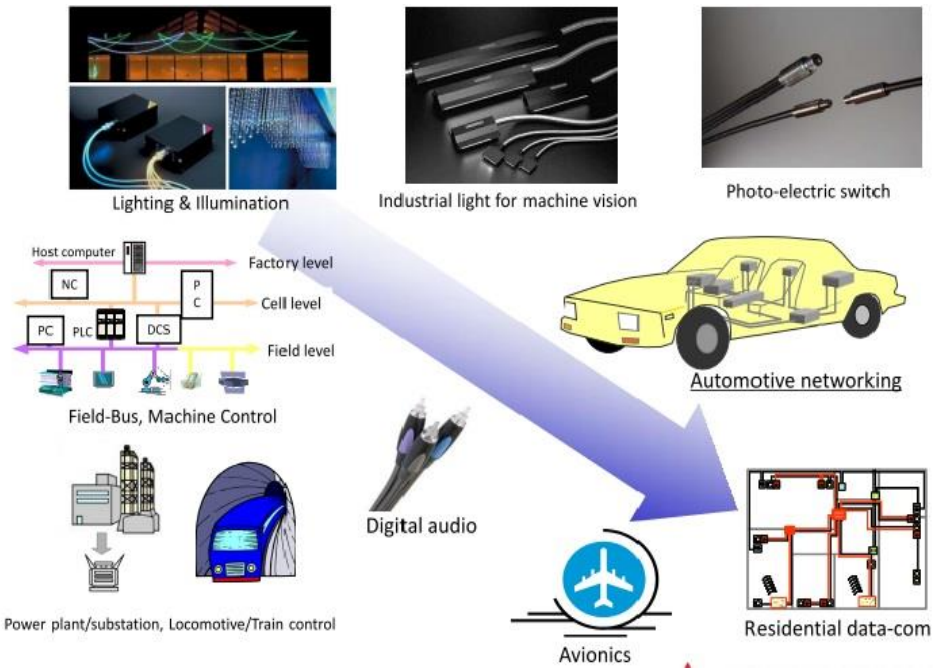

Fig. 2.1. Different application area for POF communication [23].

On the other hand, Internet-of-Things (IoT) smart home applications can be easily integrated with the physical infrastructure of these in-home POF-based high capacity solutions. This technology is increasing rapidly everywhere including the in-home scenario and with different applications like healthcare, education and building architectures with the

expectations of billions of smart devices in the near future. IoT applications key aspects are ubiquity as well as energy demands of low-power, low-cost and small-sized smart remote nodes. The current evolution of low-power IoT ecosystems enables the utilization of Power-over-Fiber (PoF) systems to remotely feed sensor nodes via optical fiber [24]. PoF provides a great advantage in environments with high electromagnetic interference (EMI) with inherent immunity to surrounding electromagnetic fields thus avoiding the use of any conventional EMI reduction technique for the power distribution. Step-index (SI) fibers are preferable over graded-index (GI) counterparts due to the mode field diameter restriction with respect to the maximum power injected into the fiber [25]. In any case, the main limitation of PoF technology over POFs comes from the polymer material itself, with POF threshold power densities of around units of KW/cm^2, being this value around three orders of magnitude lower compared to standard silica fibers [26]. In [27], this density is calculated to be 7.6 KW/cm^2 for a GI-POF with core radius of 25 μm and incident power of 75 mW which can be the same for SI-POF with same core radius but twice the incident power due to the mode field diameter (MFD) limitations [25].

Some experiments over POFs (using 1 mm core diameter standard SI-POF) reporting hundreds of mW of electrical power delivery to the load have been demonstrated [28,29] and some partial analysis of the impact of PoF on SI-POF links have been discussed [30, 31]. So that in PoF systems over POFs fiber fuse due to high power levels have to be taken into account. Energy harvesting techniques from surrounding energy sources like heat and/or electromagnetism [32] can also be employed to generate additional electrical power supply in combination with PoF. Some proposals report energy harvesting systems based VLC that can provide electrical powers of around 1.5 mW [33, 34]. A survey about utilizing energy harvesting to provide electrical power for wireless sensor networks (WSNs) and other applications can be found in [35-36]. For example, in [37] around 70 mW of power was produced by harvesting energy from piezoelectric element which can be enough to power the WSN proposed. In [38], a battery free video streaming camera was powered only by harvest energy from ambient light and RF signals that emitted from closed APs.

In this work, a real-time (RT) WDM system with maximum capacity of 4 Gbit/s over a 10 m-long SI-POF is proposed in combination with power-over-fiber (PoF) capabilities. The PoF system is implemented through the same POF fiber lead and shows the capability of providing energy to specific remote nodes and applications compatible with in-home wired/wireless IoT ecosystems. The potential of using the PoF technology in these environments is also discussed. The system efficiency in terms of power per transmitted bit (P_{Tb}) for the data signal and the maximum energy that can be delivered by the PoF channel with no penalty in the data traffic quality is evaluated. A comparative study of our proposal with respect to current state-of-the-art for Multi Gbit/s systems over SI-POF is presented. Finally, a detailed study of the scalability of our proposed PoF system for remotely feeding a smart IoT ecosystem for the in-home scenario is addressed.

2.2 Power over Fiber integration in indoor solutions

A schematic of the integration of PoF for in-home networks is shown in Fig. 2.2. It considers the use of in-home SI-POF distribution to provide gigabit per second communication as well as remote feeding purposes to the in-home IoT ecosystem. As people spend most of their time indoor, ensuring high service quality is of great importance due to rapid increase of different services as we explained previously. The distribution of small APs in each room inside home that is wired with SI-POF backbone can provide excellent wireless access to many devices within home. The integration of the PoF technology for powering smart remote IoT home nodes in the most efficient way is a major challenge in these future networks. The rapid growth in low-power integrated circuits allow the possibility of IoT devices with power consumption of even few microwatts [39]. The consideration of the wired/wireless solution to connect these in-home IoT ecosystem is of great importance.

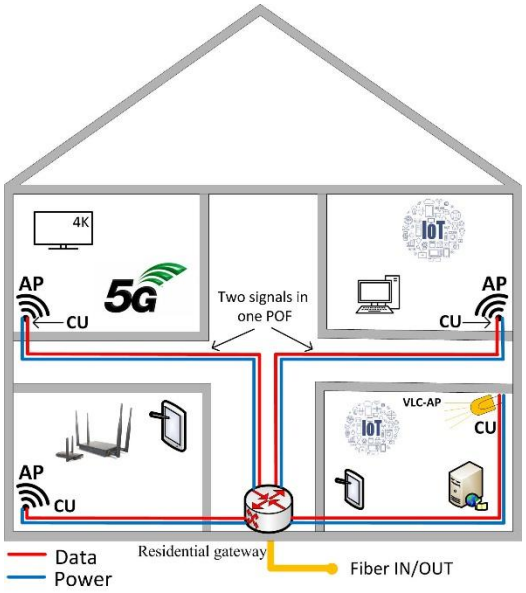

Fig. 2.2: Schematic of the proposed in-home network with PoF signal distribution.

Some aspects like maximum throughput and power consumption must be taken into account. Some technologies have been proposed to enhance the performance of wireless IoT systems in terms of energy saving by using different protocols with lower power consumption like LoRaWAN and low power WiFi [40, 41] compared to the current installed WiFi solutions. To connect the increased number of IoT devices current trends try to develop less power consumption devices but providing similar wireless connectivity. In [42] a new 28 μW ultra-low power consumption chip for wireless IoT connection is developed as a representative example. This chip can transmit data rates up to 2 Mb/s over a coverage range of 21 m and has the ability to connect many IoT sensors or other devices needed at home like phone, camera, etc.

In this application scenario, we investigate the feasibility of PoF to provide energy for an in-home IoT ecosystem. A centralized PoF system is proposed compatible with most in-home network infrastructure approaches that have been proposed and investigated [1, 7, 43], where energy is delivered from the residential gateway to feed the entire IoT system from specific units named central units (CU). These CUs may be devoted for different indoor applications such as APs or VLC communication purposes and may include different embedded smart functionality options.

The proposed system can integrate the future 5G indoor architectures where each room within the home can be equipped with high connectivity provided by POF, and simultaneously offering reliable optically feeding IoT solutions as shown in Fig. 2.2. Generally, the PoF system consists of a LD at the transmitter site to provide the power, the optical fiber link and a photovoltaic cell (PV) at the remote site/unit to convert the energy into electricity. The residential gateway can provide the energy to different elements. Different powering topologies can be designed to feed multiple battery-free smart nodes each of them with specific energy management systems for specific power consumption. Table 2.1 gives an example of main blocks of intelligent IoT nodes including smart sensors with power consumption in the μW range suitable for their use in IoT applications inside home.

Table 2.1
IoT node elements and power consumption specifications function

Function	Device	Type	Cons. (μW)
Control-intelligence	ECM3532	Artificial intelligence dual-core Arm Cortex-M3 plus NXP CoolFlux DSP	100
Communications	Ref. [42]	Wi-Fi connectivity	28
Monitoring-sensors	HTS221	Temperature and Humidity	7.2
	LPS33HW	Pressure	21.6
	H3lis331dl	Motion sensor	36
	ISM303DAC	Magnetometer sensor	17.1
	AIS2IH	Motion sensor	2.4

Using PoF can be cost-effective, achieving service continuity by remotely charging a node with a local battery and also the same fiber lead can be used to send information back about link or device status as well as the measured information to the transmitter site in the case of

a smart IoT home node. Moreover, this solution is compatible with potential energy harvesting capabilities embedded [44] in the node.

2.3 Power over Fiber System Design

2.3.1 PoF Architectures

In any PoF system over data transmission media there are mainly two architectures: a shared fiber scenario by using the same fiber for simultaneous data transmission and PoF delivery, or a dedicated fiber scenario using two independent fibers for data and PoF, respectively, as shown in Fig. 2.3.

We can see that for the dedicated fiber scenario no optical DEMUX or filtering devices are needed at the reception stage, i.e. remote site, so the power can be directly delivered to the PV. However, these elements are required in the shared fiber scenario in order to split the data traffic in coexistence with the PoF signal into the same fiber lead. This fact leads to an extra penalty in the power delivery because of their insertion losses, but with the advantage of using a single fiber serving for both purposes. MUX devices are also needed to multiplex data and PoF in the shared scenario at the transmitter site.

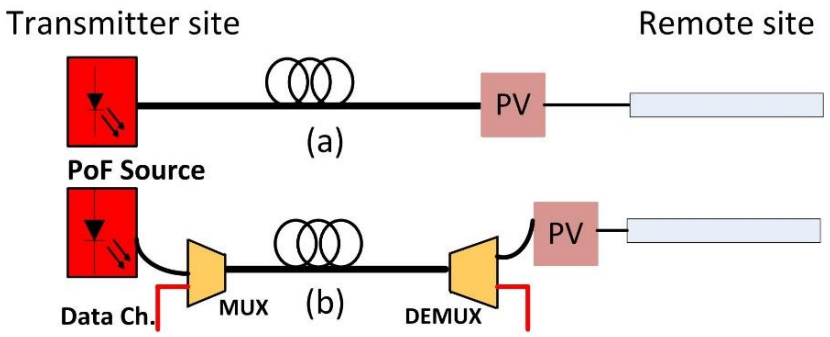

Fig. 2.3: Different powering schemes. (a) Dedicated scenario. (b) Shared scenario. PV: Photovoltaic cell.

MUX/DEMUX devices in such types of systems are critical as they should have acceptable insertion losses (IL) and high crosstalk (CT) with capability of handling high PoF power levels depending on the final application. The effect of these power levels on the data signal quality is of great importance.

2.3.2 Modeling signal to noise ratio and data transmission efficiency

When considering the shared scenario, it is important to verify how PoF power levels can affect the data transmission quality and efficiency.

The optical signal to noise ratio (SNR) model when optically delivering different levels of power on the same optical fiber needs to consider the added signal at a different wavelength from the data signal counterpart. In our calculations, we consider two laser diodes (LD), LD_1 for data transmission and LD_2 for the PoF channel, respectively. The optical power from LD_1 is P_1 providing a Relative Intensity Noise (RIN), shot noise limited. The noise contribution from RIN (σ_1) is given by [45]:

$$\sigma_1 = \eta_{FO} P_1 \sqrt{RIN\, B} \tag{2.1}$$

where: $$RIN = \frac{2h\upsilon}{P_1} \tag{2.2}$$

where η_{FO} is the fiber attenuation, *h* is the Planck constant which is equals to 6.62×10^{-34} J.s , υ is the optical frequency, and B is the bandwidth of the system.

The contributing noise terms at the detector with an incident optical power P_D, i.e. the shot noise (σ_2), dark current (I_D) noise (σ_3) and Johnson noise (σ_4), respectively, are given by [45-46]:

$$\sigma_2 = \frac{1}{\eta_{PD}} \sqrt{2q\eta_{PD} P_D B} \tag{2.3}$$

$$\sigma_3 = \frac{1}{\eta_{PD}} \sqrt{2q I_D B} \tag{2.4}$$

$$\sigma_4 = \frac{1}{\eta_{PD}} \frac{1}{\eta_{Rx}} 2\sqrt{K T_A R B} \tag{2.5}$$

where η_{PD} is the conversion efficiency of the detector, q is the electric charge, K is the Boltzmann constant equals to $1.380649\times10{-}23$ $J\cdot K^{-1}$, T_A is the absolute temperature of the resistor for Johnson noise calculations, η_{Rx} is the preamplifier gain, and R is the resistance, respectively. This resistance could be the feedback resistor value of a transimpedance amplifier, for example.

The SNR now can be expressed as follows:

$$SNR = \frac{P_D}{\sqrt{(\sigma_1)^2 + (\sigma_2)^2 + (\sigma_3)^2 + (\sigma_4)^2}} \tag{2.6}$$

The main difference in our analysis is provided by the added term in σ_1 because of the added RIN of the PoF laser; the effect will be higher for lower power levels of data channel at the

receiver, P_D. By estimating the maximum power of PoF channel allowed at the receiver for a specific SNR we can determine the minimum crosstalk required at the DEMUX device at reception, shown in Fig. 2.3. About the data transmission efficiency, we define the power per transmitted bit ($P_{Tb)}$ as [47]:

$$P_{Tb} = \frac{\beta \times I_{peak}}{T} \tag{2.7}$$

and

$$I_{peak} = m_i \times (I_{bias} - I_{th}) \tag{2.8}$$

where β is the quantum efficiency of the LD for data transmission, m_i is the modulation index, and I_{bias} and I_{th} are the optical source bias and threshold currents, respectively. T is the total network throughput and can be expressed as [47]:

$$T = R[1 - BER(P_{size} + IPG)] \tag{2.9}$$

where R is the data rate, P_{size} is the Ethernet packet size and IPG is the inter packet gap. By using these equations and depending on BER, the transmission efficiency yields:

$$\text{Transmission Efficiency} = \frac{T}{R} \times 100\% \tag{2.10}$$

Better BER values improve the transmission efficiency. For our experimental trials we select a system providing real Multi Gbit/s transmission in SI-POF [47] with BER of 10^{-10} for integrating PoF as well as testing impairment effects and energy efficiency degradation.

2.4 Experimental Results

2.4.1 Experimental testbed

The schematic diagram of the experimental setup utilized in this chapter is shown in Fig. 2.4. to investigate the feasibility of SI-POF for data transmission with Gbit/s with the integration of PoF in the shared scenario.

The setup is based on a PC equipped with a 1 Gigabit Ethernet interface in combination with a Media Converter (MC) used to generate and to receive the transmitted data bits. The MC transforms the Gigabit Ethernet frames into a 16-level Pulse Amplitude Modulation (PAM) signal (named Tx-signal), and vice versa. At the transmitter site, the Tx-signal modulates the optical source of the data channel at 650 nm. The PoF signal is generated by a LD emitting at 405 nm. In this experiment, an external LD at 650 nm is used as the optical transmitter for the data channel instead of the LED provided by the MC in order to enhance the power budget of the link. Still the MC encodes the frames into a PAM signal and vice versa. Data and power channels are multiplexed and launched into a 10 m-long PMMA SI-POF link through

a low insertion loss visible MUX device. After fiber transmission, PoF and data signals are demultiplexed. At the reception stage, the received optical signal is converted back to the electrical domain by a PIN photodiode (PD) included in the MC. This MC is part of a fully integrated system [48] that establishes a real-time data link at 1 Gbit/s without any post processing.

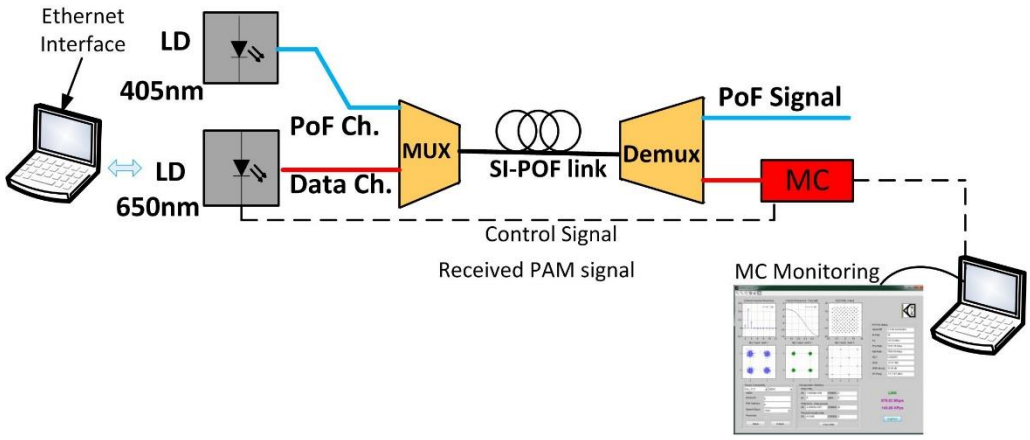

Fig. 2.4: Schematic of the experimental setup.

The MUX device is based on reflective diffraction grating technology with blazed profile and aspheric lens that can accommodate up to 6 channels with low insertion losses ILs ~ 4dB, has a 3-dB bandwidth greater than 30 nm for each channel and with a size of ~65 mm x 55 mm. The designed MUX is bidirectional so another device with the same characteristics is used at the demultiplexing stage. Fig. 2.5 shows the layout of the MUX/DEMUX devices used, however more details can be found in [22].

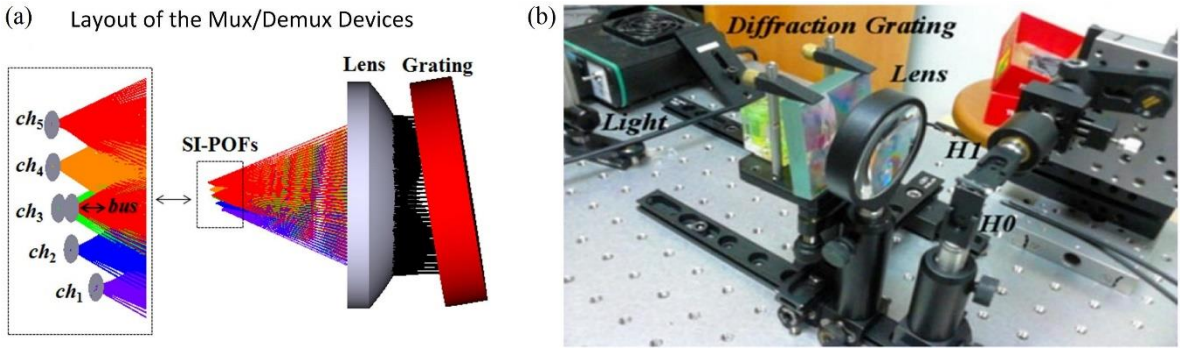

Fig. 2.5: (a) Layout of the Mux/Demux devices (b) Photo of the device [22].

This system uses Multi-level Coset Codes (MLCC) for error correction and all the BER measurements in the next subsections are taken after this error correction process. The PD is monolithically integrated with the required amplifiers, logic and lenses. It features a high linear transimpedance amplifier for Gbit/s operation. The transmission system is chosen to

have a good performance in terms of high data capacity and BER to make it compatible with the application scenario discussed within section 2.2. All link characteristics such as BER and constellation diagrams are measured depending on the monitoring features of the MC. However, Fig. 2.6 shows the recovered electrical PAM signal at reception stage capture by oscilloscope after detected by a high speed (1 GHz BW) photodiode for visible spectrum.

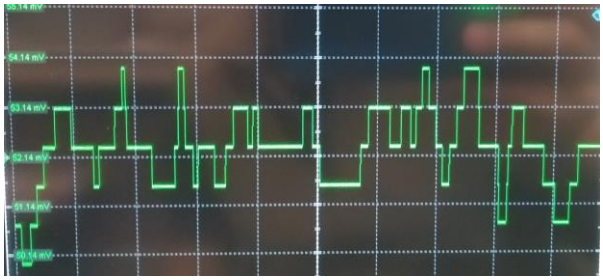

Fig. 2.6: Received PAM signal after fiber transmission.

2.4.2 Measurements of PoF impact on data transmission

In this section, the designed system is evaluated, including data signal quality and energy efficiency potential degradation due to PoF along with required devices specifications.

2.4.2.1 Shared scenario and PoF impact analysis

To analyze if there is any influence in the data transmission quality when delivering different levels of power from the PoF signal on the same optical fiber we evaluate the evolution of the signal to noise ratio (SNR) through the monitoring features provided by the MC. For doing so, different measurements of SNR_{decode} (value detected by MC) and BER are carried out. All the measurements are done over a 10 m SI-POF link length.

In the first set of measurements, there is no DEMUX in the reception stage to study the influence of the PoF signal (405 nm) into the data traffic channel (650 nm) so both signals reach the same PD. These measurements, apart from the impact effect on transmission, also provide data about the minimum crosstalk (CT) specifications required at the DEMUX in the final application. We use normalized measurements to evaluate the degradation. The reference signal is the measured SNR_{decode} when the data signal is transmitted without PoF in the proposed setup. The measured SNR_{decode} is 32.05 dB with a BER equals to zero. The PD accepts a maximum input power up to +0.5 dBm. For avoiding the damage of the PD, we configured the PoF power level at 405 nm received at the PD to be –0.2 dBm with additional received data signal of -8 dBm. In this case, the SNR_{decode} degrades in 4.1 dB. We then decrease the optical power energy delivered in steps of 3 dB resulting in a SNR_{decode} increment. This measured SNR shows negligible variations with respect to the reference signal up to a power channel level of – 12 dBm. In all the steps, the BER is $< 1\times 10^{-10}$ that represents a free error transmission. Afterwards, the input data signal is decreased, and set to – 12 dBm and the PoF optical power delivered is set to -0.2 dBm, being both power levels

measured at the PD. The same procedure to measure the SNR_{decode} is done. The measured SNR_{decode} is 28 dB when the data signal is transmitted alone. When both signals are multiplexed, the SNR_{decode} decreases in 3.9 dB with additional PoF power channel at 405 nm of -0.2 dBm in the link reaching the PD. The link is not established as the system requires $SNR_{decode} \geq 25$ dB for 1 Gbit/s transmission. The constellation diagrams of the three decoding stages at the receiver of the best and worst case are shown in Fig. 2.7.

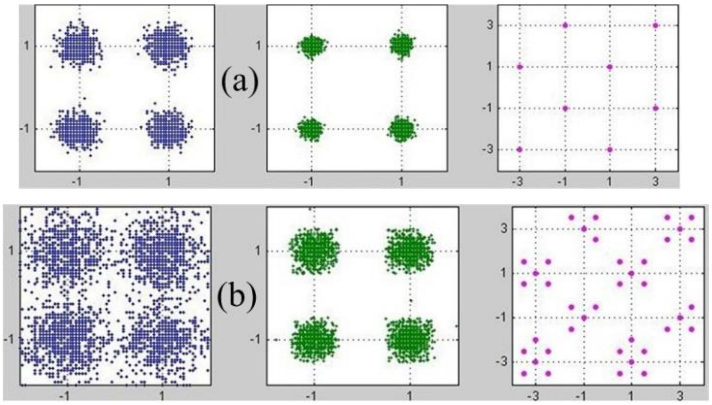

Fig. 2.7: Constellation diagram at reception of the multilevel decoding inputs: (a) Only data signal, -8 dBm at PD. (b) Both data and PoF channels at PD; data -12 dBm, PoF – 0.2 dBm.

Using the equations (2.1) - (2.6) described within section 2.3.2, normalized SNR simulations are performed considering the parameters reported in Table 2.2, chosen to emulate our experimental setup.

Table 2.2
Parameters for the SNR analysis

Parameter	Value
η_{FO}, Total fiber attenuation	0.67
h, Planck constant	6.62×10^{-34} J.s
υ, optical frequency	461.22 THz
B, Bandwidth of the system	500 MHz
η_{PD}, PD conversion efficiency	0.38 A/W
$I_{D,}$ Dark current	10 nA
q, electric charge	1.6×10^{-19} C
K, Boltzmann constant	1.38×10^{-23} J/K
η_{Rx}, Preamplifier gain	1000 V/A
R, Resistance	1000 Ω
$T_{A,}$ Temperature	300 K

We simulate two power levels reaching the PD, P_D, of –8 dBm and -12 dBm in order to have a reference SNR value for no PoF signal injected into the link. As expected the SNR degrades as the power level impinging the PD decreases. Afterwards for simultaneous transmission, we add the noise contribution from the PoF channel (LD_2) to the overall noise power. RIN of the 405 nm channel affects the SNR of the data signal thus resulting in an additional penalty. Fig.2.8 shows a comparison between both normalized calculated SNR and measured SNR_{decode} which proves that they both have the same tendency against an increasing power from LD_2. Estimated SNR penalties are around 4-5 dB similar to that of observed from the experimental setup. We show that increasing the optical power delivery signal adds more noise to the system and both the SNR and BER degrade. The maximum optical power of PoF at 405 nm, named P_{HPL}, that can reach the PD depends on the data signal power at 650 nm, named P_{DATA} reaching the PD.

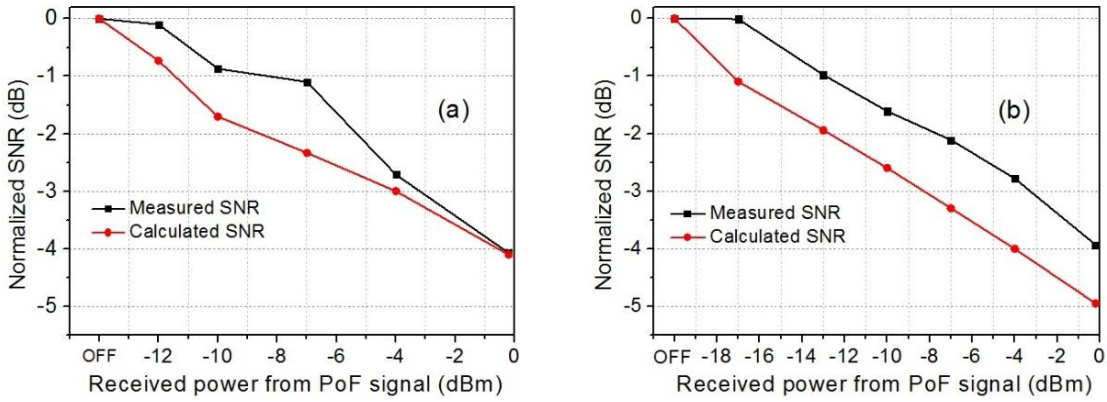

Fig. 2.8: Normalized calculated SNR and measured SNR_{decode} vs. PoF power at reception stage with input data signal power of: (a) -8 dBm (b) -12 dBm.

In any case, from the experimental results, see Fig. 2.8 - measured SNR curves, to keep the same SNR value as when there is no PoF, the relationship between the powers of both data and PoF channels at the PD can be expressed as:

$$P_{DATA}(dBm)-P_{HPL}(dBm)=5\ dB \tag{2.11}$$

The PoF power channel signal at the photodiode of the Media Converter (MC PD), named P_{HPL_DEMUX}, when using a DEMUX with a crosstalk CT at the reception stage yields:

$$P_{HPL\_DEMUX}\ (dBm)= P_{HPL}(dBm)-CT\ (dB) \tag{2.12}$$

Then the required CT for the demultiplexer is given by:

$$CT = P_{HPL} - P_{HPL\_DEMUX} = P_{HPL} - P_{DATA} - 5\ dB \quad (2.13)$$

As an example, for a 10 mW optical power delivery at the PV placed in the AP or VLC access point, see Fig 2.2, and a receiving a data signal of -8 dBm a CT of 23 dB is then required.

2.4.2.2 Shared scenario including demultiplexing and data transmission performance

In order to recover the PoF signal and to study the received data signal, we use a DEMUX at the end of the link. This device uses a diffractive grating and have a CT of around 30 dB [22], complying with the requirements analyzed in the previous section. We evaluate the link performance using the monitoring features of the MC. The link is tested using different transmitted data power levels and varying the PoF optical power delivered at 405 nm. All the measurements are carried out in a 10 m-long SI-POF link. An estimation of the power budget of the PoF is shown in Table 2.3. A PoF power level of about 20 mW is injected into the fiber. BER measurements for different PoF levels show no impact of PoF on the data signal quality transmitted at 650 nm. In all cases, BER is $< 1\times 10^{-10}$ that represents a free error transmission with the possibility of delivering 4.12 mW of optical power at the fiber end but before the demux device. In the next subsection we show how the consideration of demux devices with different insertion losses can affect PoF level at remote site. Measured SNR_{decode} of the link is 32 dB in both cases with no degradation due to the increments of the PoF signal level.

Table 2.3
Power budget of the PoF channel

Parameter	Power
PoF-LD output power (dBm)	+13
Coupling loss (dB)	0.75
MUX/DEMUX IL (dB)	4
POF link 10 m (dB)	2.1
Power at the end of link	+2.15 dBm or 1.64 mW

2.4.2.3 Shared scenario data transmission efficiency

In order to estimate the data transmission efficiency of the proposed setup, we analyze the power efficiency per transmitted bit based on the BER measurements. In our system with BER values of 10^{-10}, from Eq (2.9) and Eq. (2.10), we achieve a transmission efficiency of 100%. Table 2.4 shows recent proposals of 10 m-long SI-POF links with their general parameters. Table 2.5 includes a detailed analysis of the transmission efficiency calculation of our proposed system compared to other current state-of-the-art proposals on Multi Gbit/s

transmission over 10 m-long SI-POF links. These calculations are done for the worst-case scenario considering 64 bytes of Ethernet packet size and IPG of 96 bits where only one bit-error results in a packet-error. Our system outperforms both previous works in terms of both transmission efficiency and power per bit figures of merit, as described below.

Table 2.4
Recent proposals with 10 m-long SI-POF links

Parameter	This Work	[16]	[18]	[17]
Data Rate(Gbit/s)	1(1)	10	11	10
BER	1×10^{-10}	1×10^{-2}	1×10^{-3}	1×10^{-3}
No. of Channels	1(1)	1	3	2 bi
Simultaneous PoF	YES	NO	NO	NO
Real Time Transmission	YES	NO	NO	NO

Notes: (1) Can be extended up to 5 Gbit/s using 5 WDM-POF channels

Table 2.5
Comparison with recently reported SI-POF links.

Parameter	This work 10 m	[16] 10 m	[21]100 m
Data Rate, R (Gbit/s)	1	10	1.05
Wavelength (nm)	650	650	660
BER	1×10^{-10}	1×10^{-3}	1×10^{-3}
Data Throughput T (Gbit/s)	1	3.39	0.412
Transmission efficiency	1	0.339	0.392
Threshold Current I_{th} (mA)	20.4	20	80
Bias Current I_{bais}(mA)	23	30	45
Modulation index m_i	0.69	0.65	0.9
Quantum efficiency ß (W/A)	0.667	0.665	0.7-1.4
Power per bit P_{Tb} (pJ/b)	1.2	1.28	53.5

We further investigate the performance of the system and analyze the impact of the BER on the total throughput and transmission efficiency. We vary the received optical power near the receiver sensitivity (~ -18.80 dBm) thus decreasing the BER. The results are shown in Fig. 2.9. For a received power greater than -13 dBm a BER of $< 1\times 10^{-10}$ can be achieved with total throughput of 1 Gbit/s, meaning 100% of transmission efficiency. At BER of 1×10^{-5} the transmission efficiency is degraded to 98.46% thus leading to a throughput of 0.98 Gbit/s which still represents a good transmission performance. With the assumption of a further BER degradation to 1×10^{-3}, the transmission efficiency is 39%. These results show that the transmission efficiency of our system, which can be 100% depending on the received optical power, outperforms the other proposals at 10 m as it was 39% in [16]. Also free error transmission can be achieved with PoF capability compared to BER around $1x10^{-3}$ as in [16-

18, 21]. Moreover, a power per bit, P_{Tb}, of 1.2 pJ/b is achieved which also outperforms other works.

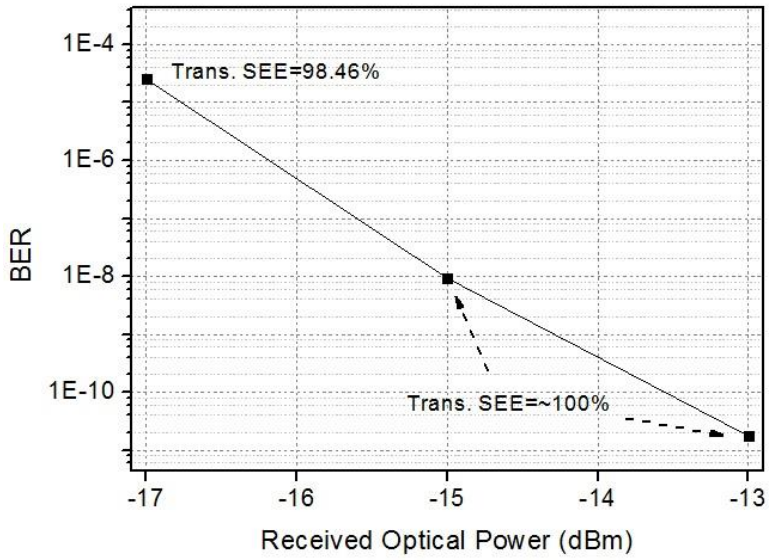

Fig. 2.9: Measured BER vs. received optical power with calculated transmission efficiency.

2.5 Discussion and scalability analysis

In this section, we discuss the use of PoF technology over the SI-POF link experimentally tested for feeding IoT nodes with the power consumption requirements provided in Table 2.1. The central IoT unit/node has a control unit, WiFi communication capabilities as well as several sensors and demands around 150 µW. Other nodes have only communications and sensing capabilities demanding 30 µW. An example of different powering distribution topologies that can be applied to any PoF system depending on the power consumption of each node/device can be found in [24].

The energy system efficiency (SEE) is a key issue in any PoF system. SEE depends directly on the optical to electrical conversion efficiency of the PV and the transmission efficiency of the fiber link. In general, SEE can be defined as follows:

$$\mathrm{SEE} = \frac{\text{Energy at the remote node}}{\text{Energy of high power laser}} \tag{2.14}$$

The SEE of the proposed system is analyzed considering the different powering architectures shown in Fig. 2.3, and depending on the PV efficiency (based on amorphous Silicon [49]), fiber attenuation and MUX/DEMUX losses. Wide bandgap materials with specific structure can be considered for higher quantum efficiency. The number of remote devices that can be powered via PoF provides information about how much the PoF solution is becoming reliable for a targeted application.

For that we consider N as the number of remote nodes that can be optically feed to determine the scalability of the system. N directly depends on the power consumption on each remote node. For the calculation, we consider a simple node (N_A) that demands 30 µW and a central node (N_B) with additional embedded smart functionalities demanding 150 µW, respectively. Thus N_A, i.e. the total number of central nodes that can be fed, follows $N_B = N_A/5$.

From the power budget analysis described within Table 2.3, after demultiplexing an optical power up to 2 mW (reaching the PV) for the PoF signal can be delivered for optimized HPL-POF fiber coupling loss. In Fig. 2.10, SEE of the proposed experimental setup is calculated for both shared and dedicated fiber scenario. The calculated electrical power at remote node (P_{elec}) is increased from 0.5 mW in the shared- to 3.14 mW in the dedicated- scenario both considering a 10m-long SI-POF link. As a result, and for this link distance, it yields $N_A = 16$ and $N_A = 104$ for the shared- and dedicated- scenarios above described, respectively. Both node types could also be fed; for instance the shared scenario may lead to simultaneous $N_A = 6$ and $N_B = 2$ remote feeding.

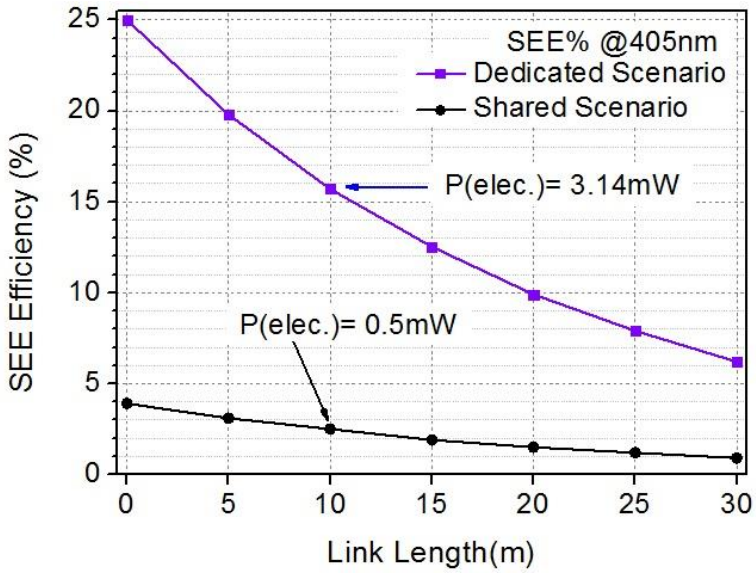

Fig. 2.10: System energy efficiency (SEE) vs link length for the proposed experimental setup with MUX/DEMUX IL~4 dB, PV efficiency= 25%.

Optimize insertion losses for the MUX/DEMUX devices can significantly enhance the SEE of the system thus increasing the resulting P_{elec} at the remote node. For that we analyze different cases as the fiber bundle approach proposed in [50] for POF multiplexing. This MUX comprises a fiber bundle made of graded index plastic optical fibers of 1m and numerical aperture (NA) of 0.185, having a total diameter of less than 1mm; being faced to the SI-POF fiber using ST-ST connectors. At the DEMUX stage two cases are considered: our DEMUX device used for the experimental setup [22] as well as a potential improved version of the latter with extremely low losses (IL 1.5 dB). LD (PoF source) output power is

considered to be 20 mW as aforementioned to fit with the experimental values. Fig. 2.11 shows the impact of these considerations onto the current experimental setup.

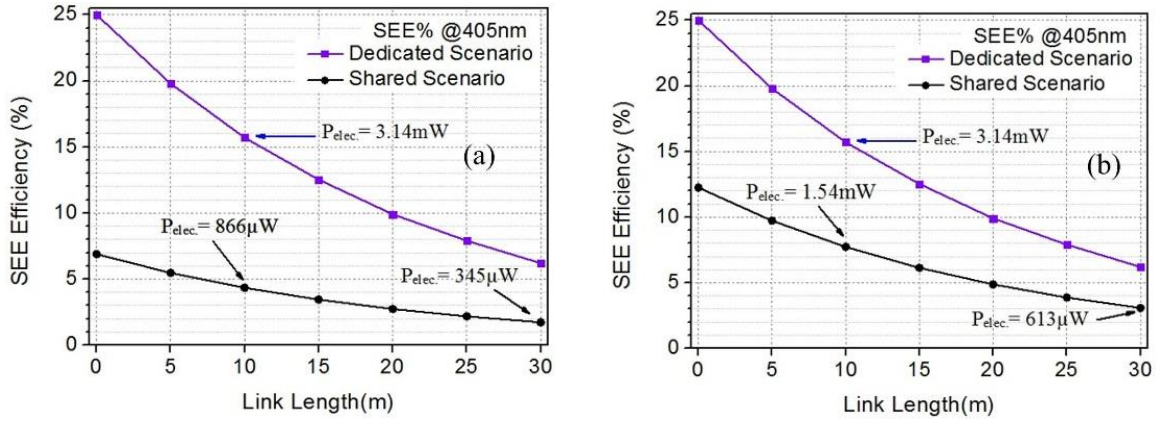

Fig. 2.11: System energy efficiency (SEE) vs link length for the proposed experimental setup considering a fiber bundle for multiplexing, PV%= 25%:(a) DEMUX IL~4 dB, (b) DEMUX IL 1.5 dB.

Fig. 2.12 shows a comparison between the two shared scenarios depicted in Fig. 2.11. SEE is increased from 4.1% to 8.9% for a 10m-long link by using the low-loss DEMUX device proposed. For this SI-POF link distance the remote delivered electrical power rises from 866 µW to 1.54 mW. This leads to an increase in the remote power delivery capability of the PoF system: N_A may increase from 28 to 51 while the N_B counterpart from 5 to 10. Right vertical axis in Fig. 2.12 shows the evolution vs link distance of number of smart N_B IoT nodes that could be remotely fed considering the case of a low insertion loss DEMUX device.

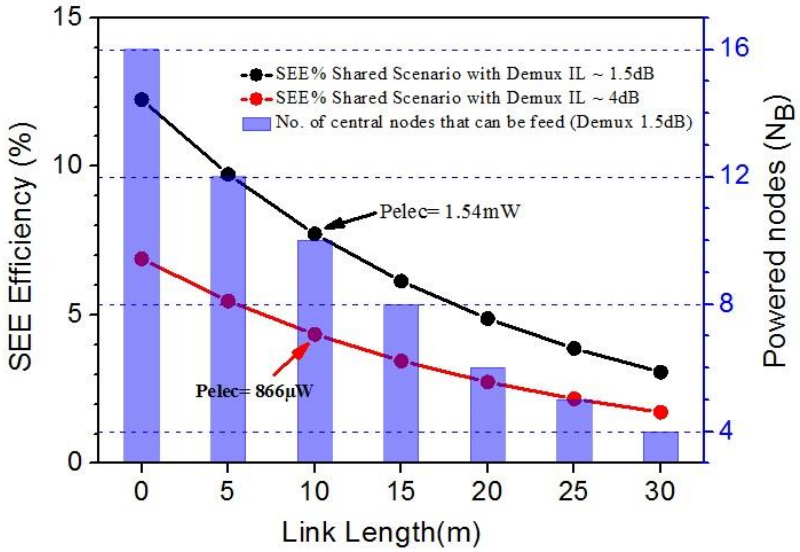

Fig. 2.12: System energy efficiency (SEE) vs link length for the shared scenarios for PoF at 405 nm with different DEMUX losses. Right vertical axis: number of smart N_B IoT nodes that could be remotely fed considering different DEMUX devices in the link.

Other parameters that can affect the SEE should be considered like fiber attenuation and PV efficiency. Both depend on the operating wavelength of the PoF source. We consider a new wavelength for our study thus being 520 nm. At 520 nm both lower fiber attenuation coefficient (0.104 dB/m) and higher PV efficiency (~ 38%) are expected compared to the 405 nm case.

Additionally, the DEMUX device shows a less insertion loss at this wavelength [22, 50] being of around 3.5 dB. In Fig. 2.13(a), the SEE vs link length of the proposed setup with PoF at 520 nm is estimated for both shared- and dedicated- fiber scenario. At 10 m-long SI-POF link the remote electrical power delivered, P_{elec}, results in 1.99 mW and 5.96 mW for the shared- and dedicated scenarios. This means an increase of 129% and 90%, respectively, if we compare these values with the electrical power delivered, P_{elec}, at 10 m-long SI-POF, as shown in Fig. 2.11(a). Accordingly, Fig 2.13(b) depicts the expected similar figures of merit by considering the improved version of the DEMUX device with IL ~1.5 dB. Following similar considerations to that of for the previous figure, for this specific case study N_A increases from 66 to 105 while the N_B counterpart from 13 to 21, respectively.

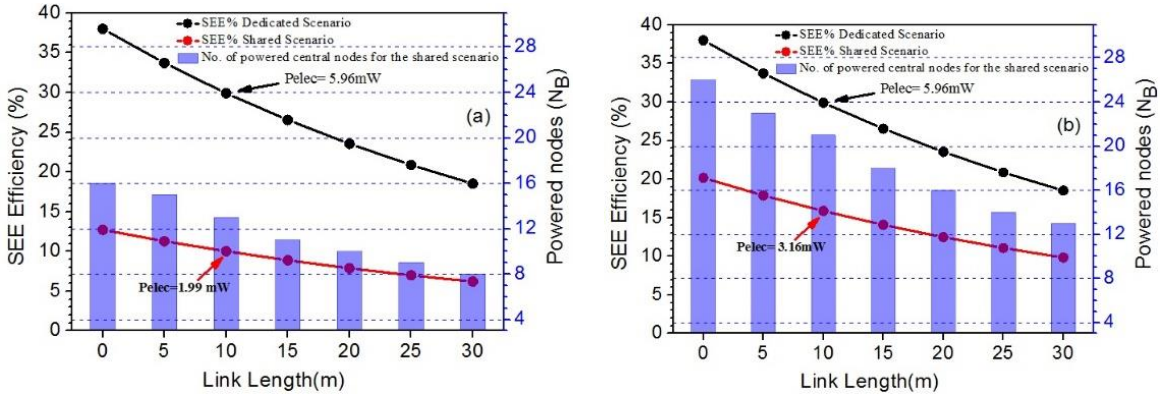

Fig. 2.13: System energy efficiency (SEE) vs link length for the proposed system considering a PoF system operating wavelength of 520 nm, PoF-LD output power: 20 mW, PV%= 38%, (a) DEMUX IL~ 3.5 dB, (b) DEMUX IL 1.5 dB. Right vertical axis: number of smart N_B IoT nodes that could be remotely fed.

Moreover, utilizing the presented MUX/DEMUX devices with high CT and acceptable ILs, the capacity of the proposed system can be extended to five channels. Data transmission of 4 Gbit/s can be integrated with the PoF levels concluded from Figures 2.10 to 2.13 by considering a shared scenario with four channels for data transmission and one for PoF purposes. On the other hand, the maximum delivered energy at the remote node can be even increased by applying more channels for optical feeding purposes.

Finally, in Fig. 2.14 we show the overall SEE vs link length for the shared scenario by using 4 channels for PoF (405 nm, 470 nm, 520 nm, 590 nm) and one channel for data (650 nm). The attenuation losses, MUX/DEMUX ILs for the rest of the channels are all extracted from [22, 50, 51]. The delivered P_{elec} for a 10 m-long 5-channel WDM SI-POF link can be

increased up to 6.36 mW. For this maximum energy delivery, NA= 212 or NB= 42 nodes could be remotely fed via PoF means which can be greatly enough for in-home scenarios.

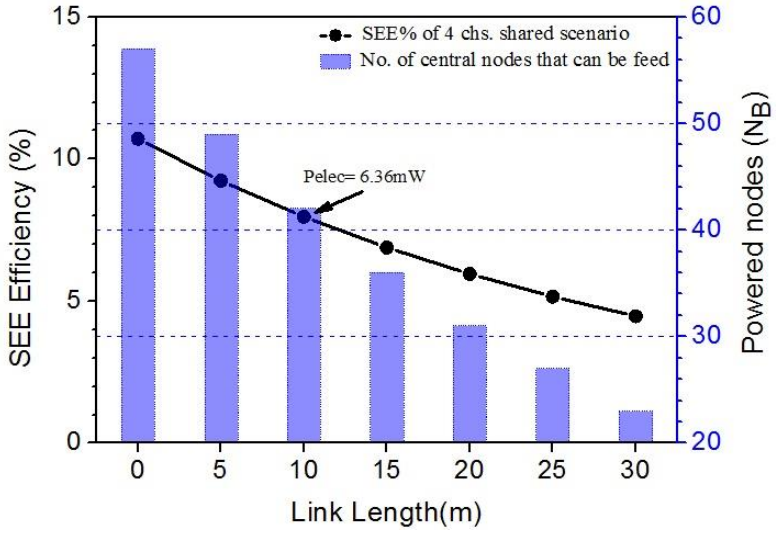

Fig. 2.14: System energy efficiency (SEE) vs link length for the proposed system considering 4 channels for PoF and one channel for data in a WDM-POF link for in-home networking.

For optical feeding based SI-POF (using the proposed channel at 405 nm), and depending on the power level, the long term stability of the fiber is of great importance. High temperature and humidity may cause aging problems as it can affect the optical properties of the fiber [52]. However, these problems can be expected in systems with high power levels increasing the fiber temperature up to 60º C [53], which is not the case in the proposed system as it uses low power values, being aging problems negligible. For high PoF system, this issue needs to be addressed. In [21], the same wavelength of 405 nm is used in the data channel with the same power level we use.

The above analysis shows the feasibility of the designed PoF system to provide remote energy to multiple IoT devices with low power consumption. The numbers of optically feeding nodes can be increased by increasing the output power provided by PoF light source. Thanks to current state-of-the-art of low power consumption devices for IoT purposes provided in Table 2.1, the total PoF power can be reduced being able to operate in eye safety limit while providing sufficient energy to fulfill smart IoT ecosystem needs.

2.6 Conclusions

In this Chapter we provide a detailed analysis of the impact of simultaneous data transmission and energy delivering over the same plastic optical fiber (POF) lead for the in-home networking scenario, for the power-over-fiber input powers considered. A real-time data link at a data rate of 1 Gbit/s with BER < 1×10^{-10} over 10 m-long POF integrated with different energy delivery scenarios is evaluated. The transmission capacity of the proposed system can be expanded to 5 Gbit/s with the use of the presented MUX/DEMUX devices to achieve a WDM-POF based solution to expand the POF fiber data traffic capabilities and meet user's data rate demands in the home. Our system outperforms in terms of transmission efficiency and power per bit figures of merit.

We present shared- and dedicated- fiber scenarios over POF to integrate our PoF solution in the above POF communication link where no impact on the data traffic (BER < 1×10^{-10}), neither on transmission efficiency is noticed for delivered optical power levels up to several mW at the fiber end. Design rules on the required crosstalk on the demultiplexer at the receiver stage are also provided. The use of this energy to remotely feed different sensor nodes for in-home IoT applications is discussed. The scalability of the system is analyzed showing the PoF feeding capabilities for different case studies that fulfill smart IoT in-home ecosystem needs.

2.7 References

[1] A. M. J Koonen and E. Tangdiongga, *"*Photonic home area networks,*" IEEE Journal of Lightwave Technology,* vol. 32, no. 4, pp. 591-604, 2014.

[2] P. Polishuk, "Plastic optical fibers branch out," *IEEE Communications Magazine*, vol. 44, no. 9, pp. 140-148, Sept. 2006.

[3] O. Ziemann, J. Krauser, P. Zamzow, and W. Daum, POF-Handbook: Short Range Optical Transmission Systems, 2nd ed. Berlin, Germany: Springer-Verlag, 2008.

[4] R. Gaudino *et al*., "Perspective in next-generation home networks: Toward optical solutions?," *IEEE Communications Magazine*, vol. 48, no. 2, pp. 39-47, February 2010.

[5] D. Cardenas et al., "100 Mb/s Ethernet Transmission over 275 m of Large Core Step Index Polymer Optical Fiber: Results from the POF-ALL European Project," *IEEE Journal of Lightwave Technology,* vol. 27, no. 14, July 2009.

[6] A. M. J. Koonen et al., "POF Application in Home Systems and Local Systems," in *Proc. of International Conference on Plastic Optical Fiber,* Yokohama*,* 2005.

[7] Y. Shi, E. Tangdiongga, A. M. J. Koonen, A Bluschke, P. Rietzsch, J. Montalvo, M. De Laat, G. Van den hoven, and B. Huiszoon, "Plastic-optical-fiber-based in-home optical networks," *IEEE Communication Magazine,* vol. 52, no. 6, pp. 186–193, 2014.

[8] I. Mollers *et al*., "Plastic optical fiber technology for reliable home networking: overview and results of the EU project pof-all," *IEEE Communications Magazine*, vol. 47, no. 8, pp. 58-68, August 2009.

[9] "Indoor 5G Scenario Oriented White Paper" Huawei, Version 3.0, October, 2019, Available Online, Accessed on December 2020 https://carrier.huawei.com/~/media/CNBGV2/download/products/servies/Indoor-5G-Scenario-Oriented-White-Paper-en.pdf

[10] P. Polishuk, "Top 40 Actual and Potential Plastic Optical Fiber Markets for 2008" p. 136, 2008.

[11] I. N. Osahon, E. Pikasis, S. Rajbhandari, and W. O. Popoola, "Hybrid POF/VLC link with M-PAM and MLP equaliser″ in *Proc. IEEE International Conference on Communication (ICC*), Paris, pp.1-6, 2017.

[12] C. Lethien, D. Wake, B. Verbeke, J. Vilcot, C. Loyez, M. Zegaoui, N. Gomes, N. Rolland, and P. Rolland, "Energy-Autonomous Picocell Remote Antenna Unit for Radio-Over-Fiber System Using the Multiservices Concept," *IEEE Photonics Technology letters*, vol. 36, no. 8, pp. 649-651, 2012.

[13] C. R. B. Correa, F. M. Huijskens, E. Tangdiongga, and A. M. J. Koonen, "POF feeding in Li-Fi systems with MIMO approach'' in *Proc. 24th annual IEEE Photonics Benelux Symposium*, Amsterdam, Netherlands, 2019.

[14] B. Huiszoon, M. M. de Laat, Y. Shi, B. Eman, and G. N. van den Hoven, "Beyond a Gigabit on plastic optical fibre at the FTTH gateway," in *Proc. 15th International Conference on Transparent Optical Networks (ICTON),* Cartagena, pp. 1-4, 2013.

[15] D. Fujimoto, H. Lu, K. Kumamoto, S. Tsai, Q. Huang, and J. Xie, "Phase-Modulated Hybrid High-Speed Internet/WiFi/Pre-5G In-Building Networks Over SMF and PCF with GI-POF/IVLLC Transport," *IEEE Access,* vol. 7, pp. 90620-90629, 2019.

[16] I. N. Osahon, M. Safari, and W. O. Popoola, "10-Gbit/s transmission over 10-m SI-POF with MPAM and multilayer perceptron equalizer" *IEEE Photonics Technology Letters*, vol. 30, no. 10, pp. 911-914, 2018.

[17] X. Li et al., "Micro-LED-based single-wavelength bi-directional pof link with 10 Gbit/s aggregate data rate," *Journal of Lightwave Technology* vol. 33, no. 17, pp. 3571-3576, 2015.

[18] X. Li *et al*., "11 Gbit/s WDM transmission over SI-POF using violet, blue and green μLEDs," in *Proc. Optical Fiber Communications Conference (OFC),* California, 2016.

[19] J. Vinogradov, R. Kruglov, R. Engelbrecht, O. Ziemann, J. K. Sheu, K. L. Chi, J. M. Wun, and J. W. Shi, "GaN-based cyan light-emitting diode with up to 1-Ghz bandwidth for high-speed transmission over SI-POF," *IEEE Photonics Journal*, vol. 9, pp. 1-7, 2017.

[20] J. F. C. Carreira, E. Xie, R. Bian, C. Chen, J. J. D. Mckendry, B. Guilhabert, H. Haas, E, Gu, and D. Dawson, ''On-chip GaN-based dual-color micro-LED arrays and their application in visible light communication,'' *Optics Express,* vol.27, no. 20, pp. 1517-1528, 2019.

[21] R. Kruglov, S. Loquai, J. Vinogradov, O. Ziemann, C. A. Bunge, G. Bruederl, and U. Strauss, "10.7 Gbit/s WDM transmission over 100-m SI-POF with discrete multitoned," in *Proc. Optical Fiber Communication Conference (OFC),* paper W4J.5, pp. 1-3, California, 2016.

[22] P. Pinzon, I. Pérez, and C. Vázquez, "Efficient Multiplexer/Demultiplexer for visible WDM transmission over SI-POF technology," *Journal of Lightwave Technology*, vol. 33, no. 17, pp. 3711-3718, 2015.

[23] IEEE 802.3 Gigabit Ethernet over Plastic Optical Fiber meeting, 2014, Available Online, Accessed on 2020: https://www.ieee802.org/3/GEPOFSG/public/May_2014/Tsukamoto_GEPOF_01_0514.pdf

[24] J. D López-Cardona, D. S. Montero and C. Vázquez "Smart remote nodes fed by power over fiber in internet of things applications," *IEEE Sensors Journal*, vol. 19, no. 17, pp. 7328-7334, 2019.

[25] J. D. López-Cardona, C. Vázquez, D. S. Montero, and P. Contreras, "Remote optical powering using fiber optics in hazardous environments," *Journal of Lightwave Technology,* vol. 36, no. 3, pp. 748-754, 2018.

[26] Y. Mizuno et al, "Propagation mechanism of polymer optical fiber fuse" *Scientific Reports*, vol. 4, no. 4800, 2014.

[27] Y. Mizuno et al, "Observation of polymer optical fiber fuse," *Applied Physics letters*, vol. 104, no. 4, pp. 1-4, 2014.

[28] C. Vázquez, J. D. López-Cardona, D. S. Montero, I. Pérez, P. C. Lallana and F. M. A. Al-Zubaidi, "Power over Fiber in Radio over Fiber Systems in 5G Scenarios," in *Proc. 21st International Conference on Transparent Optical Networks (ICTON)*, pp. 1-4, Angers, France, 2019.

[29] C. Vázquez, D. S. Montero, P. J. Pinzón, J. D. López-Cardona, P. Contreras, and A. Tapetado, "Integration of power over fiber on RoF systems in different scenarios,*"* in *Proc. of SPIE (Broadband Access Communication Technologies),* 2017.

[30] Fahad M. A. Al-Zubaidi, D. S. Montero, C. Vázquez and P. J. Pinzón,,"Noise analysis and Multi-Gbit/s transmission in PoF scenarios over SI-POF," in *Proc. of XI Spanish Optoelectronics Meeting (OPTOEL),* Zaragoza, Spain*,* 2019.

[31] Fahad M. A. Al-Zubaidi, D. S. Montero, A. Lopez, J. Zubia and C. Vázquez, "Investigation of power over fiber impact on gigabit data transmission in SI-POF," in *Proc. of International Conference on Plastic Optical Fiber,* Yokohama, Japan, 2019.

[32] V. Sharma, U. Mukherji, V. Joseph, and S. Gupta, "Optimal energy management policies for energy harvesting sensor nodes*"* *IEEE Transactions Wireless Communication*, vol. 9, no. 4, pp. 1326–1336, Apr. 2010.

[33] X. Liu, X. Wei, L. Guo, Y. Liu, Q. Song, and A. Jamalipour, "Turning the signal interference into benefits: Towards indoor self-powered visible light communication for IoT devices in industrial radio-hostile environments," *IEEE Access*, vol. 7, pp. 24978-24989, 2019.

[34] G. Pan, J. Ye, and Z. Ding, "Secure hybrid VLC-RF systems with light energy harvesting," *IEEE Transactions Commun*ication, vol. 65, no. 10, pp. 4348–4359, Oct. 2017.

[35] S. Chalasani and J. M. Conrad, ''A survey of energy harvesting sources for embedded systems,'' *in Proc. IEEE SoutheastCon*, pp. 442–447, 2008.

[36] F. Akhtar and M. H. Rehmani, ''Energy replenishment using renewable and traditional energy resources for sustainable wireless sensor networks: A review,'' *Renewable and Sustainable Energy Review*, vol. 45, pp. 769–784, May 2014.

[37] Ottman G K, Hofmann H F, Bhatt A C, and Lesieutre G A "Adaptive piezoelectric energy harvesting circuit for wireless remote power supply," *IEEE Transactions Power Electronics*, vol. 17, no. 5, pp 669–676, 2002.

[38] A. Saffari, M. Hessar, S. Naderiparizi and J. R. Smith, "Battery-Free Wireless Video Streaming Camera System," *in Proc. IEEE International Conference on RFID*, pp. 1-8, Phoenix, AZ, USA, 2019.

[39] D. Tokmakov, S. Asenov, and S. Dimitrov, "Research and development of ultra-low power LoraWan sensor node," *in Proc. IEEE XXVIII International Scientific Conference Electronics (ET),* pp. 1-4, Bulgaria, 2019.

[40] J. Lee, Y. Su, and C. Shen, "A Comparative Study of Wireless Protocols: Bluetooth, UWB, ZigBee, and Wi-Fi," in *Proc. 33rd Annual Conference of the IEEE Industrial Electronics Society (IECON),* Taipei, November 2007.

[41] A. Nikoukar, S. Raza, A. Poole, M. Güneş and B. Dezfouli, "Low-Power Wireless for the Internet of Things: Standards and Applications," *IEEE Access*, vol. 6, pp. 67893-67926, 2018.

[42] P. Wang, C. Zhang, H. Yang, D. Bharadia, and P. Mercier, "A 28μW IoT Tag that can communicate with commodity WiFi transceivers via a Single-Side-Band QPSK backscatter communication technique," in *Proc. of ISSCC Conference, San Francisco,* Feb. 2020.

[43] F. Forni, Y. Shi, N. C. Tran, H. P. A. van den Boom, E. Tangdiongga, and A. M. J. Koonen, "Multiformat wired and wireless signals over large-core plastic fibers for in-home network," *Journal of Lightwave Technology,* vol. 36, no. 16, pp. 3444-3452, 15 Aug.15, 2018.

[44] S. Mondal and R. Paily, "On-Chip photovoltaic power harvesting system with low-overhead adaptive MPPT for IoT nodes," *IEEE Internet of Things Journal,* vol. 4, no. 5, pp. 1624-1633, Oct. 2017.

[45] R. Dahlgren, "Noise in Fiber Optic Communication Links," *Technical Report*, SVPhotonics, 2000. Available Online, Accessed on 2019: http://www.svphotonics.com/pub/pub029.pdf

[46] A. D. Ellis, M. E. McCarthy, M. A. Z. Al Khateeb, M. Sorokina, and N. J. Doran, "Performance limits in optical communications due to fiber nonlinearity," *Advances in Optics and Photonics*, no. 9, pp. 429-503, 2017.

[47] P. J. Pinzón, I. Pérez, and C. Vázquez, "Visible WDM system for Real Time Multi-Gbit/s bidirectional transmission over 50m SI-POF," *IEEE Photonics Technology Letters*, vol. 28, no. 15, pp. 1696-1699, 2015.

[48] Knowledge Development for POF (KDPOF). "Simple introduction to gigabit communications over POF," Available online: http://www.kdpof.com/wp-content/uploads/2012/07/Easy-Introduction-v1.1.pdf, accessed Jan. 15, 2016.

[49] E. J. H. Skjølstrup and T. Søndergaard, "Design and optimization of spectral beamsplitter for hybrid thermoelectric-photovoltaic concentrated solar energy devices," *Solar Energy*, vol. 139, pp. 149–156, 2016.

[50] P. J. Pinzón, "Birefringent and diffractive devices for implementing MultiGbit/s transmission systems using visible WDM over SI-POF technology," *doctoral thesis*, Universidad Carlos III de Madrid, Spain, 2015.

[51] P. J. Pinzón, J. Moreno, and C. Vázquez, "Energy efficiency of a WDM link at Multi-Gbit/s over plastic optical fiber," in *Proc. of XXXI National Symposium of the International Scientific Radio Union (URSI), Madrid,* 2016.

[52] K. Bhowmik and Gang-Ding Peng, "Polymer Optical Fiber," book chapter, March, 2019.

[53] A. D. Alobaidani, D. Furniss, M. S. Johnson A. Endruweit and A.B. Seddon, "Optical transmission of PMMA optical fibres exposed to high intensity UVA and visible blue light," *Optics and Laser for Engineering,* vol. 48, pp. 575-582, 2010.

Chapter 3:

Analysis of the Impact of Non-linear effects on the HPL System Efficiency for MCF and SMF

Chapter Three discusses the potential of using Power-over-Fiber (PoF) technology in optical access networks. We analyze the limits of the power delivery in PoF systems. An extensive simulation study is presented to analyze different design parameters including the High Power Laser (HPL) source parameters and fiber non-linearities. The analysis includes a comparison between the both powering architectures, shared and dedicated, for various types of optical fibers. The power levels that can be delivered for powering purposes without any degradation due to fiber nonlinear effects are addressed. Finally, the chapter revises the impact of PoF transmission in data signal quality because of these effects in terms of Bit Error Rate (BER) penalty.

3.1. INTRODUCTION

Power over fiber (PoF) starts to be seen as an attractive technology that can be used to supply energy in different applications including sensing and communication. Due to various advantages as mentioned in **Chapter one**, this technology can be applied in different hazardous and noisy environments [1-2].

One of the key features for this technology is the small attenuation of optical fibers being <0.2 dB/km for the standard single mode fiber (SMF) currently installed, including in access networks. The three basic components of any PoF system are High Power Laser (HPL) source, optical fiber and photovoltaic cells (PV), respectively. More recently, inexpensive HPL sources become commercially available while the works towards higher conversion efficiency for PV cells are in progress.

Efficient fiber media is very important in PoF systems. For longer distances to achieve optically powered networks, SMFs working in the third window, are preferred over Multi-Mode Fibers (MMF) due to the higher attenuation of the latter being of around 3 dB/km at 850 nm. In recent years and with research focus on developing energy efficient networks with low power consumption components, a new niche for PoF technology appears. Utilizing the currently installed SMF to integrate PoF can save costs and provide more reliability for the designed systems.

However, one of the limiting factors is the small core area of the fiber which limits the maximum power that can be injected. As very high power level can damage the fiber, there is a fiber damage power intensity threshold [3] of around 2.5 MW/cm^2. However still acceptable power levels can be delivered at the remote site using SMF. For example, 3.5 W of optical power is delivered [4] using 5 km of SMF. The delivered power level is strongly dependent on the power consumption for the devices to be powered. Apart from the damage power intensity, non-linear fiber effect is become of great interest if high power levels are injected to this small core area. Generally, after losses due to fiber attenuation, Stimulated Brillouin Scattering (SBS) and Stimulated Raman Scattering (SRS) become the most limiting factors that can cause losses in the PoF transmitted power [4].

Identifying the power limits in PoF systems due to these effects not only depend on the fiber diameter or design parameters but also on some additional PoF system parameters. In order to design an optical power delivery system with a good performance, we analyse the impact that these nonlinear effects can cause and degrade such systems. This can help for proper choice of HPL source for PoF system, the limits of powers that can be transmitted and also to properly design the adequate transmission distances.

On the other hand, the integration of silica multicore fibers (MCF) for future front-haul technologies can build flexible mobile networks. In some proposals of future 5G front-haul

architectures with Software Defined Network (SDN) capabilities, PoF is also integrated considering the use of MCF [5]. Also for the rapid increase of demand for high data rates, Space division multiplexing (SDM) is proposed to meet this requirement and to increase network capacity. MCF is found as optimal solution to adopt SDM technology [6-7]. As with the next generation 5G radio access networks (RAN), low power consumption Remote Radio Units (RRU) can be installed due to integration of different technology like Radio over Fiber (RoF) so PoF can replace the usual electric power supplies in specific cases to save cost and space or when the existence of such electric sources are not recommended [2].

The combination of PoF and MCF to integrate centralized RAN (C-RAN) can add more flexibility to the network. Fig. 3.1 shows a schematic diagram for future cellular networks that uses a MCF-based PoF configuration that can be utilized to integrate different technologies like Fiber-to-the-Home (FTTH) and also Passive Optical Networks (PON). MCF can also add more reliability to cope with large number of RRU to be installed in the future to support high data rate of 5G. The schematic is also valid considering bundles of SMFs instead of MCF.

Exploiting PoF in PON networks can solve the complexity with the network architectures due to this increased number of RRU and also save installation costs as one optical fiber which is used to connect the central office (CO) to different RRUs is used as powering line [8]. Of course, some additional passive components will be required like optical splitters to deliver power from that fiber to multiple RRUs. Such network topologies will eliminate the use of batteries at the remote site [9]. In [10], PoF technique is used to feed PON extenders based on semiconductor optical amplifiers (SOA) and turning them all to passive mode compared to conventional powering techniques.

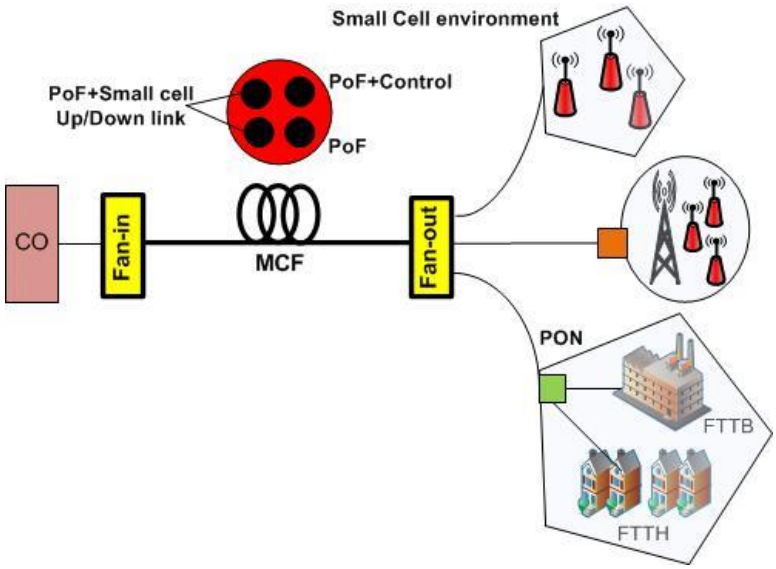

Fig. 3.1: MCF based PoF configuration considered for future cellular networks.

From Fig. 3.1 we can also see that different powering scenarios can be applied. These scenarios are 'shared cores/fiber scenario' where all or some individual cores of MCF (or each or all fibers of the bundle of fibers) transmit simultaneously data and PoF signals and 'dedicated cores/fibers scenario' where some cores (or fibers) are used only for PoF transmission. Due to the small core area in most MCFs and SMFs, analysing the power limit in these fibers due to non-linear effect is of major interest too to decide the proper powering scenario. The crosstalk between adjacent cores in high power levels in MCFs can have its impact too [3]. However, in link lengths < 10 km the crosstalk can be negligible (< -50 dB). Hence in this chapter we firstly address the limit in the PoF system efficiency due to non-linear effects, and then explore the potential of PoF delivery in different powering scenarios and compare between both of them in terms of power levels and the number of devices that can be powered. It also addresses the data transmission quality due to this high optical power transmission. Different powering configuration are proposed using different fibers including SMF and MCF. The chapter investigates the maximum link length that can be used in mobile front-hauling with negligible impact of non-linear effects. For that, a deep analysis is performed using the VPI Photonics^{TM} virtual photonic instrumentation software tool. Table 3.1 shows the different fibers consider for the analysis in this chapter.

Table 3.1
Fibers specifications

Fiber	A_{eff} (μm^2) each core/fiber
SMF	80
4-MCF	50.6
7-MCF*	27
7-MCF	75

Throughout this chapter, MCF with 7 cores with an effective area of 27 μm^2 in each core is written as 7-MCF* to be recognized from other MCFs with 7 cores and other effective areas.

3.2 Impact of Fiber Non-linear Effects on Power Delivery

In this section a detailed analysis of Stimulated Brillouin Scattering (SBS) and Stimulated Raman Scattering (SRS) induced losses in PoF systems is presented. The analysis is based on simulations in VPI software tool. The simulation setup used is shown in Fig. 3.2 where HPL at 1480 nm is considered as the PoF source. The WDM source is used to generate data signals at the C-band for simulating a shared power scenario. Both data and power are multiplexed by using a MUX, and then injected in the fiber. After transmission, a Fiber Bragg Grating (FBG) filter is used to separate HPL and data signals (specifically in the shared scenario). In order to simulate the impact on different fibers as those proposed in Table 3.1, parameters such as the core area and Raman gain files are varied depending on the fiber under test. Generally, we use the universal fiber module which can be used to simulate wideband

non-linear signal transmission for silica fibers, mainly SMF. However, for the case of MCF, the fiber module is considered for simulating each individual core of a specific MCF. This is done by modelling the fiber with a new Raman gain curve of silica fibers considering the new effective area of the targeted MCF. This effective area varies to model the different MCFs mentioned in Table 3.1. For that, it is worth mentioning that the crosstalk effect is not considered for MCF with this fiber module. This is the case for all MCF simulation results presented in this chapter. This fiber module also allows bidirectional signal analysis that is present in many applications such as WDM systems and discrete Raman amplifiers. However, this model has some limitations for direct solutions of the bidirectional Nonlinear Schördinger equations (NLSE) due to the required computation time and excessive memory. VPI software considers some assumptions to simplify the interaction of counter-propagating waves. Some effects are neglected in the opposite direction such as dynamic effects, Fabry-Perot resonance and Four Wave Mixing (FWM). So that counter-propagating waves are restricted only to time averaged powers. Power meters are placed at different stages in the simulation setup in order to monitor the power levels. The used power meter is the (PowerMeterVPA) module that displays the optical power of the input signal. It includes options to decide the output signal units and also to decide the central frequency and the bandwidth in which to measure the power at a specific frequency band. So that the different power meters used in the simulation are set with different center frequency and bandwidth depending on the needs. These power meters are used specifically to measure the delivered PoF levels after fiber transmission (at 1480 nm), the Received Optical Power (ROP) for data signals at C- band region (at 1550 nm) and also backscattered power.

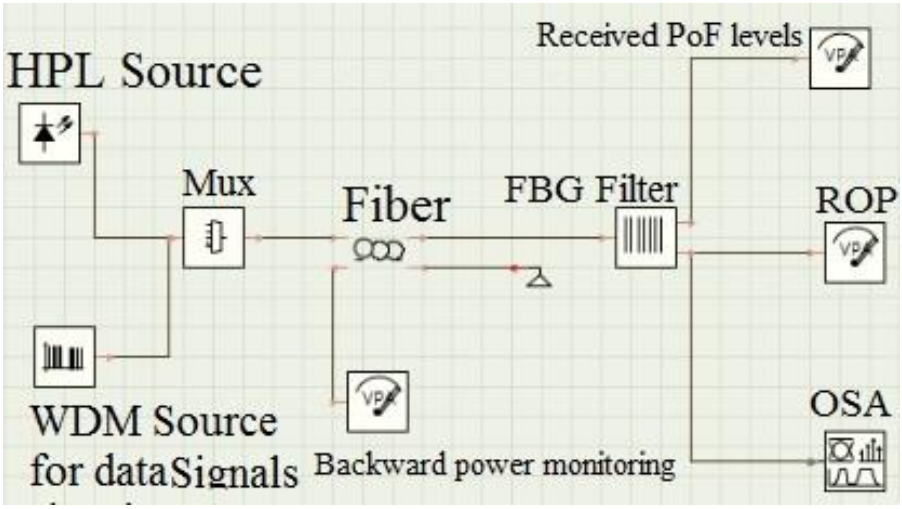

Fig. 3.2: Schematic diagram of the simulation setup used for the analysis of fiber non-linear effects.

In the next subsection, a brief theoretical background for each effect (SBS and SRS) is described. Then simulation results are shown and discussed for shared and dedicated PoF scenarios. In terms of methodology firstly, the impact of each effect (SBS and SRS) is studied

separately to address their specific influence accurately. So that in Section 3.2.1 when SBS impact is analyzed, SRS is not activated in all cases and vice versa in Section 3.3.3 for SRS impact analysis.

3.2.1 Stimulated Brillouin Scattering

In this section, we investigate the limits in the PoF systems in SMF and MCFs chosen above due to SBS effect. Generally, this effect depends on the linewidth of HPL source for PoF system. Fiber parameters such as effective area (A_{eff}) and link length can have its impact too. Optimizing all these parameters can help in choosing the proper HPL source depending on the required delivered energy at the remote side.
The threshold power of SBS is given by [4]:

$$P_{th\_SBS} = \frac{\triangle \nu_B + \triangle \nu_P}{\triangle \nu_B} \frac{21\, K\, A_{eff}}{g_{B0}\, L_{eff}} \tag{3.1}$$

where $\triangle \upsilon_B$ is the Brillouin gain bandwidth, $\triangle \upsilon_P$ is the HPL source linewidth, k is a polarization factor (for silica k=2), A_{eff} is the effective area of the fiber, g_{B0} is Brillouin gain coefficient and L_{eff} is the effective transmission distance for this threshold power and it is given by [3]:

$$L_{eff} = \frac{1-\exp(-\alpha L)}{\alpha} \tag{3.2}$$

where α is the attenuation loss.

Hence in the following, different simulation cases are performed using the simulation setup shown in Fig. 3.2 in order to investigate the SBS impact on the performance of PoF systems. HPL source at 1480 nm is used for the analysis as this wavelength will be experimentally used later in this thesis (**Chapter Five**) as the PoF source for the different testbeds. The different fiber types described in Table 3.1 are simulated. Different HPL output power levels and linewidths are considered in order to choose the proper HPL parameters and for different link lengths. In all cases, the Brillouin gain parameter is set to 6×10^{-11} m/W while the Brillouin gain bandwidth is set to 35 MHz. The output power after fiber transmission is used to evaluate system performance and SBS impact.

Firstly, SMF is simulated. Different HPL linewidths are considered for different power levels and transmission distances. First in Fig. 3.3, 10 km is simulated with input power levels up to 3 W; it is clearly seen the SBS impact for small HPL linewidths as in the case of 1 GHz and 500 MHz as degradation due to SBS is resulted even at small input powers. For 100 GHz there is no degradation due to SBS and power loss is mainly caused by fiber attenuation, which is represented by dot lines in Fig. 3.3 too. As aforementioned, the attenuation loss (α) is set to 0.2 dB/km in all cases. For 3 W input optical power, the penalty of PoF channel at

remote the site for the case of 100 GHz is 40% (caused only by attenuation) while losses are increased to 71.67% and 80% for 1 GHz and 500 MHz linewidths respectively (caused by attenuation and SBS).

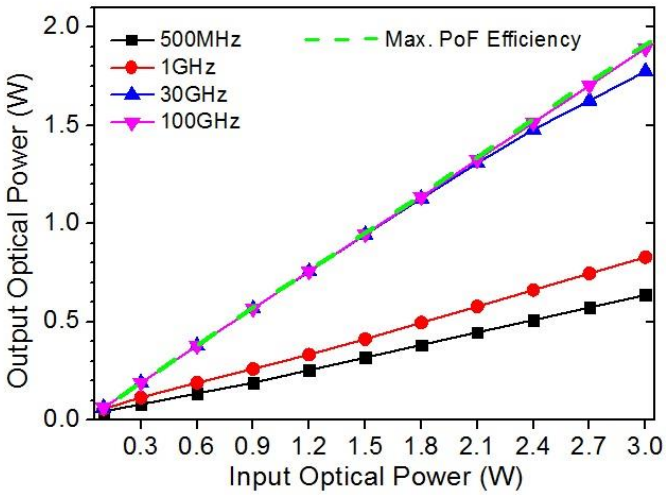

Fig. 3.3: Output power vs. input power for PoF channel at 1480 nm for different HPL source linewidth to investigate SBS impact for 10 km of SMF. α = 0.2 dB/km, SRS OFF.

For higher input power levels up to 5 W, 100 GHz HPL linewidth is still quite enough to suppress SBS impact as shown in Fig. 3.4 for 5 km link length of SMF. Also small HPL linewidths still induce huge penalty in the delivered power due to SBS. As an example only 36% of the input power will reach the load located 5 km away, if a 5 W HPL with 1 GHz linewidth is used. For 5 W input optical power, the penalty in the output optical power in the case of 100 GHz is 20% (caused by attenuation only) while its increased for example in the case of 1 GHz to 64% (caused by attenuation and SBS).

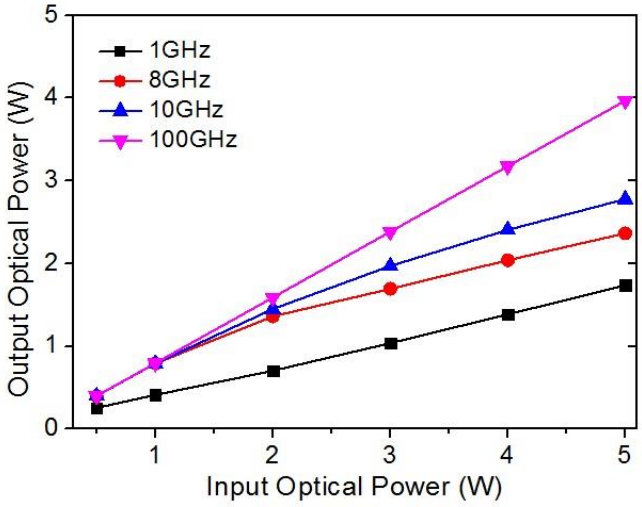

Fig. 3.4: Output power vs. input power for PoF channel at 1480 nm for different HPL source linewidth to investigate SBS impact for 5 km of SMF. α = 0.2 dB/km, SRS OFF.

For 1 km of SMF, SBS impact can be suppressed even with 8 GHz of HPL linewidth and with input power levels of 5 W as shown in Fig. 3.5. At 1 GHz, 2 W of input power is possible with small degradation due to SBS. For example, the penalty in the output power when the injected power is set to 5 W is 40% compared to 64% in the case of 5 km simulated above.

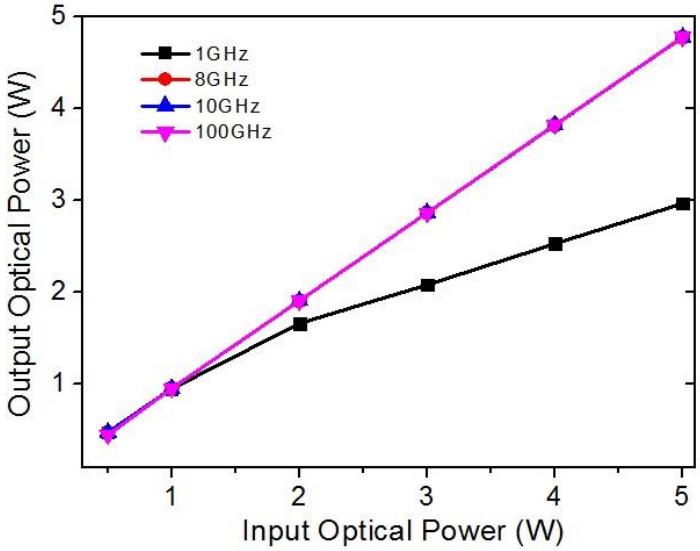

Fig. 3.5: Output power vs. input power for PoF channel at 1480 nm for different HPL source linewidth to investigate SBS impact for 1 km of SMF. α = 0.2 dB/km, SRS OFF.

Some simulations are performed for different MCFs to investigate SBS impact as shown in Fig. 3.6 where 5 km of 2 MCFs are simulated, 4-MCF (A_{eff} of 50.6 μm^2) and 7-MCF* (A_{eff} of 27 μm^2) for 50 and 100 GHz HPL linewidths. The attenuation loss is set to 0.2 dB/km in both cases. As in the case of SMF, for 4-MCF 100 GHz linewidth can be enough to eleminate any impact due to SBS up to 3 W. However in the case of 7-MCF there is a small degradation at 3 W of input power. This degradation is increased when linewidth is reduced to 50 GHz.

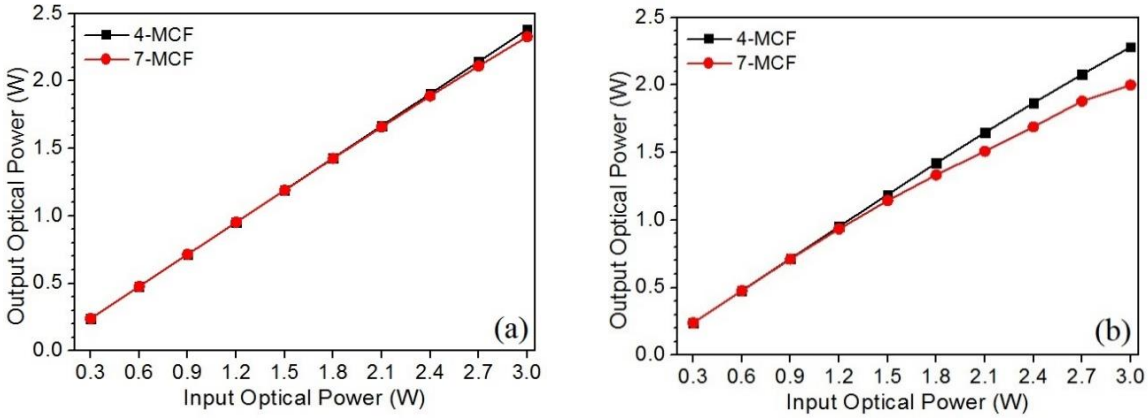

Fig. 3.6: Output power vs. input power for PoF channel at 1480 nm for different HPL source linewidth to investigate SBS impact for 5 km of 4-MCF (A_{eff} of 50.6 μm^2) and 7-MCF (A_{eff} of 27 μm^2). (a) 100 GHz (b) 50 GHz. α = 0.2 dB/km, SRS OFF.

3.2.2 Stimulated Raman Scattering

This section investigates the limits in the optical power delivery of PoF system due to SRS effect. After using proper laser bandwidth for HPL sources in order to suppress SBS impact, transmission loss and SRS effect become the most limiting parameters for the efficiency of PoF system. The threshold power for SRS effect can be given by [4]:

$$P_{th\_SRS} = \frac{16\, A_{eff}}{g_R\, L_{eff}} \tag{3.3}$$

where, A_{eff} is the effective area of the fiber, g_R is the Raman gain coefficient and L_{eff} is the effective transmission distance for this threshold power and as given in eq. (3.2).

SRS effect in optical fibers have been widely discussed in the literature [11] as it represents the basic principle of a very important kind of optical amplifiers, namely Raman Amplifier. Many proposals have discussed and showed the important role that this kind of amplification can play in optical communication systems [12-14]. Generally, power transfer from higher to smaller frequencies is expected due to Raman amplification and the related frequency shift. Raman gain has triangular shape in silica fibers and can have its peak at 13 THz of frequency difference between two transmitted signals in the fiber [15]. Apart from the frequency difference, this is also depending on other parameters as shown in the above equations. For that and due to the frequency difference between the considered PoF sources in this study at 1480 nm (202.70 THz) with C-band frequencies (193.5 THz) for data transmission, it is of prime importance to analyze power degradation in PoF channel or the amount of power transferred to C-band because of this phenomenon.

The same simulation setup described at the beginning of section 3.2 and as shown in Fig. 3.2 is used to investigate the SRS effect. The different fibers that were described in Table 3.1 are also considered for the simulation. Both scenarios are simulated separately. First, we show the results for the dedicated scenario, then for the shared one and finally we simulate the impact for PoF on data signal quality by measuring the BER for the simultaneous transmission with the modulated signals.

As we have mentioned before, Universal fiber module is used in all cases to simulate SRS impact. Firstly, the curve for Raman gain coefficient (g_R) is shown in Fig. 3.7 which is used for Raman gain file located in VPI software tool. In order to simulate all fibers mentioned in Table 3.1, the Raman gain curve is obtained for all these fibers by dividing g_R by the effective core area of each fiber. The different Raman gain profiles used in the simulation are shown in Fig. 3.8 where the effect of decreasing the effective core area is clearly seen. However, it also shows that the differences between SMF and 7-MCF can be negligible.

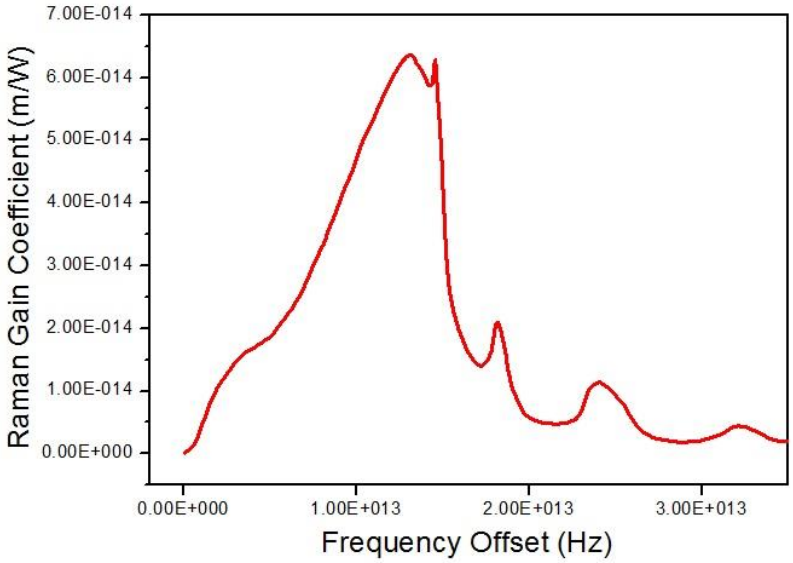

Fig. 3.7: Raman gain coefficient used in the simulation (g_R).

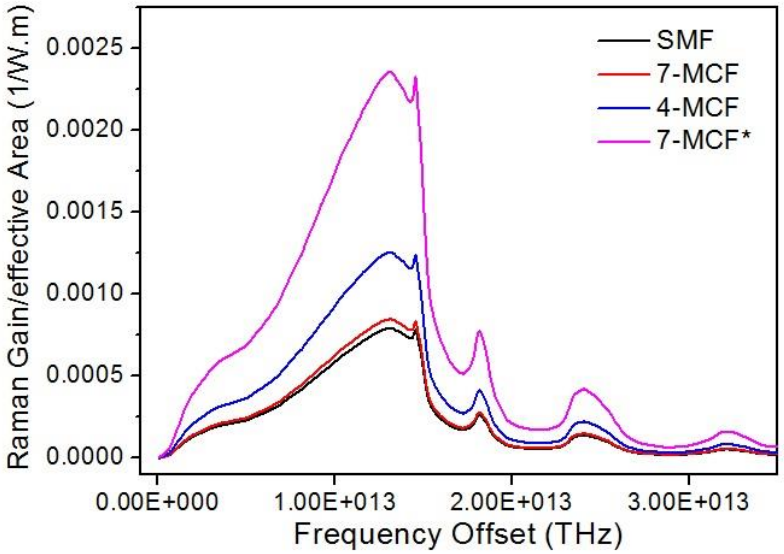

Fig. 3.8: Raman gain curves used in the simulation for the different fiber mentioned in Table 3.1.

3.2.2.1 Dedicated Scenario

Here we show the impact of SRS on the power delivery efficiency for the fiber types stated in Table 3.1. The attenuation loss is set to 0.2 dB/km in all cases. We first simulate SMF for different link lengths up to 20 km and HPL up to 2 W. The linewidth of HPL is set to 100 GHz to avoid any influence of SBS as previously discussed. From the results shown in Fig. 3.9, total optical power of 0.8 W is delivered at remote site for 20 km distance and 2 W HPL input power. This power is increased to 1.25 W for 10 km distance. The results show almost

no power degradation due to SRS. The penalty for 10 km and 20 km are 37.5% and 60.5% respectively for 2 W HPL input power.

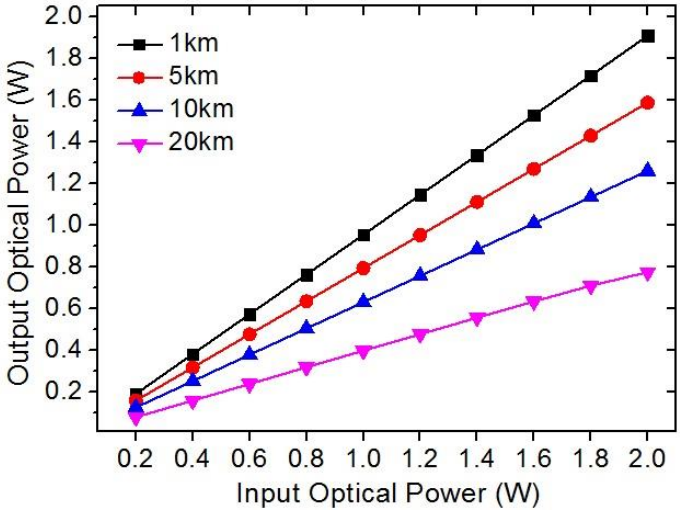

Fig. 3.9: PoF channel output power vs input power at 1480 nm for different SMF link lengths in the dedicated scenario, and including the SRS effect in the simulations. α = 0.2 dB/km.

Initially in the dedicated scenario, no filter or Demux devices are needed after fiber transmission, thus the FBG filter is used to monitor the amount of scattered power at 1550 nm when no data channel is transmitted. The results are shown in Fig. 3.10 a where this power is linearly increased with HPL input power increased. However, the power level is very low; being the highest –13 dBm for 10 km while for 20 km is increased up to 0 dBm (1 mW) for a HPL input level of 2 W. Fig. 3.10 b shows the SRS backscattered power for 20 km and 10 km. There is an increment from – 0.02 dBm in the case of 10 km to around +16 dBm for 20 km.

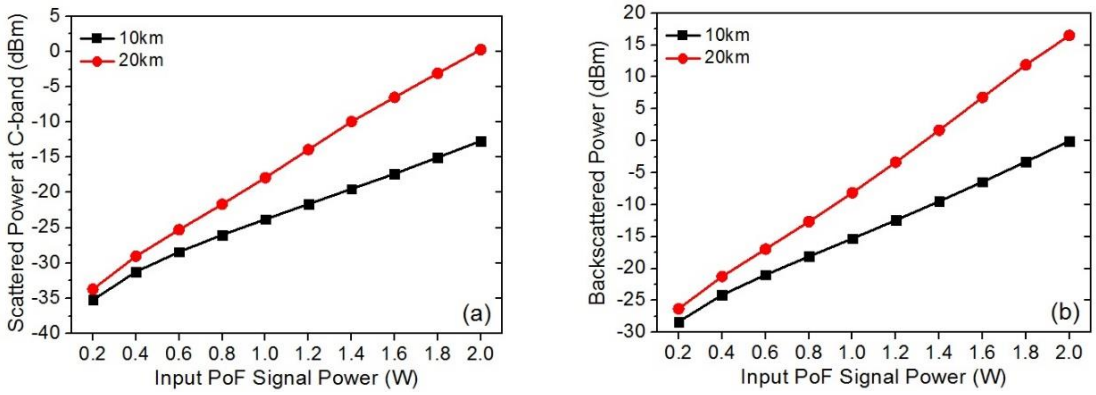

Fig. 3.10: Scattered power at 1550 nm vs. HPL input power at 1480 nm, for 10 km and 20 km SMF (a) Forward (b) Backwards. SRS effect in dedicated scenario. α = 0.2 dB/km.

From the last two figures, we can conclude that SMF can provide an efficient solution for power delivery in a dedicated scenario up to 2 W.

As in the case of SBS analysis, three types of MCFs are simulated. First 7-MCF with each individual core having an A_{eff} of 75 μm^2. As the core area for this fiber is close for the simulated SMF in the first case, the results are almost the same for 1, 5 and 10 km as shown in Fig. 3.11. For 20 km there is a very small degradation compared to SMF when HPL input is set to 2 W; as the penalty increased to around 64% compared to 60.5% in the case of SMF.

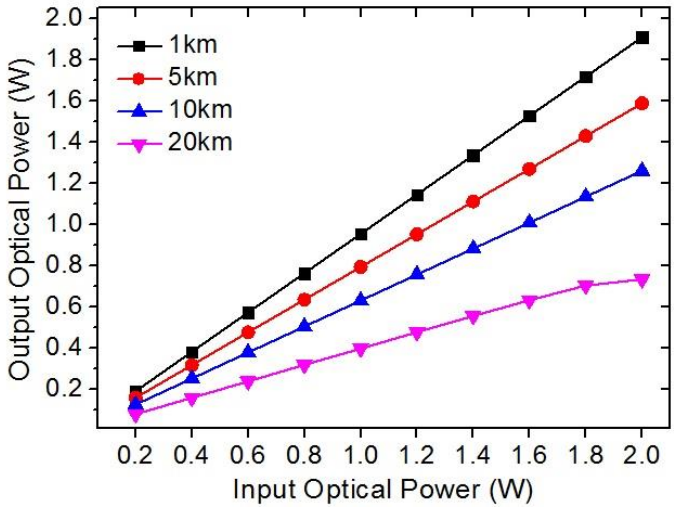

Fig. 3.11: Output power vs. input power for PoF channel at 1480 nm for different link lengths of 7-MCF (A_{eff} of 75 $\mu m^{2)}$ for the dedicated scenario considering SRS effect, α = 0.2 dB/km.

For 4-MCF, almost the same results are obtained as in the case of SMF and 7-MCF up to 10 km as shown in Fig 3.12.

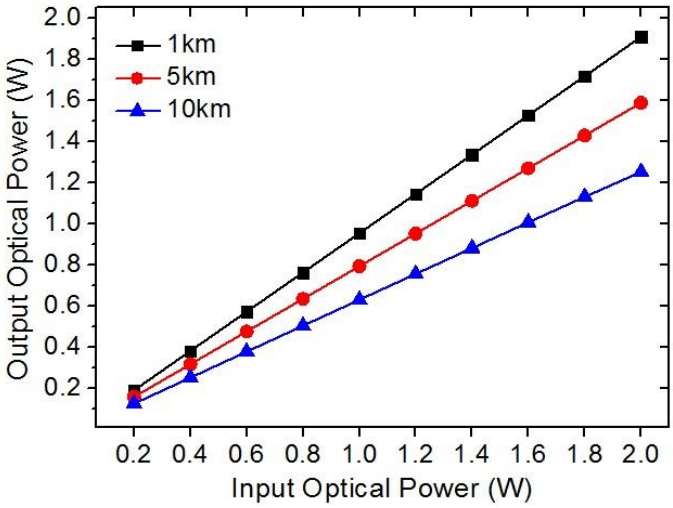

Fig. 3.12 output power vs. input power for PoF channel at 1480 nm for different link lengths of 4-MCF. (A_{eff} of 50.6 $\mu m^{2)}$ for the dedicated scenario considering SRS effect, α = 0.2 dB/km.

However, this is not the case for 7-MCF* with A_{eff} of 27 μm^2 especially for long link lengths as the maximum possible input power in the case of 10 km is limited to 1.4 W, with resulted in an output power of 0.78 W as shown in Fig 3.13.

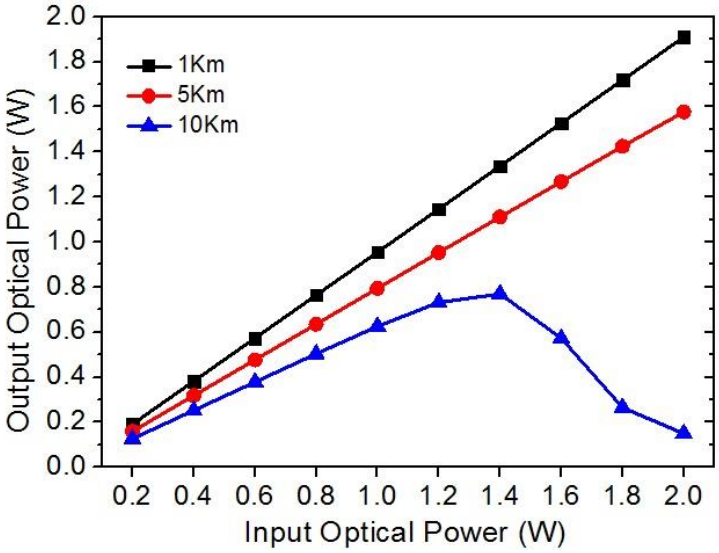

Fig. 3.13 Input power vs. output power for PoF channel at 1480 nm for different link lengths of 7-MCF* (A_{eff} of 27 $\mu m^{2)}$ for the dedicated scenario considering SRS effect, α = 0.2 dB/km.

More simulations are performed for the case of 7-MCF* with 10 km transmission distance to check scattered powers both at the forward direction within C-band and in the backward direction due to SRS. The results in Fig. 3.14 for both powers clarify that most of the power is backscattered. This can be expected due to the very small core area of the fiber and because the 1480 nm channel is transmitted alone with no signal transmission in the C-band. However, there is part of the input power scattered at the C-band, around +9 dBm when launching 2 W of HPL output power. This is quite high compared to the case of SMF for the same transmission distance, being around – 12.5 dBm (see Fig. 3.10 a).

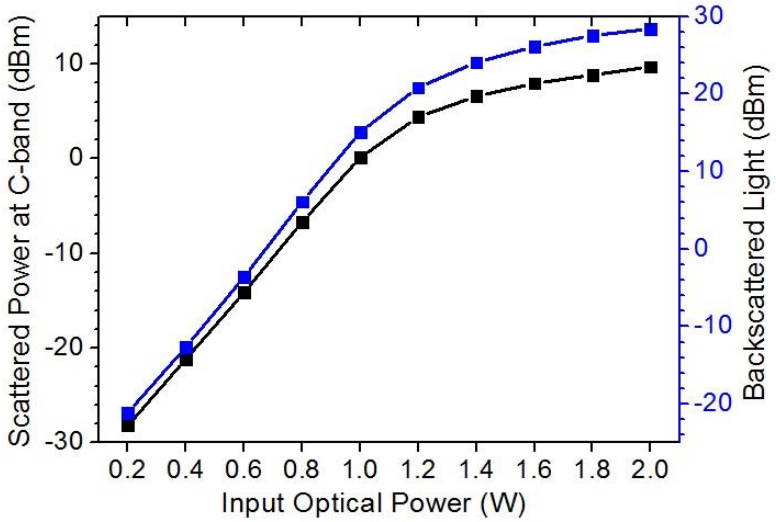

Fig. 3.14 Scattered power at C-band and backscattered power vs. input optical power from 1480 nm channel for 10 km of 7-MCF* in the dedicated scenario.

3.2.2.2 Shared Scenario

In this subsection, we analyze the impact of SRS on power delivery efficiency in the shared scenario. As in the previous subsection, the simulation setup in Fig. 3.2 is considered, but this time, we activate the WDM source to generate data signals at C-band. HPL source with a maximum power of 2 W is considered too. SRS can be more dominant in the shared scenario compared to the dedicated one. This simultaneous transmission not only affects the delivered energy in the remote site, but can also have impact on the data signal quality. So first in this section, we address the power levels that can be delivered and in the next section, we analyze its impact on the data signal quality.

The four types of fibers (see Table 3.1) are initially considered. However, as for 7-MCF with A_{eff} of 75 μm^2, we expect the same results of SMF, this fiber is not finally considered here. In Fig.3.15, the results are shown for SMF for two links lengths, 10 km and 20 km for simultaneous transmission with a single data channel at 1550 nm. As shown in the figure for 10 km, the response is linear and the losses are due to the fiber attenuation, which is set in all cases to 0.2 dB/km. This will also be the case for the other links lengths shorter than 10 km. For 20 km, the power degradation started with HPL input of 1.8 W, this is not the case as compared with the dedicated scenario (see Fig. 3.9). We compared that with the maximum PoF efficiency at 20 km transmission (dashed line) by considering only attenuation losses where the impact of HPL degradation at remote site is mainly due to SRS. The penalty in the PoF channel for 10 and 20 km is 40% and 80.5%, respectively, for 2 W input optical power. This is high in comparison with the case of dedicated scenario with 37.5% and 60.5% for 10 and 20 km respectively.

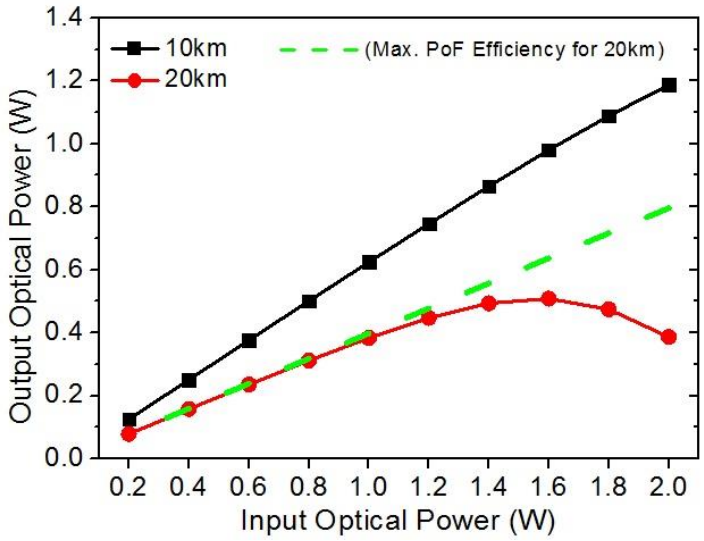

Fig. 3.15: Output power vs. input power for PoF channel at 1480 nm for different link lengths of SMF for shared scenario with a single data channel at 1550 nm, data power: 0 dBm, α = 0.2 dB/km.

In Fig. 3.16, we monitor the scattered power at the C-band and total backscattered power for the different input PoF levels simulated in Fig. 3.15 when SRS is activated. As expected, due

to SRS effect both powers increased as HPL input power is increased. The transferred power to C-band is quite high compared to the dedicated scenario (see Fig. 3.10 a) which is also expected due to the interaction between HPL signal and data signal at 1550 nm. The backscattered power is slightly lower than in the case of dedicated scenario. This also can be due to the simultaneous transmission of HPL signal and data signals as the majority of power will be scattered in the forward direction.

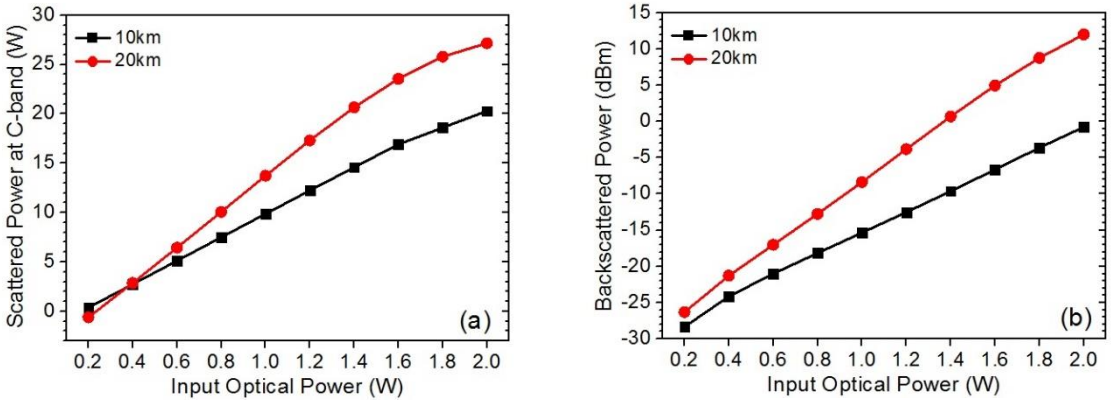

Fig. 3.16: Scattered power at 1550 nm vs. HPL input power at 1480 nm, for 10 km and 20 km SMF (a) Forwards (b) Backwards. SRS effect in shared scenario. α = 0.2 dB/km.

In the following, we show the difference between co-propagating and counter-propagating signals for 10 km SMF, in the case of shared scenario with one data channel. The same simulation setup is used but now by placing HPL source at the end of the link by utilizing the bidirectional analysis feature of the Universal fiber module used. By comparing the scattered power at the forward direction in the C-band from co-propagating (see Fig. 3.16 a) and that resulted from counter-propagating, it is seen that this power is slightly higher in the case of the co-propagating signal case.

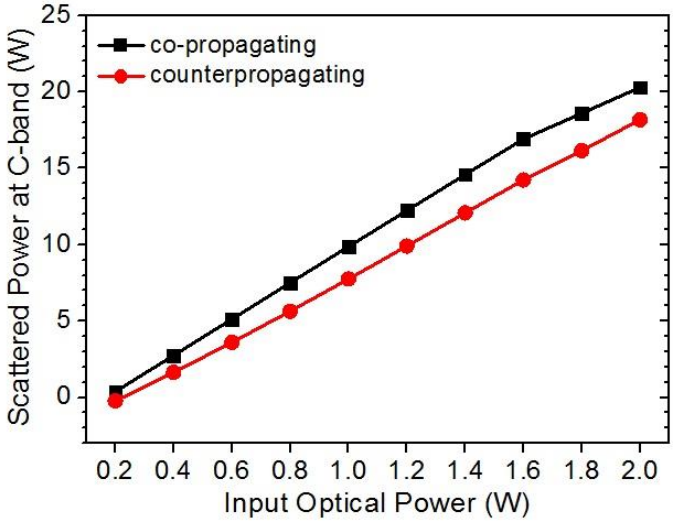

Fig. 3.17: Scattered power at 1550 nm vs. HPL input power at 1480 nm for 10 km SMF for the shared scenario with one data channel considering SRS effect with co-propagating and counter propagating for HPL signal. α = 0.2 dB/km.

To investigate the reason behind this difference we compare the delivered HPL power at 1480 nm for both cases. In the case of counter-propagating it will be the power monitored at the data transmitter site. The results are shown in Fig. 3.18 where counter-propagating delivered energy is slightly higher. This proves that Raman interaction increases in the forward direction.

The counter-propagating analysis is important for powering scenarios when both data signals and PoF signal are transmitted in opposite directions. For example when data are sent back from remote node to the central office while PoF is located in the central office. This scheme can also provide more protection to the photodiode.

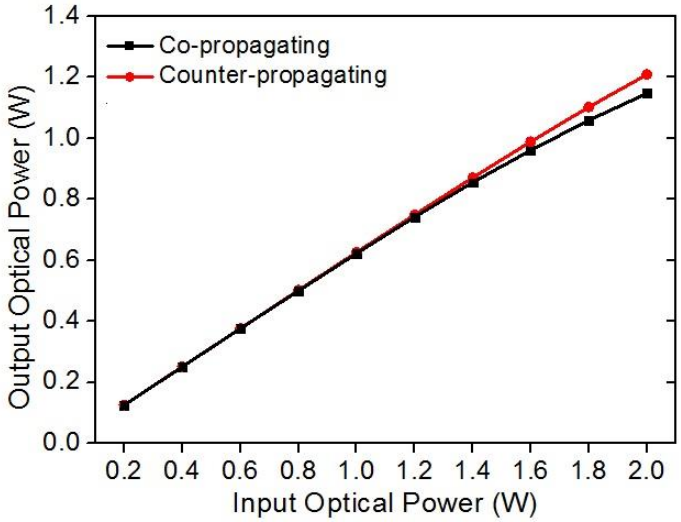

Fig. 3.18: Input power vs. output power for PoF channel at 1480 nm with co-propagating and counter-propagating for 10 km of SMF in the shared scenario with one data channel considering SRS effect, $\alpha = 0.2$ dB/km.

The following results are performed in the forward direction. To investigate the impact of the number of channels in the C-band on the delivered energy at the remote site, two different cases are simulated by using 10 and 25 channels, as shown in Fig. 3.19. Compared with the case of a single data channel as in Fig. 3.15, it is clearly seen that the number of channels can affect the PoF system performance. For example, the total powers at the fiber output after splitting data channels are ~ 1 W and ~ 0.81 W for 10 and 25 channels respectively while it is ~ 1.2 W for a single data channel. For the case of 20 km, the power starts to degrade after 1.2 W and 1.4 W for 10 and 25 channels, respectively. For a single data channel, it is degraded after 1.6 W input power, with a maximum output power of 0.45 W at that specific input power level. The penalty in the PoF channel increases with the number of data channels being around 91% and 97% for 20 km with 2 W input optical power for 10 and 25 data channels, respectively.

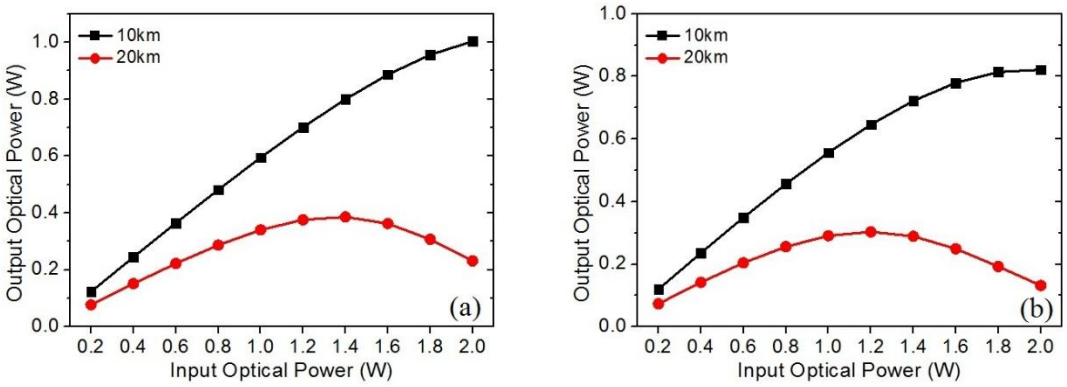

Fig. 3.19: Input power vs. output power for PoF channel at 1480 nm for different link lengths of SMF for shared scenario with C-band channels from 1530 nm to 1550 nm, Single data channel power: 0 dBm, α = 0.2 dB/km. (a) 10 channels with 200 GHz spacing (b) 25 channels with 100 GHz spacing.

In the following, we investigate how the number of channels in the C-band and their frequency difference with HPL wavelength can affect the power delivery performance. This can be useful if optical feeding purposes are considered simultaneously with WDM systems (or even if HPL source is considered for data amplification in long haul links). 25 data channels are considered for a wavelength range from 1530 – 1550 nm with channel spacing of 100 GHz. This is compared with channels in the band (1541-1561 nm). The results are depicted in Fig. 3.20, showing the great impact of considering the frequency difference between HPL wavelength and C-band data channels. For 10 km, working with 25 channels almost near 1550 nm and beyond (1541-1561 nm) makes the maximum input power limited to 1.2 W with output power ~ 0.4 W while for data channels ranging from (1530-1550 nm), there is a maximum output power of 0.81 W which represents twice the value when compared with the other data channels band. For 2 W input optical power, the penalty in the output power is increased from 59.5% in the case of (1530-1550 nm) data channels to 87.5% in the case of (1541-1561 nm) data channels.

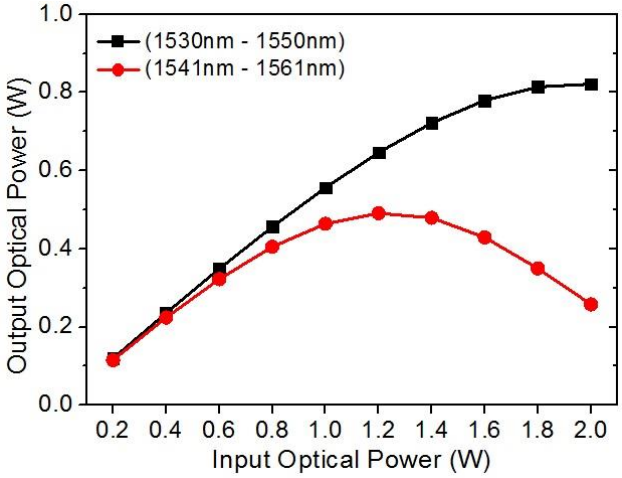

Fig. 3.20: Output power vs. input power for PoF channel at 1480 nm for 10 km of SMF for a shared scenario with 25 data channels at different C-band channels considering SRS effect, α = 0.2 dB/km.

For MCF, we simulate SRS impact in the shared scenario for two fibers, 7-MCF* and 4-MCF. As the small core area can increase fiber non-linear operation regime due to SRS, as shown in eq. 3.3 and Raman gain curves in Fig 3.8, we use the channels in the frequency band from (1530-1550 nm) compared to the case of (1541-1561 nm) as less power degradation due to SRS is expected as we shown above. In this case, the maximum simulated length is 15 km. Firstly, for 4-MCF with A_{eff} of 50.6 μm^2, the results for a single data channel in the shared scenario are shown in Fig. 3.21 for 5, 10 and 15 km. The maximum output power is 0.68 W for 10 km and 0.42 W for 15 km before the power starts to degrade. There is a clear difference in comparison with the case of SMF.

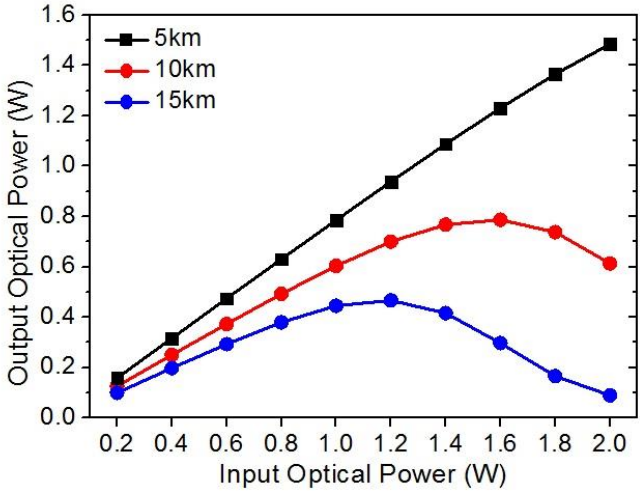

Fig. 3.21: Output power vs. input power for PoF channel at 1480 nm for different link lengths of 4-MCF for shared scenario with one data channel at 1550 nm, data power: 0 dBm, α = 0.2 dB/km.

For 10 data channels, the maximum possible power is reduced to ~ 0.55 W and 0.3 W for 10 km and 15 km respectively, as shown in Fig. 3.22.

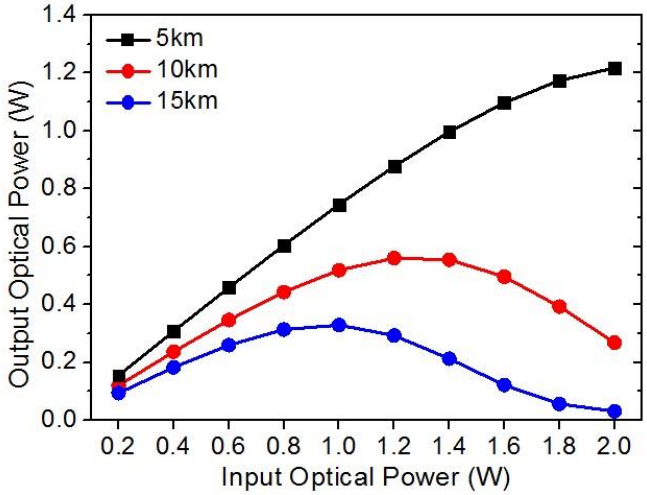

Fig. 3.22: Output power vs. input power for PoF channel at 1480 nm for different link lengths of 4-MCF for a shared scenario with 10 data channels at C-band channels from 1530 nm to 1550 nm with 200 GHz spacing, the input optical power of each data channel is: 0 dBm, α = 0.2 dB/km.

Increasing the data channels up to 25 channels in the same band (1530-1550 nm) leads to an increment of the penalty even in the case of 5 km. The maximum output power being of 0.98 W compared to 1.22 W and 1.55 W in the case of 10 and a single data channels respectively. The results are shown in Fig. 3.23.

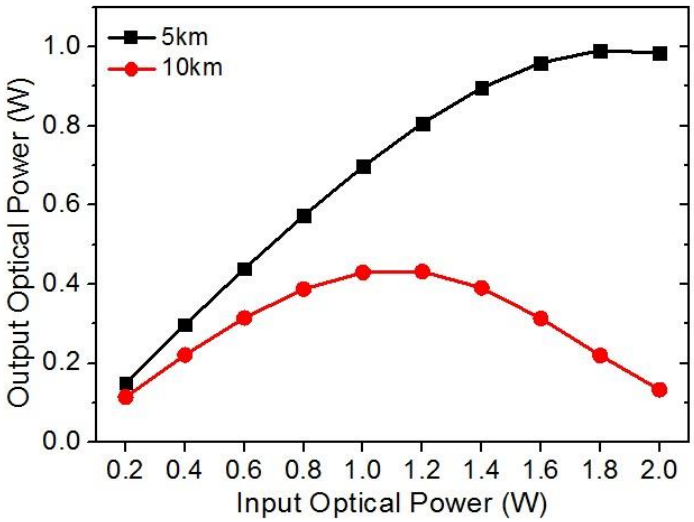

Fig. 3.23: Output power vs. input power for PoF channel at 1480 nm for different link lengths of 4-MCF for a shared scenario with 25 data channels at C-band channels from 1530 nm to 1550 nm with 100 GHz spacing, data power of each channel is 0 dBm, α = 0.2 dB/km.

For 7-MCF* with A_{eff} of 27 μm^2, the results for a single channel and 25 channels are shown in Fig. 3.24 and 3.25 respectively. As with this small core area SRS can mostly degrade the power so shorter distances are simulated too (i.e 1 km). As shown from Fig. 3.19, with one data channel, the SRS can affect even 5 km transmission being 0.82 W the maximum output power. This power is reduced to 0.41 W and 0.2 W for 10 km and 15 km respectively.

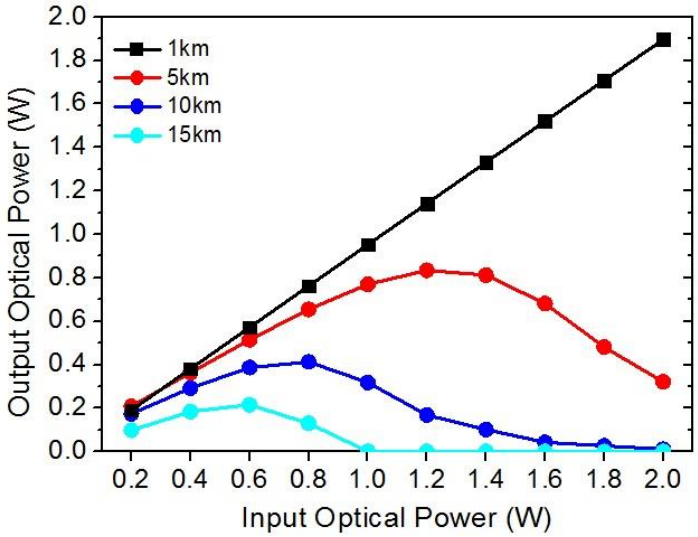

Fig. 3.24: Output power vs. input power for PoF channel at 1480 nm for different link lengths of 7-MCF* for shared scenario with one data channel at 1550 nm, data power: 0 dBm, α = 0.2 dB/km.

For the case of 25 data channels, as shown in Fig. 3.25, the maximum output power is reduced to less than 0.6 W and 0.2 W for 5 km and 10 km respectively.

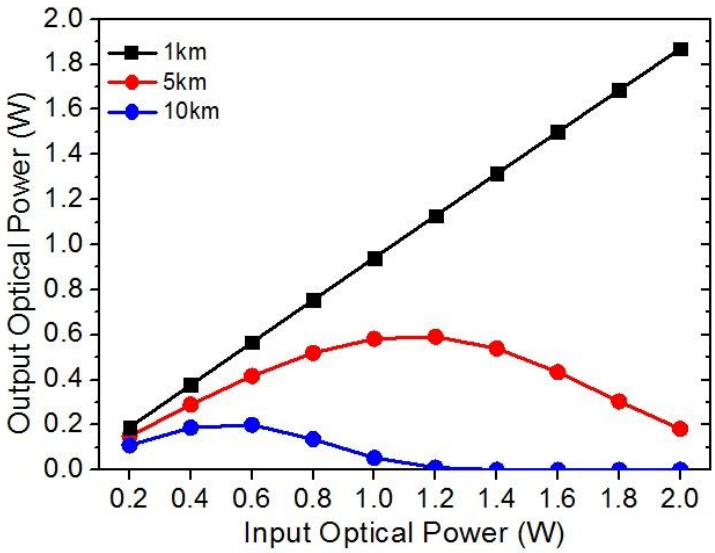

Fig. 3.25: Output power vs. input power for PoF channel at 1480 nm for different link lengths of 7-MCF* for shared scenario with 25 data channels at C-band channels from 1530 nm to 1550 nm with 100 GHz spacing, data power of each channel is: 0 dBm, α = 0.2 dB/km.

Comparing the penalty in the output power for 5 km of 4-MCF and 7-MCF* for 2 W input optical power and 25 data channel transmitted, there is an increment from 52.4% (in the case of 4-MCF) to 90% (in the case of 7-MCF*).

Finally, as we stated before in this section, the most important aspect is to calculate the penalty introduced in PoF channel due to fiber non-linearities as this can degrade PoF system efficiency and to monitor the scattered power in the different directions.

3.2.2.2 Impact of PoF on Data signal quality

When considering simultaneous transmission of data and PoF signals, i.e (shared scenario) one of the most important aspects is to ensure that these PoF power levels do not affect the data signal quality. For that, in this section we simulate different cases for different fibers (SMF and MCF) to investigate this issue.

The simulation setup shown in Fig. 3.26 is used for that purpose. Tx_OOK module is used to generate a modulated light signal at 1550 nm with NRZ modulation formats and data traffics at 1.25 Gbps. Then the data traffic is multiplexed with PoF signal and injected into the fiber where different fiber types are simulated. After data traffic is filtered out by FBG filter, Variable Optical Attenuator (VOA) is used to adjust ROP for BER simulation results which is measured by Rx_OOK.

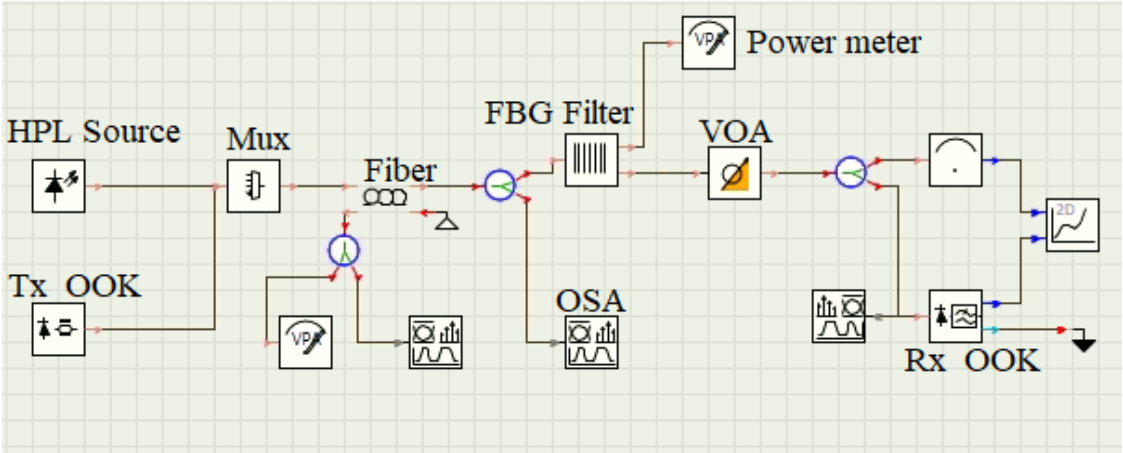

Fig. 3.26: Schematic diagram of the simulation setup used for the analysis of PoF impact on data signal quality.

For small core area MCFs (i.e 4-MCF and 7-MCF*) we investigate the data signal quality with the coexistence of PoF signal in the shared scenario for 5 km transmission distance. We choose the maximum injected power of 500 mW into the fiber input as with that power level there is no degradation in the PoF efficiency for both fibers in the shared scenario. The results for 4-MCF are shown in Fig. 3.27. BER is measured at the receiver for different input powers by using a VOA, first with no PoF and then with 250 mW and 500 mW of injected HPL power to the fiber. The results show that there is no impact on the data signal quality due to the PoF transmission as BER for ON and OFF HPL status is almost the same.

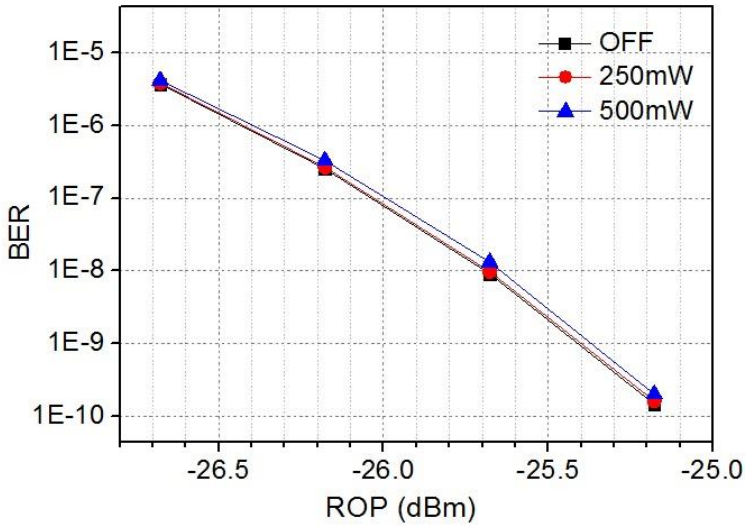

Fig. 3.27 VPI simulations of BER in a power over 4 core-MCF link of 5 km in a shared core scenario for different HPL powers: 500mW & 250mW.

The same results are obtained for 7-MCF* as shown in Fig. 3.28 with 500 mW injected power. However, there is a very small variation compared to 4-MCF.

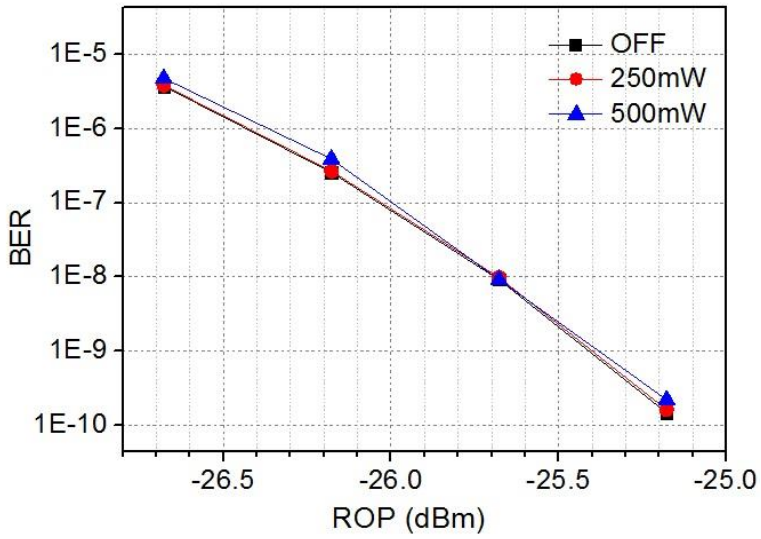

Fig. 3.28 VPI simulations of BER in a power over 7 core-MCF* link of 5 km in a shared core scenario for different HPL powers: 500 mW & 250 mW.

In PoF configurations over MCF, the other design parameter that have to be taken into account is the crosstalk (CT) of the fiber, that is the transfer of power or undesired signals between different fiber cores. Many proposals have studied the impact and limits of CT on the transmission quality and distance [16-18]. However, still its value varies and depends a lot on fiber manufacturing. So that with the integration of PoF and especially with higher power levels, investigating MCF CT becomes of prime importance. In MCF dedicated scenario, and when one MCF is used only for powering so that all cores only propagate energy (i.e no data traffic transmission) the CT power transfer between cores analysis can be neglected. However, also with the same dedicated scenario, but with some cores delivering data, and in a shared core scenario, (i.e the same core delivers energy and data) those undesired signals could affect the data transmission quality. The propagation of higher power levels can also saturate the photo-detector (PD). The power transferred from other cores at 1480 nm can be filtered out by placing filter at 1550 nm at the end of the link. However, the signal at 1550 nm that resulted from SRS can be transferred too between adjacent cores and it is not possible to filter them out. For that some calculations/simulations are performed here as a first step towards addressing the CT impact on data signal quality in different PoF scenarios. The CT between two cores in MCF is given by [19]:

$$CT(z) = \frac{1-e^{-2.\frac{\eta}{L_c}.z}}{1+e^{-2.\frac{\eta}{L_c}.z}} \tag{3.4}$$

which depends on transfer power efficiency (η) which is given by:

$$\eta = sin^2\left(\frac{\pi .z}{2 .L_c}\right) = sin^2(k .z) \tag{3.5}$$

where L_c is the coupling length and is equal to $\pi/2.\mathrm{k}$. K is the coupling coefficient and z is the propagation distance.

The transfer power efficiency also depends on the MCF manufacturing properties like relative refractive index or the fluctuations on the core radius [19]. Core to core pitch (intercore distance) can also affect the coupling length and the coupling coefficient. The CT between adjacent cores can be quite higher than between those that are not. Different methods are proposed to calculate CT in MCF like the one detailed in [20]. Some propose the use of heterogeneous MCF to reduce CT [21]. As a very first approximation, some calculations are performed to determine CT in MCF with core radius of 40 μm. We use equations (3.4) and (3.5) and some parameters that are extracted from [19-20]. The results are shown in Fig. 3.29 for different link lengths (by varying z in the equations) where CT increases with the length. However, we consider here CT between two adjacent cores depending on coupling length and coupling coefficient. This value is reduced for two cores that are far from each other in the fiber as the results shown in [20].

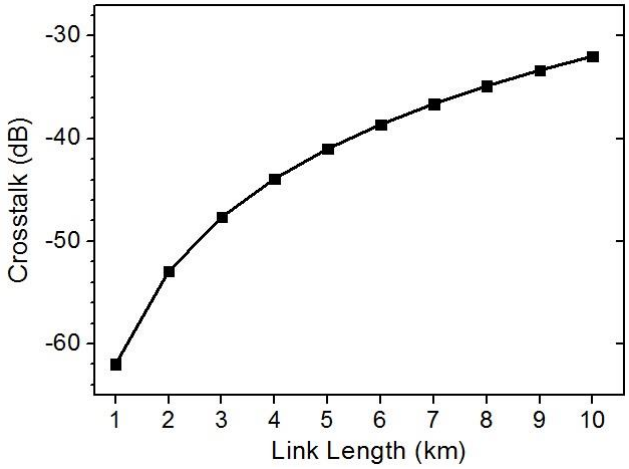

Fig. 3.29 CT vs. link length calculation between two adjacent cores in MCF.

Some simulations are performed in this section too to investigate the effect of having CT between cores and how the transfer of power between cores can affect the data signal quality. The same simulation setup described in Fig. 3.26 is used. We consider the case of having 5 km of 4-MCF in a shared scenario, having some cores for energy and others for data. We analyze the impact of having some optical power at 1550 nm which can be transferred through CT and SRS from the core used for energy to the one used for data. The universal fiber model does not support the simulation of CT, so as a first approximation we placed one source at 1550 nm with the required power level to act as CT source. This power depends on the PoF power level in the first place. We showed previously in Fig. 3.12 that for 4-MCF, an output power of around 1.6 W at 1480 nm resulted with 2 W input optical power at 5 km when the core is used only for energy. In the C-band for the same core the optical power is around – 9 dBm. From this power and by considering different CT values, we predict the power of CT source at 1550 nm which represents the transfer to the data transmission core

due to CT. VOA attenuator is used to fix an attenuation value and in steps of 0.5 dB for all cases. The results are shown in Fig. 3.30 where up to -30 dB of CT there is a very small variation in BER that can be negligible. This is in parallel with delivering 1.6 W of optical power for feeding purposes. However, BER variation is increased as CT increases and becomes more noticeable at CT equals to -15 dB.

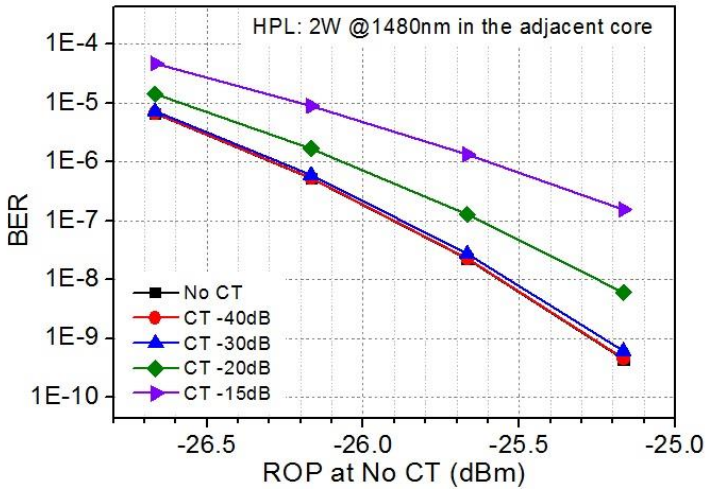

Fig. 3.30: VPI simulations of BER with different CT for 4-MCF in shared MCF fiber scenario. HPL: 2 W at the adjacent core.

Some experimental results about the impact of PoF signal on the data signal quality in MCF can be found in [22], which are related to the work presented here.

The case of 10 km SMF in the shared scenario, using the same simulation setup described above and for the same parameters of the data channel, is also reported here. For HPL source we also found that adding noise with RIN of -130 dB/Hz and noise bandwidth of 1 THz around 1480 nm does not affect the data signal quality as shown in Fig. 3.31

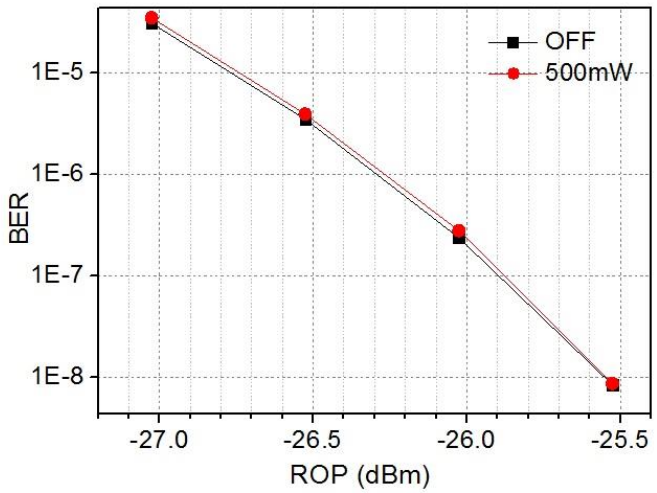

Fig. 3.31 VPI simulations of BER in a power over SMF link of 10 km in a shared scenario for HPL powers of 500mW, RIN -130 dB/Hz.

3.3 Experimental results

Some experimental measurements are performed in order to compare with the simulation results, to address the impact of non-linear effects on the data signal quality in the shared scenario. We used BER of the received signal after fiber transmission as the metric to quantify the impact. These measurements are made in collaboration with PhD student J. D. López-Cardona.

The experimental setup is shown in Fig. 3.32. A BER tester using a Coarse Wavelength Division Multiplexing (CWDM) SFP transceiver operating at 1550 nm of wavelength is used to generate and evaluate the BER performance of a 2.6 Gbps bit-rate data traffic signal (NZR, PRBS=2^{31}-1). The optical circulator provides additional isolation at 1480 nm to the SFP optical source. Then, a variable optical attenuator (VOA) is used to adjust the signal power injected from the optical data source to allow BER measurements. A continuous-wave high-power laser (HPL) at 1480 nm and an output optical power up to 2W is employed as a PoF source. The linewidth for PoF source is 2 nm so that according to our analysis in this chapter, SBS impact can be neglected.

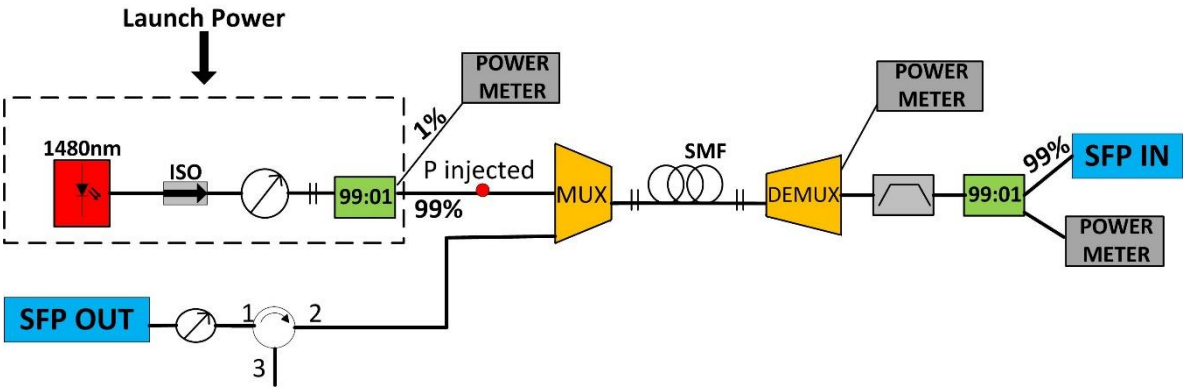

Fig. 3.32: Schematic diagram of the experimental setup used for the analysis of PoF impact on data signal quality.

We use the case of SMF with 10 km link length where results for different input powers levels are shown in Fig. 3.32. The input optical power from PoF source to the system (i.e before Mux) is monitored at point $P_{injected}$, see Fig. 3.32. Although there is small penalty in BER, it keeps < $1*10^{-5}$ for different injected PoF power levels to the system up to 900 mW. We also measured the delivered optical feeding power (after demux) to be around 316 mW (+25 dBm) for an injected PoF level of 900 mW. This small degradation in signal quality can be explained due to two reasons. Firstly, for 10 km SMF with one data channel and with this injected power, Raman amplification is not dominant and only a small part of the power is transferred to C-band. This is concluded from the simulations done is section (3.2.2.2) for

the shared scenario with one data channel as in Fig. 3.13. However, the experimental injected power (900 mW) is compared with 0.6 W at fiber input in the simulations in that graph by considering losses due to Mux/connector in the experimental case. Secondly, the utilized PoF source has a wide spectrum with a peak of maximum power at 1480 nm, but with additional signals, even at the C-band, which may additionally degrade BER. However, we show that 316 mW of optical feeding power can be delivered after 10 km transmission distance with BER below Forward Error Correction (FEC) limit which is 1×10^{-3}.

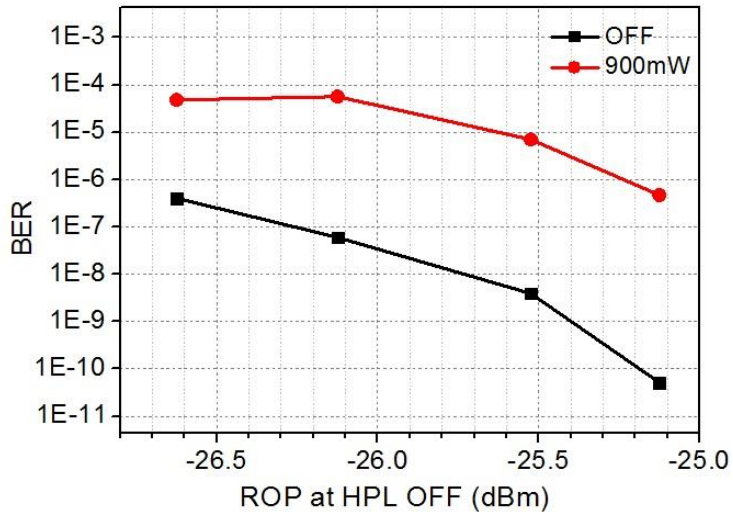

Fig. 3.33 Experimental results of BER in 10 km SMF in the shared scenario for injected power of 900 mW.

3.4 MCF PoF configurations migration towards integration in access networks

In this section, we provide some scalability analysis for PoF systems exploiting the potential of spatial division multiplexing using MCF technology. We compare both powering scenarios in terms of energy that can be delivered and the number of elements that will be required. For doing so, different powering configurations are proposed. Two MCFs are considered (4-MCF and 7-MCF), from Fig. 3.1, and different cases are taken into account in terms of the number of cores that can be used for the different purposes, i.e optical powering, up/down link data transmission for different RRU, control signals and PON. Table 3.2 illustrates a performance comparison considering two aforementioned MCFs, in terms of the energy delivered to the RRU units for both scenarios as well as for different link lengths, respectively.

The delivered energy is considered, for example, to feed RRUs in a mobile front-haul infrastructure. However, in any case the first aspect to be considered is the limit in the amount

of the delivered power in the fiber. It is clearly seen from Fig.3.1 that for the dedicated core scenario no optical demultiplexers (DEMUX) or filter devices are needed at the reception stage, whereas these elements are required for the shared core scenario in order to split the data traffic from the feeding power. This fact leads to an extra penalty in the power delivery because of their insertion losses that reduce the overall power delivery efficiency. Multiplexing devices should be also needed at the central office. In the dedicated core scenario, one individual core or two individual cores are considered for the PoF feeding in the case of a 4-core and a 7-core MCF, respectively. Rest of (free) MCF cores are used for up/down link purposes to provide small cell connectivity in both directions within the infrastructure and for a control channel. In the case of the 7-core MCF the two remaining cores may be employed to support up/down stream PON data traffic. The maximum power assumed to be injected on each individual MCF core is 500 mW. Injecting this power level shows no degradation in PoF efficiency due to non-linear effects up to 5 km (as we showed earlier in this chapter) which is the maximum distance considered in this section. We showed also by simulations that there is no impact on data signal quality up to 5 km.

From our optical budget analysis, the power reaching the RRU unit for the 5 km-long link results in 194.52 mW and 389.04 mW for the 4-core and 7-core, respectively. The power doubles in the 7-core MCF as the total input power is 1W for the two available cores, i.e. 500 mW per individual core. The considered power losses are due to the fan-in device (FI) (~ 1.9 dB), the fan-out device (FO) (~ 1.2 dB) and transmission loss (0.2 dB/ Km), all extracted from [23]. For the shared core scenario, the same configuration is considered for the transmission channels where simultaneously all the cores are used for optical powering purposes. There is a maximum input power of 2 W and 3.5 W for 4-core and 7-core with reaching powers at the RRU site after 5 km of distance of 618.04 mW and 1081.5 mW respectively.

FI and FO devices have crosstalk levels of around -30 dB, being more restricted than MCF crosstalk values that are negligible even at the highest length of 5 km considered in our analysis (> -50 dB). This FI and FO crosstalk, which depends on the ratio between data traffic signal power and PoF levels, could affect the signal transmission quality not only in the shared but also in the dedicated core scenario. If this is the case, optical filters centered on the channel wavelength could be used for more isolation. In this case, the PoF wavelength should be easily demultiplexed from the data channel, as it can be the case if transmitting data traffic at 1550 nm and the PoF signal at 1480 nm. According to our analysis, the shared core scenario provides a better performance in terms of the total amount of delivered power and so the number of the devices that could be remotely powered by light, but at the cost of using more optical elements and more complex topologies. The proposed architecture utilizing the MCF can build flexible Radio Access Network (RAN) as in [6] that can address its future challenges through SDM with the additional advantages of the integration of PoF.

Table 3.2
MCF designs with different cores usage and configurations

Cores Configurations (Dedicated Scenario)							
Fiber Type	Small cell	Control	PON	Power	Link Length	P(mW) at RRU	No. of elements
4-Core Fiber	1 upstream 1 downstre-am	1	0	1	20 m	244.66	3
					1 km	233.82	
					5 km	194.52	
7-Core Fiber	1 upstream 1 downstre-am	1	1 upstrea-m 1 downst-ream	2	20 m	489.32	3
					1 km	467.65	
					5 km	389.04	
Cores Configurations (Shared Scenario)							
	Small cell	Control	PON	Power	Link Length	P (mW) at RRU	No. of elements
4-Core Fiber	1 upstream 1 downstre-am	1	0	4	20 m	777.24	11
					1 km	742.92	
					5 km	618.04	
7-Core Fiber	1 upstream 1 downstre-am	1	1 upstrea-m 1 downst-ream	7	20 m	1360	17
					1 km	1300	
					5 km	1081.5	

3.5 Conclusion

In this chapter, we introduce the limits in the PoF system due to non-linear effects for the integration of these systems in next generation access networks. Limitation on PoF efficiency for shared and dedicated fiber (or core) scenarios are provided. We show that working with HPL (PoF source) linewidth of 100 GHz and beyond can suppress SBS effect in SMF and other MCFs (namely 4-MCF and 7-MCF) and for different transmission distances up to 20km and injected optical powers of even 5 W as in the case of SMF. For 7-MCF* higher linewidths have to be considered, especially for transmission distances longer than 5 km.

For SRS impact we show how the link length, number of data channels, wavelength of data channels and injected power levels can limit system performance. The analysis shows how critical is the consideration of data channels frequencies within C-band as working with (1530-1540) nm band for example, can save noticeable power level of PoF channel at remote side compared with (1550-1560) nm. 25 data channels can be successfully transmitted without affecting PoF efficiency due to non-linear effects with injected power levels up to 2 W and 1.4 W for 10 km and 20 km SMF links respectively. The same results are obtained for 7-MCF. For 4-MCF and 7-MCF* injected power levels are limited to 1.2 W and 0.8 W for 10 km link length. Some simulation cases show the difference between co-propagating and counter-propagating for SMF showing that higher gains are achieved when both signals are transmitted in the forward direction.

The impact of PoF on data signal quality is investigated by simulating BER for data traffic signal transmitted with 1.25 Gbps in different fibers. The analysis shows that both signals (PoF and data traffic signals) can be transmitted with no problem. The impact of crosstalk in MCF arising from high PoF level on data signal quality is calculated. Some simulations show that with – 40 dB of CT no signal degradation is resulted. However, with higher values its impact has to be carefully addressed depending on the input PoF signal power. Some experimental results are provided thus showing the potential of delivery remote feeding power up to 316 mW with BER as low as 1×10^{-5}. Scalability analysis and comparison between both powering scenarios in terms of power levels and the required elements are provided.

The study provided in this chapter can help in the design of power by light systems for SMF and MCF in future access network infrastructures and well as in current network deployments.

3.6 References

[1] J. Werthen, "Powering Next Generation Networks by Laser Light over Fiber," in *Proc. of Optical Fiber Communication/National Fiber Optic Engineers Conference*, San Diego, CA, USA, pp. 1-3, 2008.

[2] J. D. López-Cardona, C. Vázquez, D. S. Montero and P. C. Lallana, "Remote Optical Powering Using Fiber Optics in Hazardous Environments," *Journal of Lightwave Technology,* vol. 36, no. 3, pp. 748-754, 1 Feb.1, 2018.

[3] C. Vázquez *et al*., "Multicore Fiber Scenarios Supporting Power Over Fiber in Radio Over Fiber Systems," *IEEE Access*, vol. 7, pp. 158409-158418, 2019.

[4] Lin Ma, Kyozo Tsujikawa, Nobutomo Hanzawa, and Fumihiko Yamamoto, "Design of optical power delivery network based on power limitation of standard single-mode fiber at a wavelength of 1550 nm," *Applied Optics*, vol. 54, pp. 3720-3724, 2015.

[5] G. Otero, J. D. López-Cardona, R. Muñoz, C. Vázquez, D. Larrabeiti, R. Vilalta, J. A. Hernández, and J. M. Fábrega, ‘‘SDN-based multi-core power-over-fiber (PoF) system for 5G front-haul: Towards PoF pooling,’’ in *Proc. European Conference On Optical communication (ECOC)*, Rome, Italy, pp. 1–3, 2018.

[6] J.M. Galve et al., “Reconfigurable Radio Access Networks using Multicore Fibers,” *IEEE Journal of Quantum Electronics*, vol. 52, no. 1, 0600507, 2016.

[7] T. Umezawa et al "100-GHz Radio and Power Over Fiber Transmission Through Multicore Fiber Using Optical-to-Radio Converter," *Journal of Lightwave Technology*, Vol. 36, no. 2, pp. 617-623, 2018.

[8] Y. Lee, K. Suto, H. Nishiyama, N. Kato, H. Ujikawa and K. Suzuki, "A novel network design and operation for reducing transmission power in cloud radio access network with power over fiber," in *Proc. IEEE/CIC International Conference on Communications in China (ICCC)*, pp. 1-5, Shenzhen, China, 2015

[9] J. B. Rosolem, "Power-over-Fiber applications for telecommunications and electric utilities," book chapter, Intech Open, June 2017.

[10] R. S. Penze, J. B. Rosolem, U. R. Duarte, G. E. R. Paiva and R. B. Filho, "Fiber powered extender for XG-PON/G-PON applications," *IEEE/OSA Journal of Optical Communications and Networking*, vol. 6, no. 3, pp. 250-258, March 2014.

[11] J. Bromage, "Raman amplification for fiber communications systems," *Journal of Lightwave Technology*, vol. 22, no. 1, pp. 79-93, Jan. 2004.

[12] T. N. Nielsen, et. al, “1.6 T b/s (40 40 Gb/s) transmission over 4 100 km of nonzero-dispersion fiber using hybrid Raman/erbium-doped inline amplifiers,” in *Proc*. of *European Conference on Optical Communication (ECOC)*, pp. 236-238, 1999.

[13] P. B. Hansen, L. Eskildsen, S. G. Grubb, A. J. Stentz, T. A. Strasser, J. Judkins, J. J. DeMarco, R. Pedrazzani, and D. J. DiGiovanni, “Capacity upgrades of transmission systems by Raman amplification,” *IEEE photonic Technology Letters*, vol. 9, pp. 262–264, 1997.

[14] S. Namiki and Y. Emori, “Ultrabroad-band Raman amplifiers pumped and gain equalized by wavelength-division-multiplexed high-power laser diodes,” *IEEE Journal of Selected Topics in Quantum Electron*nics, vol. 7, pp. 3–16, 2001.

[15] A. R. Chraplyvy, “Optical power limits in multi-channel wavelength-division multiplexed systems due to stimulated Raman scattering,” *Electronics Letters*, vol. 20, pp. 58–59, 1984.

[16] R. S. Luís, G. Rademacher, B. J. Puttnam, Y. Awaji, and N. Wada, “Long distance crosstalk-supported transmission using homogeneous multicore fibers and SDM-MIMO demultiplexing,” *Optics Express*, vol. 26, no. 18, pp. 24044–24053, 2018.

[17] B. J. Puttnam et al., “Impact of intercore crosstalk on the transmission distance of QAM formats in multicore fibers,” *IEEE Photonics Journal*, vol. 8, no. 2, Art. no. 0601109, 2016.

[18] J. M. Gené and P. J. Winzer, "A Universal Specification for Multicore Fiber Crosstalk," *IEEE Photonics Technology Letters*, vol. 31, no. 9, pp. 673-676, 2019.

[19] K. Takenaga, S. Tanigawa, N. Guan, S. Matsuo, K. Saitoh, and M. Koshiba, ‘‘Reduction of crosstalk by quasi-homogeneous solid multi-core fiber,’’ in *Proc. Optical Fiber Communication Conference*, (OFC/NFOEC), San Diego, CA, USA, pp. 1–3, Mar. 2010.

[20] J. K. Mishra, B. M. A. Rahman and V. Priye, "Rectangular Array Multicore Fiber Realizing Low Crosstalk Suitable for Next-Generation Short-Reach Optical Interconnects with Low Misalignment Loss," *IEEE Photonics Journal*, vol. 8, no. 4, pp. 1-14, Aug. 2016.

[21] M. Koshiba, K. Saitoh, and Y. Kokubun, “Heterogeneous multi-core fibers: Proposal and design principle,” *IEICE Electronic Express*, Vol. 6, no.2, pp. 98–103, 2009.

[22] C. Vázquez, D. S. Montero, F. M. A. Al-Zubaidi and J. D. López-Cardona, "Experiments on Shared- and Dedicated- Power over Fiber Scenarios in Multi-core Fibers," in *Proc. European Conference on Networks and Communications (EuCNC)*, pp. 412-415, Valencia, Spain, 2019.

[23] H. Takara et al, “1000-km 7-core fiber transmission of 10*96-Gb/s PDM-16QAM using Raman amplification with 6.5 W per fibers,” *Optics Express*, vol. 20, no. 9, pp. 617-623, 2012.

Chapter 4:

Radio-over-Fiber Design Parameters for 5G New Radio

In this chapter, we design, analyze and test the Radio Frequency (RF) transmission over different fiber links following 5G New Radio (NR) numerology by using Analog Radio over Fiber (ARoF) technique. We discuss the potential of the designed system to support wireless communication networks in 5G. Different design parameters and fiber link impairments are considered. Sets of experiments considering different advanced modulation formats and link lengths are implemented. Simulation studies are presented to support the experiments. Metrics such as constellation diagram, recovered RF power and Error Vector Magnitude (EVM) are used to evaluate the performance. The results show the system feasibility to transmit high data rates with EVM in compliance with 5G standard requirements. The designed and tested system presented represents first step towards the design of optically powered RoF system by applying Power over Fiber (PoF) technology. The concept of PoF-RoF system will be deeply studied and analyzed in **Chapter Five.**

4.1 Introduction

The fifth generation (5G) communication network is being developed so fast due to the rapid increase in the data traffic of mobile communications [1–3]. Much higher bandwidth and less power consumption requirements are expected. The deployment of 5G technology is expected to depend on the installation of many small cells to improve the capacity and coverage of the network. Additionally, the small cell design will result in flexible 5G mobile networks with higher throughput and more energy efficiency [4].

The research is now focusing on developing new front-haul solutions beyond 4G Common Public Radio Interface (CPRI) to design efficient and cost-effective networks that can support 5G wireless traffic and in turn supporting legacy services such as Fiber to the Home (FTTH) and fixed broadband services [5]. In order to deliver this high data throughput from the cloud centre to different wireless subcarriers, the integration of radio access network (RAN) with fiber based mobile front-haul is important. The 4G mobile front-haul used technologies such as Common Public Radio interface (CPRI) [6] which uses Digitalized-Radio over fiber (D-RoF) technique to transmit IQ radio signals depending on available resources with limited bandwidth [7]. However, such technologies will not be able to support the high data rate expected by 5G. Analog RoF (ARoF) technology is recognised as solution to integrate 5G mobile front-haul [8-10]. The user data can be directly up-converted to different carrier frequencies and transmitted over optical fiber without any signal format conversion or digitalization [9]. This can extremely provide more bandwidth and simplify the Base Band units (BBU) and Remote Radio Units (RRU). For 5G mm-wave communication with high frequencies the direct modulation of RF signals is limited by the modulator bandwidth. The use of optical carriers with ARoF technology gives the advantages of high modulation bandwidths of different optical components and also the feasibility of the generation of optical signals with offset frequency [10]. ARoF has other advantages also like low transmission loss which can be very helpful for long-reach networks.

On the other hand, moving towards centralized RAN (C-RAN) can bring many potentials to the network architectures compared to distributed RAN (D-RAN). In general, C-RAN is composed of three basic components, BBU, front-haul network and RRU as shown in Fig. 4.1. BBU units are centralized in the central office (CO) where all data processing is done their compared to traditional networks where it is done at every remote site. This can help in reducing cost and the complexity of maintenance [11]. Moreover, considering large number of small cells in 5G networks to carry the high data rate requirements brings many challenges to the transport networks to achieve low latency and greener communication [12]. The introduction of C-RAN in 5G networks can address these requirements. The central BBU in C-RAN can be connected to multiple RRU at the remote site by the front-haul segment [13]. ARoF based C-RAN for 5G front-haul can be an optimal solution to meet with the bandwidth requirements and the planned broadband connectivity to final destination where high data

rates up to 1 Tb/s have already been recorded for fiber communication [14]. 5G networks capacity are expected to increase by 1000 times by considering signals in millimetre wave (mm-band) band. Designing flexible access networks based ARoF and C-RAN is essential to support the large number of cells and to provide the required Quality of Service (QoS) [15]. The integration of small cells, i.e microcells, picocells or even femtocells, with current mobile front-haul solutions based on C-RAN architectures using ARoF has advantages as it offers the simplicity at the RRU and also it allows inter-cell coordination so that some solutions like Multiple-input Multiple-output (MIMO) technology can be easily integrated [16]. This centralized management can support network architectures like Passive Optical Networks (PONs) which with Wavelength Division Multiplexing (WDM) technology can be an option to increase the capacity [17]. Wireless access networks based passive optical networks (PON) have been widely investigated including future 5G networks [18].

With the aim of increasing the capacity in future 5G optical access networks at a reduced cost and to make it possible utilizing the existing access network based infrastructure, Single Mode Fiber (SMF) can be considered. Even using bundles of SMF if spatial division multiplexing (SDM) is required [13]. Radio over SMF for medium distances mobile front-haul solutions is reported in [19].

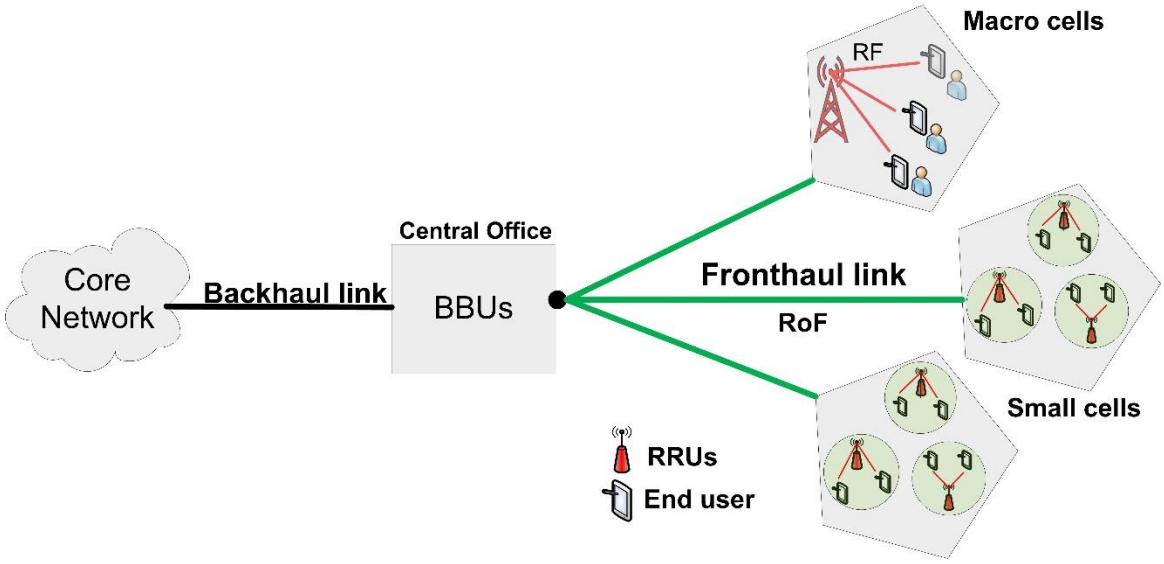

Fig. 4.1: Schematic diagram of studied C-RAN configuration. BBU: Base Band Unit. RRU: Remote radio unit. RoF: Radio-over-Fiber.

5G New Radio (NR) access technology is expected to operate in the frequency range from 1 GHz to100 GHz [20] and support different applications such as Internet of Things (IoT), artificial intelligence, big data analytics, Massive Machine Type Communications (MMTC) and Enhance Mobile Broadband (eMBB) [20]. 5G NR is standardized through the 3rd generation partnership project (3GPP) [21]. And Cyclic-Prefix Orthogonal Frequency Division Multiplexing (CP-OFDM) waveform has been considered for the new 5G access

networks. This multi-carrier waveform is essential to support 5G high data rates. CP-OFDM is selected as NR waveform for 5G due to different key performance such as high spectral efficiency, powerful for frequency selective channels, well localized in time domain and robust to timing synchronization errors [22]. OFDM numerology (cyclic prefix and subcarrier spacing) will add more flexibility to support variety of services. The sub-carrier spacing for OFDM in 5G NR was agreed to be 15×2^n kHz where n is an integer number that can be chosen depending on the type of service, hardware requirements and mobility [20]. 15 kHz is the subcarrier used by 4G in the Long Term Evolution (LTE). CP is necessary for inter-symbol-interference (ISI) removal where its length depends on the channel model for a specific standard. Fig 4.2 shows a general vision of the services that can be supported by 5G NR and the operating frequencies. For the great wireless data rate demands, 5G approved the use of mm-wave frequencies above 30 GHz [23], in parallel with the use of the microwave region (< 10 GHz) [24].

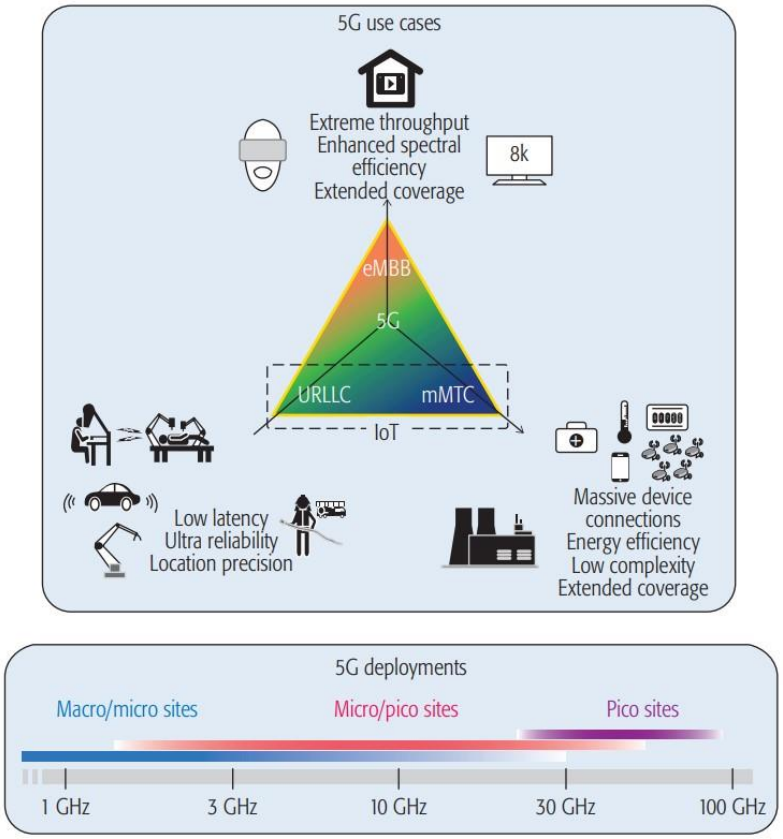

Fig. 4.2: 5G uses cases and utilized spectrum ©2018 [20].

Hence, in this chapter we analyze the performance of 5G NR signal transmission using ARoF technology. We focus mainly on SMF as there is a considerable interest by the operators in the reuse of the already deployed broadband fiber networks, being SMFs the most popular and widely used mean for these optical fiber-based infrastructures. The proposed system uses 5G NR baseband signals to emulate user data and uses different electrical and optical

component/devices to achieve the data transmission. The performance is tested using different modulation formats including QPSK, 16-QAM, 64-QAM, 256-QAM and different RF carrier frequencies bands up to 20 GHz. SMF links up to 10 km are implemented.

The chapter is organized as follows, first the impact of the design parameters including chromatic dispersion is discussed. Next, the ARoF transmission system is modelled using VPI software tool and the different design parameters are simulated in detail. Afterwards, the experimental setup and characterization are described and the main results are discussed. Finally, the chapter is concluded and the bibliography is listed at the end.

4.2 Performance of Radio over Fiber links transmission following 5G NR

In this section we design and analyze the transmission of modulated radio signals over a standard SMF fiber. The most important parameters in the design of a Radio over fiber link are addressed. A series of simulations based on Virtual Photonic Instrumentation software tool (VPI) are implemented and firstly discussed in this section for different carrier frequencies, link lengths and other parameters of interest. We analyze the frequency band that can be selected for the desired link length depending on the final application. The 5G NR waveform format considered in this study is based on CP-OFDM (Cyclic Prefix – Orthogonal Frequency Division Multiplexing) with adaptive modulation including QPSK,16QAM, 64QAM and 256QAM following the 5G NR numerology, as aforementioned in the above section.

To the date of writing this document there is no research work reported that analyzes in detail the impact of chromatic dispersion in the transmission of 5G NR signals in a standard fiber. A simulation study to address the chromatic dispersion limits in the ARoF transmission distance is presented. Nonlinear effects such as self-phase modulation (SPM) and Kerr effects can also affect the overall performance. The simulation study will also address its impact in some cases.

4.2.1 Radio over Fiber Simulation Design Model

All the results presented in this section are based on VPI simulations. We simulate different case studies to test the analog transmission of RF signals modulated with 5G NR basebands in SMF. The general schematic of the VPI simulation layout is shown in Fig. 4.3. The OFDM transmitter generates the electrical CP-OFDM signal up-converted at the desired RF carrier frequency to emulate the user data. This signal is optically modulated with an optical signal carrier at 1532 nm and an optical power of 10 mW using a Mach-Zehnder intensity modulator (MZM). After propagating in SMF, the data signal is filtered-out with a Fiber Bragg Grating

(FBG filter) and finally detected by Photodiode (PD). RF input power is set to +15 dBm in all cases.

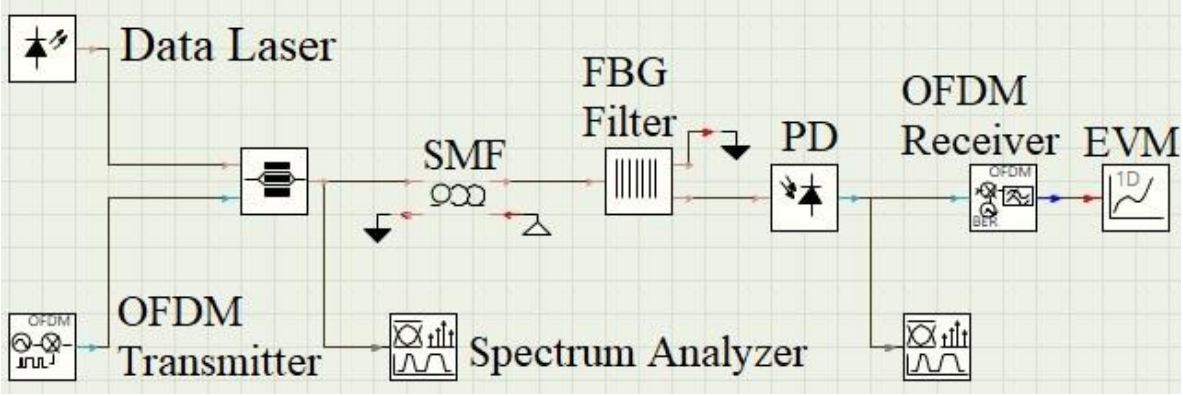

Fig. 4.3: Schematic of the general VPI simulation layout.

Afterwards the signal is fed to an OFDM receiver which is used to decode the received OFDM signal and evaluate the performance, where the EVM value and the constellation diagram of the received signal can be obtained. The spectrum analyzer is used at different stages of the setup to obtain both the optical and electrical spectrums. Different optical components are additionally used to run the different simulation cases. They will be clarified later in this section.

As we are interested in the evaluation of the transmission of 5G signals over SMF fiber, we will focus in this chapter on the impact of the optical fiber to support the design of future 5G front-haul solutions. Fig. 4.4(a) shows the CP-OFDM signals after being optically modulated (at MZM output) with an RF carrier frequency at 10 GHz. Fig. 4.4(b) shows the recovered RF signal after being detected by the PD and decoded by the OFDM receiver in Back-to-Back (B2B) conditions (i.e. no fiber transmission) for reference purposes.

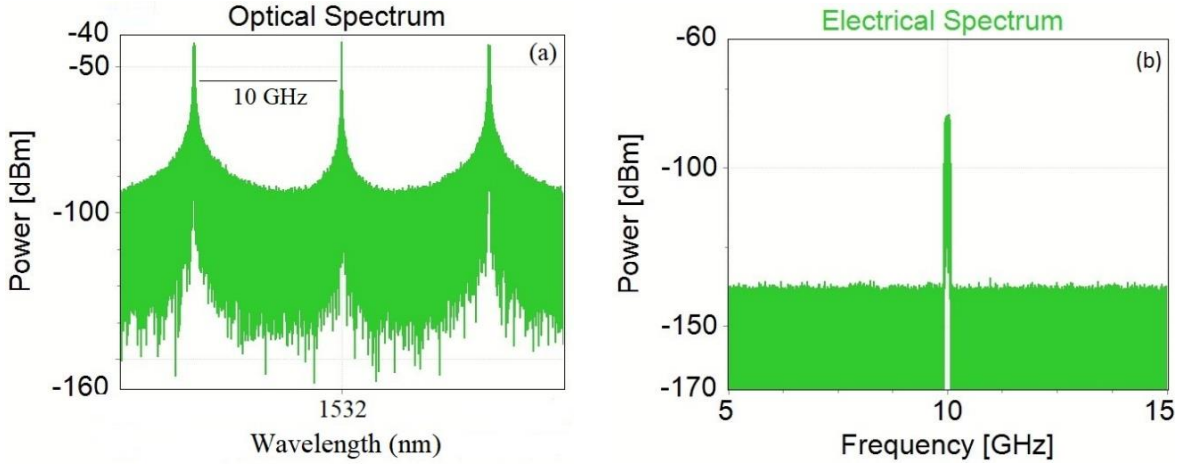

Fig. 4.4: (a) Optically modulated RF signal with MZM at 10 GHz carrier frequency. (b) Electrical spectrum of recovered RF signal at 10 GHz after PD detection.

In the following, different cases are considered to evaluate the fiber response for RF transmission. As the focus will be mainly on the fiber channel, a linearizer is placed before the MZM to ensure the linear response and to compensate for the modulator nonlinearity. Figures of merit to evaluate the system performance will be the EVM, the received constellation diagram and the recovered RF power. The simulated EVM values obtained will be always compared with the EVM requirements for downlink transmitted signals from base stations provided within the 5G NR standard as shown in Table 4.1 [14]. PD responsivity is set to 1 for ideal Optical/Electrical conversion.

Table 4.1
EVM standard requirements for downlink transmission in 5G NR [14].

Modulation formats	EVM%
QPSK	17.5-19%
16-QAM	12-14%
64-QAM	8-9%
256-QAM	3.5%

4.2.2 RF Power Fading and Chromatic Dispersion Impact in Intensity modulated RF signals

In general, one of the limiting factors for ARoF transmission is the chromatic dispersion, especially for long mobile front-haul solutions and high bandwidth systems, being the most critical effect which needs to be carefully addressed [25]. Considering this effect is an important design parameter to decide the feasibility of the current infrastructure based on SMF and the maximum distance that radio transmission can propagate with no or acceptable degradation due to link impairments. In microwave and mm-wave links, and after signal is intensity modulated on the optical fiber with double sideband modulation (DSB), the optical carrier signal within both bands can suffer from different phase shifts because of chromatic dispersion after propagating along the fiber channel. This fact can degrade the microwave signal power at detection [26]. Due to this phase shifts, the optical carrier and the two modulated sidebands will propagate in different velocities inside fiber and after received by photodetector, heterodyne signal component will be generated at RF carrier frequency. The modulation transfer function is given by [27]:

$$k(\omega, L) = \cos^2\left(\frac{\omega^2 \beta_2 L}{2}\right) \tag{4.1}$$

where L is the fiber link length, ω is the modulation frequency and β_2 is the mode propagation constant.

This degradation caused by chromatic dispersion is increased for higher carrier frequencies as the offset between the optical carrier and these bands is increased. This can greatly distort

and attenuate the RF signal which may be even canceled out at specific conditions. At a specific link length and RF carrier frequency the two modulation sidebands will be in counter phase which resulted in zero in the recovered RF amplitude by photodiode [28]. As a result, the phase shifts resulted from the chromatic dispersion can lead to the well-known periodic RF power fading [26-27]. This RF power fading limits the transmission distance, especially for high carrier frequencies, and its impact appears as notches in the frequency response of the RF signals after fiber transmission [29]. For that it is of great interest to analyze the chromatic dispersion impact on the 5G NR signals transmission over SMF and to address the distances that can be reached at the desired RF frequency. Different simulation cases are performed for this purpose in this section and the metrics that have been used are EVM, RF frequency response and constellation diagram, respectively.

SMF is considered with α=0.2 dB/km of fiber attenuation coefficient at 1532 nm. Firstly, all non-linear effects are not included to study the chromatic dispersion impact separately. The study focuses on the link lengths that can be utilized in access networks up to few tens of kilometers where chromatic dispersion limitation dominates. The impact of polarization mode dispersion (PMD) is not included. Its impact can be neglected up to 40 km which is the longest distance considered in this study as the PMD coefficient is < 0.1 ps/√km for the fibers considered. High RF frequency carriers are simulated, specifically from (10 to 30 GHz), aligned with the frequency bands of 5G NR (Frequency Range 2). At first QPSK modulation is considered for all cases. As reference, the 20 GHz carrier frequency will be considered in most cases. Fig. 4.5 shows the EVM performance for radio transmission with a 20-GHz RF carrier over SMF with chromatic dispersion parameter (D) set to 17 ps/nm/km. Fiber length up to 20 km in steps of 1 km are simulated. As we can see, EVM is dramatically degraded at a specific link length which is 9 km. Afterwards, the EVM is enhanced up to 20 km.

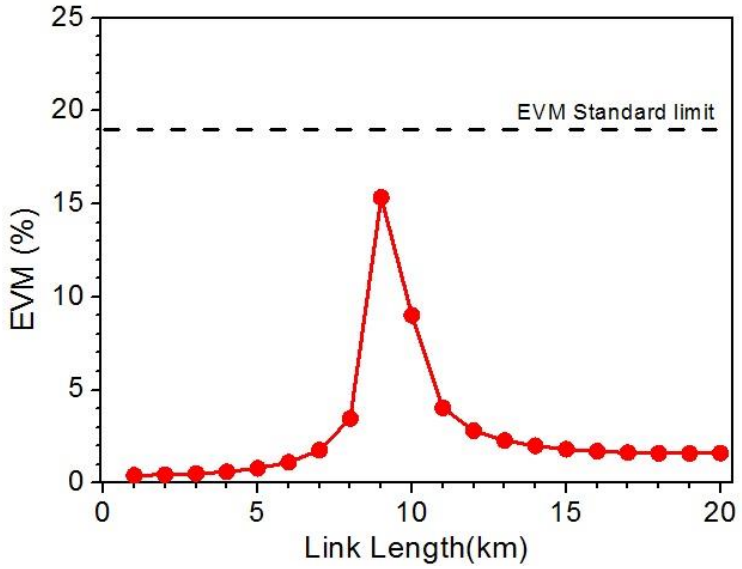

Fig. 4.5: Simulation of EVM vs. Link length for SMF, D=17 ps/nm/km, α 0.2 dB/km, RF 20 GHz.

This behavior can be due to the dispersion induced penalty into the two modulated side bands where they both can suffer from different phase shifts being the RF signal attenuated too. Fig. 4.6 shows the constellation diagrams for the EVM results depicted in Fig. 4.5 at specific link lengths, including the 9 km-long link that shows the worst EVM performance. It's clearly seen at the 9 km how the symbols are distorted which leads to this EVM degradation.

To prove that this power fading is due to the chromatic dispersion impact, different chromatic dispersion values are simulated for the same conditions (RF 20 GHz, QPSK). The results are shown in Fig. 4.7. From that figure we can see that as the chromatic dispersion value increases, the link length where EVM takes its worst-case is decreased, being the signal faded at shorter link lengths. At some conditions, the resulting EVM even exceeds the standard limits for the QPSK modulation considered. So that its clearly seen that different critical lengths are observed where EVM shows it peaks for different chromatic dispersion values. This shows how important considering the chromatic dispersion for efficient system performance. For that, further cases are investigated.

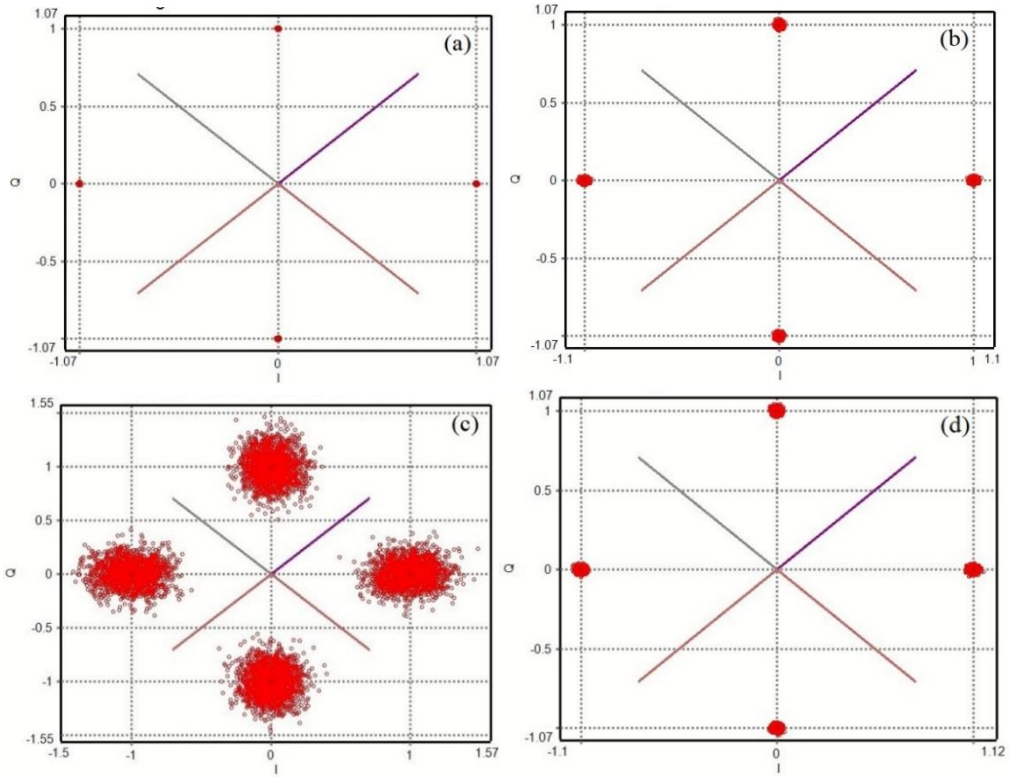

Fig. 4.6: Constellation diagrams for the EVM results of Fig. 4.5: (a) B2B, (b) 5 km, (c) 9 km, (d) 15 km.

The other figure of merit used to evaluate the designed system performance and to investigate the chromatic dispersion impact is the power of the recovered RF signal after O/E conversion. The frequency response for the same simulated cases of Fig. 4.7 is shown in Fig. 4.8. The chromatic dispersion impact is shown as notches in the signal frequency response as chromatic dispersion values vary.

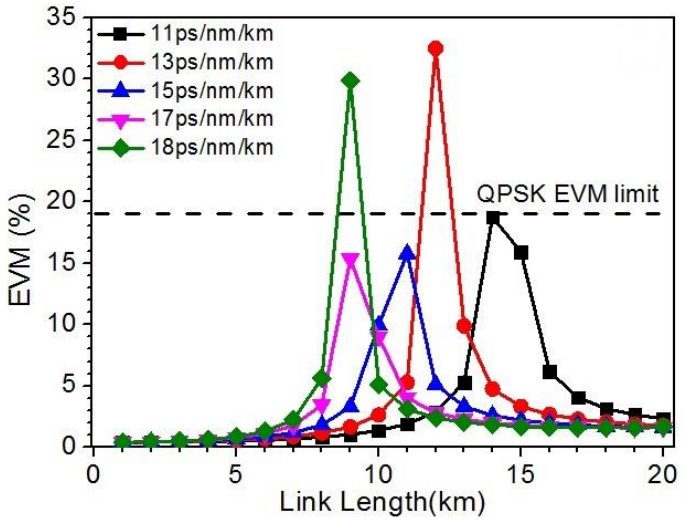

Fig. 4.7: EVM vs. link length with L swept in steps of 1 km for different dispersion parameters, α=0.2 dB/km, RF carrier =20 GHz.

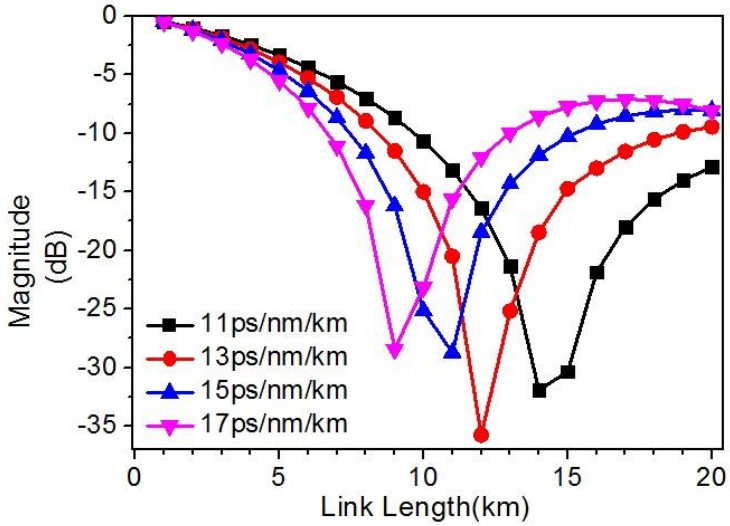

Fig. 4.8: Frequency response for different dispersion parameters with L swept in steps of 1 km, α=0.2 dB/km, RF=20 GHz.

The vertical axis in Fig. 4.8 represents the difference between the recovered electrical power at the back to back conditions with respect to fiber transmission for the different link lengths. At this specific fiber link length (9 km) this attenuation or power degradation is rapidly increased which result in power fading [25,2]. This length can be defined as follow [26]:

$$L_1 = \frac{c}{2D\,\lambda^2 {f_c}^2} \tag{4.2}$$

where c is the speed of light, D is the chromatic dispersion parameter, λ is the optical wavelength and f_c is the carrier frequency, respectively.

This link length L_1 will be defined as the critical length throughout this section.
Fig. 4.9 combines the results of the previous two figures for a dispersion parameter equals to 17 ps/nm/km to show how the critical length affects the two metrics, EVM and frequency response, both dramatically penalised at 9 km. Considering these parameters as a reference, we further investigated the chromatic dispersion impact for different carrier frequencies.

The link length is increased up to 40 km. The results for three carrier frequencies (10, 15 and 20 GHz) are shown in Fig. 4.10. The figure shows the high sensitivity of RF frequency carrier to the dispersion. The critical length is also shifted to longer lengths as the carrier frequency decreases. At 10 GHz this length is 38 km which is far from the case of other carrier frequencies. At 20 GHz, two peaks for EVM degradation are clearly observed. This cyclic behaviour of the signal degradation (i.e power fading) is expected. The length period between two consecutive notches is given by [26]:

$$\triangle \mathrm{L} = \frac{c}{D\lambda^2 {f_c}^2} \tag{4.3}$$

where $\triangle$L is the link length period between two notches, c is the speed of light, D is the chromatic dispersion parameter, λ is the optical wavelength and f_c is the carrier frequency.

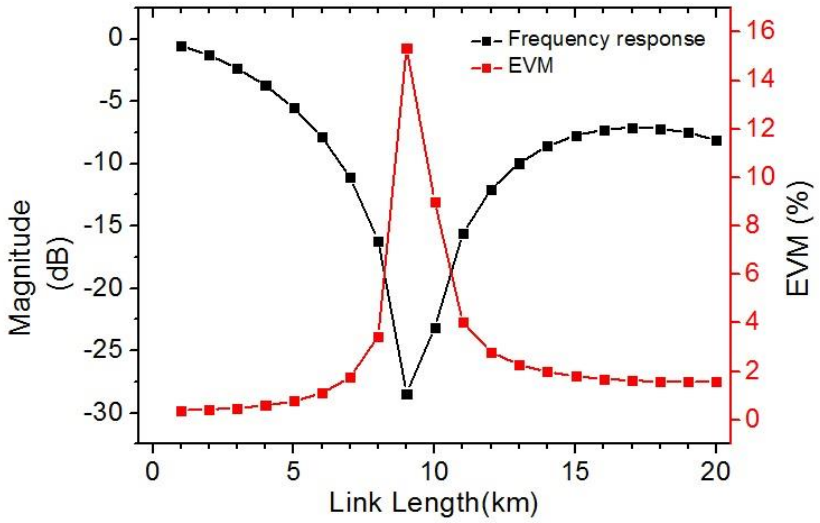

Fig. 4.9: EVM and frequency response vs. link length with L swept in steps of 1 km for a dispersion parameter D=17 ps/nm/km, α=0.2 dB/km, RF carrier=20 GHz.

As the RF carrier frequency increases, more notches appear in the link length range considered up to 40 km. For example, for a RF carrier frequency of 25 GHz, 3 notches would appear in the frequency response while for 30 GHz the notches would be 5. Their corresponding EVM peaks are illustrated in Fig. 4.11.

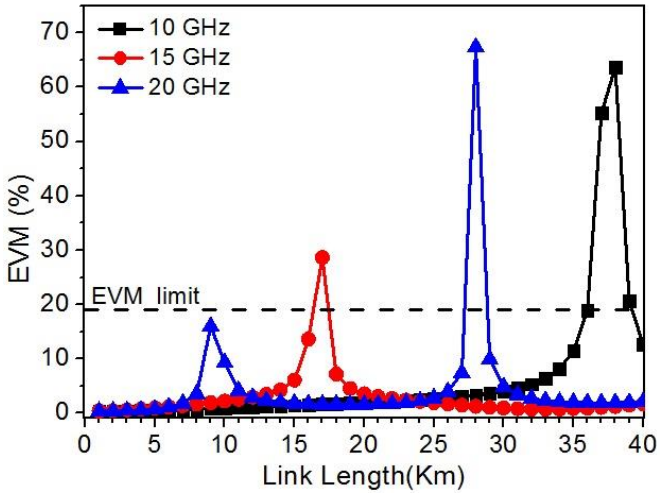

Fig. 4.10: EVM vs. link length with L swept in steps of 1 km for carrier different frequencies, α=0.2 dB/km, D=17 ps/nm/km.

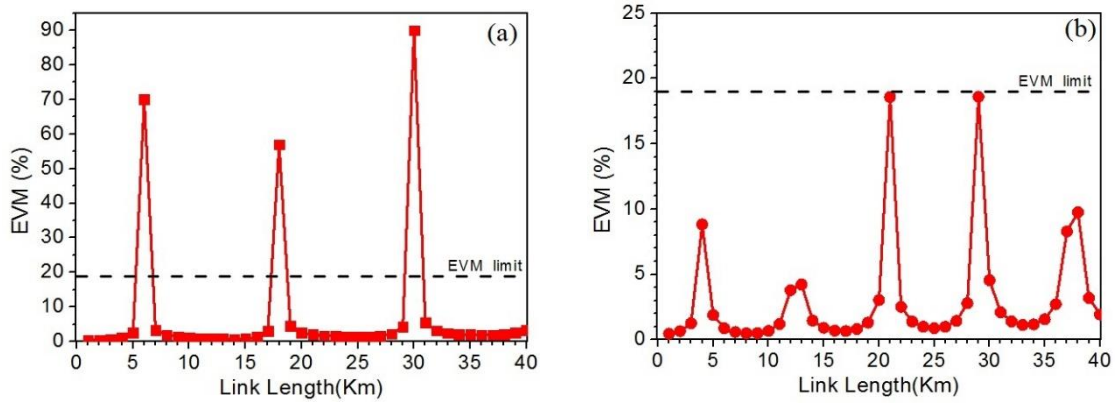

Fig. 4.11: EVM vs. link length with L swept in steps of 1 km for a RF carrier frequency (a) 20 GHz, (b) 30 GHz. α=0.2 dB/km.

Fig. 4.12 shows how these notches are represented in the frequency response for 15 GHz and 30 GHz RF carrier frequencies. These notches are exactly the same for the EVM peaks observed in figures 4.10 and 4.11, respectively.

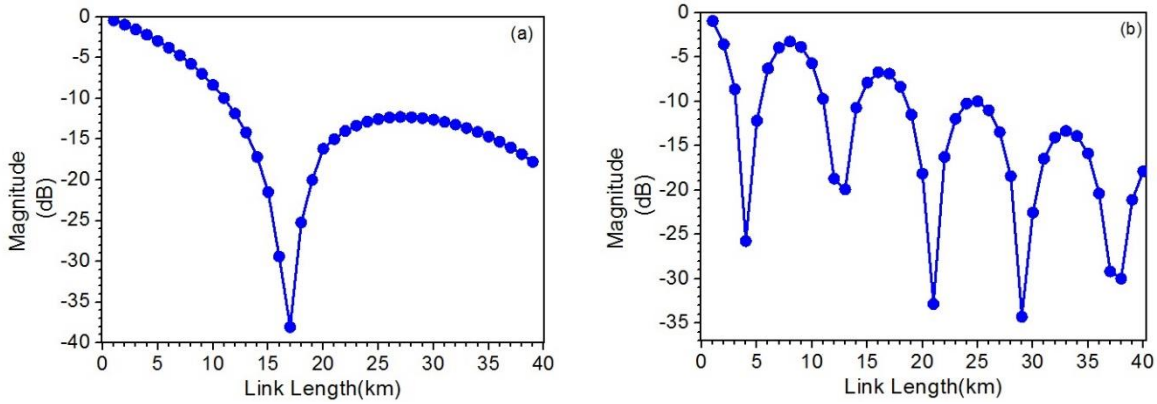

Fig. 4.12: Frequency response with L swept in steps of 1 km for a RF carrier frequency(a) 15 GHz, (b) 30 GHz. α=0.2 dB/km.

Back to our reference case with a dispersion parameter equals to 17 ps/nm/km at RF 20 GHz, the critical length L_1 for these conditions is 9 Km (see Fig. 4.5). Further investigation around this critical length shows that even greater peaks for EVM degradation can be obtained, as depicted in Fig. 4.13. In this figure L is swept in steps of 100 m for different dispersion parameters in steps of 0.1 ps/nm/km. This clearly indicates how the radio transmission is sensitive to this periodic impact of chromatic dispersion. The dramatic EVM values observed at this specific conditions indicate that the signal might be totally faded due to carrier suppression because of the chromatic dispersion impairment.

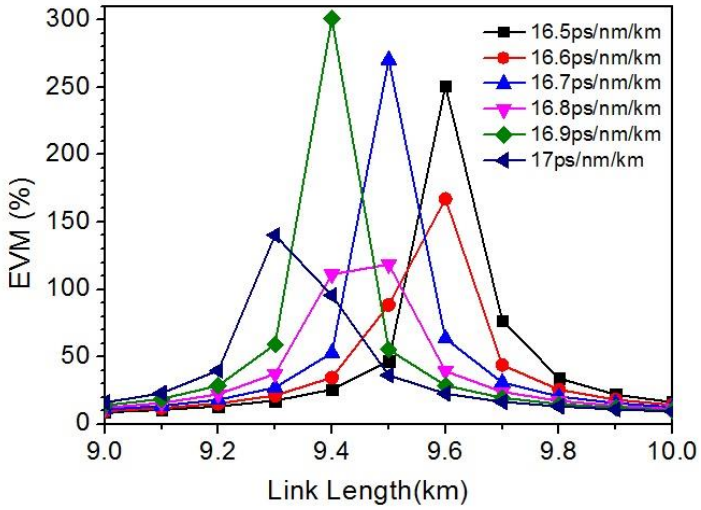

Fig. 4.13: EVM vs. link length with L swept in steps of 100 m for different dispersion parameters, α=0.2 dB/km, RF carrier frequency=20 GHz.

In Fig. 4.14, the constellation diagram at reception at a link length of 9.4 km and for a dispersion parameter of 16.9 ps/nm/km (green curve in Fig. 4.13) is shown. The figure shows how the symbols are canceled because of power fading which leads to this very high EVM value.

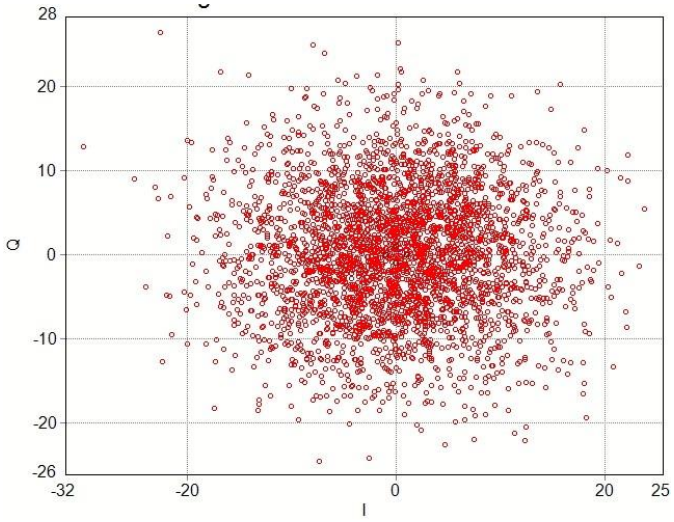

Fig. 4.14: Constellation diagram for L=9.4 Km, D=16.9 ps/nm/km, RF=20 GHz.

These EVM values can even be greater around L_1 with D swept in only 0.05 ps/nm/km (fine tune) as shown in Fig. 4.15 and Fig. 4.16. Two link lengths are chosen depending on the results shown in Fig. 4.13.

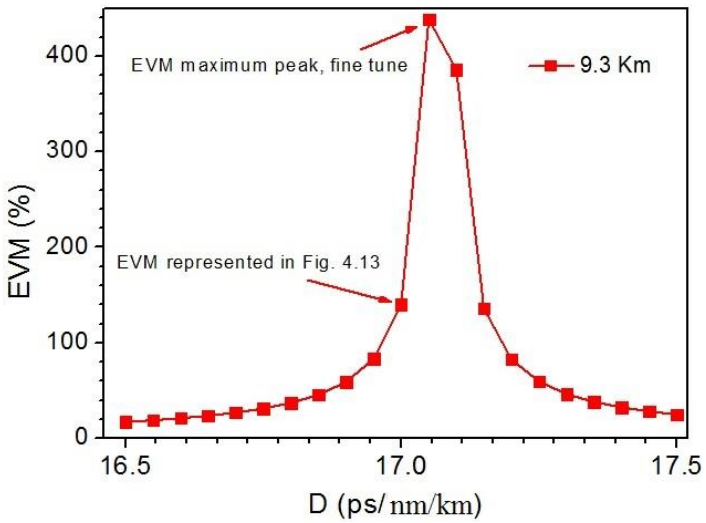

Fig. 4.15: EVM vs. dispersion parameter with swept of 0.05 ps/nm/km, L=9.3 km, α=0.2 dB/km, RF=20 GHz.

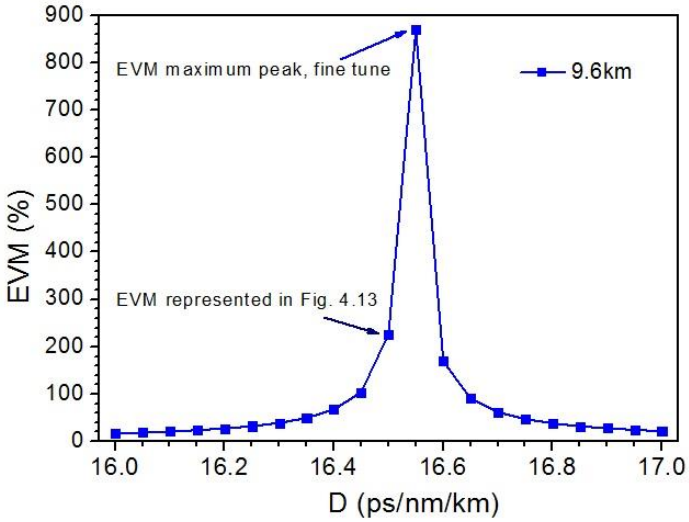

Fig. 4.16: EVM vs. dispersion parameter with swept of 0.05 ps/nm/km, L 9.6 km, α 0.2 dB/km, RF=20 GHz.

Table 4.2 compares the calculated and simulated results for L_1 and $\triangle L$ for different carrier frequencies. The calculated results are based on equations (4.2) and (4.3) for an operating wavelength (λ) of 1532 nm. The simulation results are done with link lengths in steps of 200 m to achieve more accurate results near the critical length. The calculated and simulated results are in good agreement.

Table 4.2
Calculated and simulated L_1 and $\triangle L$ for different carrier frequencies for 1532 nm data channel

RF carrier frequency (GHz)	L_1 (km)		$\triangle L$ (km)	
	Calculated	Simulated	Calculated	Simulated
10	37.59	37.60	75.19	75
15	16.71	16.60	33.42	33.4
20	9.39	9.4	18.80	18.80
25	6	6	12.03	12
30	4.17	4.2	8.35	8.4

For a deep investigation of this power fading effect, further simulations are performed for other modulation formats. In Fig. 4.17 (a) and (b) EVM and frequency response for both 64-QAM and 256-QAM modulation formats are shown, respectively. As expected, the behavior is the same as in the case of QPSK for a RF carrier frequency of 20 GHz. The frequency spectrum shows a notch at 9 km which in turn results in a dramatic EVM degradation at this specific length. Nevertheless, the EVM result is slightly different for the three modulation formats considered, and this difference is increased at the critical length. For 64-QAM case, only 9 km is out of standard limit while for 256-QAM both 9 and 10 km exceed the limit. Additionally, link lengths of 8 km and 11 km show a critical EVM near standard limit. This indicates how important is consider this impact for the design of ARoF links.

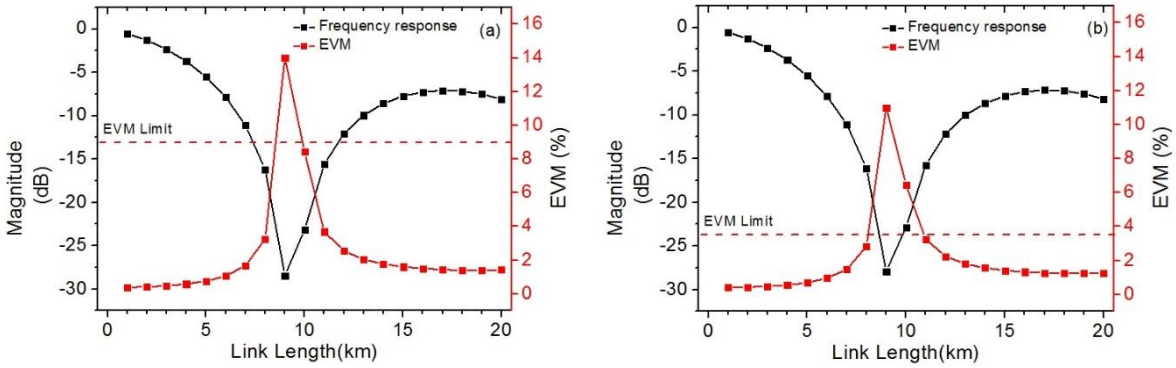

Fig. 4.17: EVM and frequency response vs. link length with L swept in steps of 1 km for dispersion parameter D=17 ps/nm/km, α=0.2 dB/km, RF 20 GHz (a) 64QAM modulation formats (b) 256QAM modulation formats.

For 16-QAM modulation format, we simulate the 30 GHz carrier frequency case in order to compare with other modulation format (QPSK, see Fig. 4.11b) and to investigate the cyclic behavior of EVM. The results are shown in Fig. 4.18 where the same parameters are used as in the case of QPSK modulation. For 16-QAM a similar behavior is obtained, with EVM degradation peaks at the same distances. However, some of these peaks exceed the EVM standard limit. In addition, the EVM values obtained showed some differences mainly at the critical lengths.

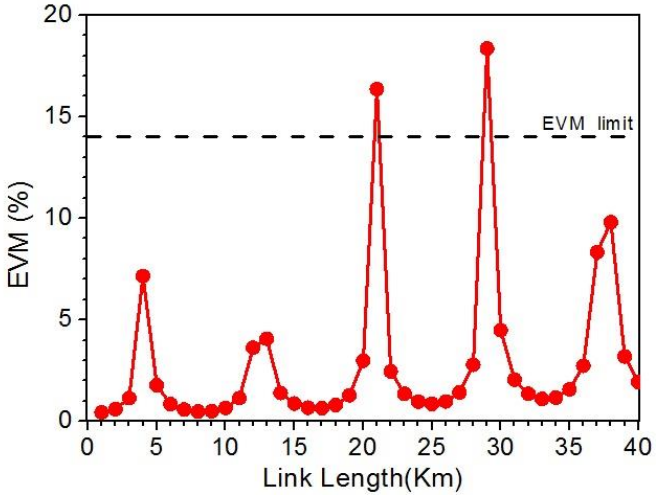

Fig. 4.18: EVM vs. link length with L swept in steps of 1 km for RF= 30 GHz, 16-QAM modulation format, α=0.2 dB/km, D=17 ps/nm/km.

One of the common ways to compensate for this chromatic dispersion issue is the use of the Dispersion Compensation Fiber (DCF), as shown in Fig. 4.19. In Fig. 4.20 we show by simulation how the use of commercially available dispersion compensating fibers (DCF) may extend the link length before first notch due to fading occurs. For instance, a 3 km-long DCF fiber with a dispersion parameter of -40 ps/nm/km placed after the SMF link shifts L_1 from 9.3 km to 16.5 km

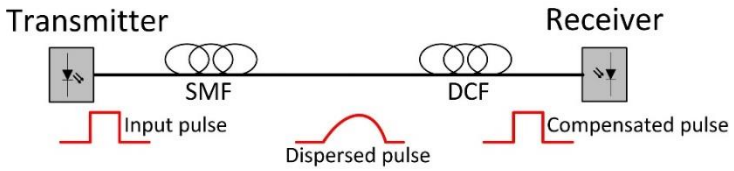

Fig. 4.19: Schematic diagram showing the principle of using a DCF fiber for chromatic dispersion compensation.

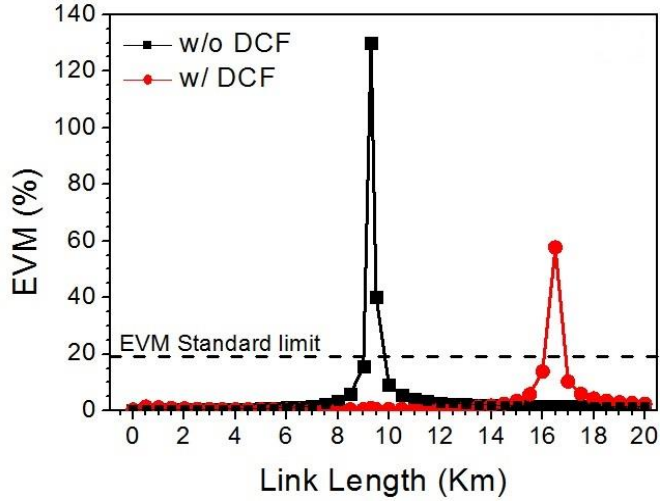

Fig. 4.20: EVM vs. link length with L swept in steps of 200 m showing the effect of adding a DCF fiber (3 km, D= -40 ps/nm/km) after transmission link. D =17 ps/nm/km, α=0.2 dB/km, RF= 20 GHz.

4.2.3 Impact of data channel power and fiber non-linear effects

In this section, series of simulations are performed to investigate the impact of the optical carrier power on the performance of the data transmission. In Fig. 4.21 different link lengths are considered for RF 20 GHz and D=17 ps/nm/km. As expected, worst EVM cases are obtained at the critical length L_l=9 km or around (10 km). In all cases EVM is improved as the input optical power of the data channel is increased and then it stabilizes at 20 mW and beyond. A similar performance is obtained considering a RF carrier frequency of 30 GHz and the same dispersion parameter. Results are depicted in Fig. 4. 22. Link lengths of 4 km and 13 km show the worst EVM performance as they represent L_l and $\triangle L$ for a RF carrier frequency of 30 GHz, respectively, while EVM shows a better performance for the other cases under study (5 km and 8 km).

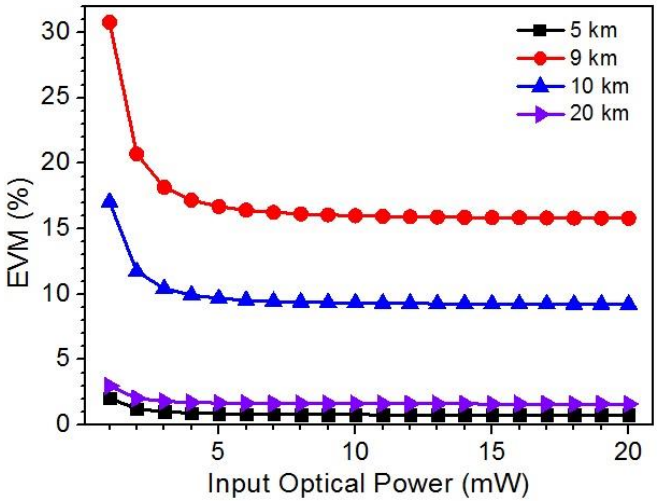

Fig. 4.21: EVM vs. Input Optical Power (data channel) for different link lengths. D=17 ps/nm/km, , α=0.2 dB/km, RF=20 GHz, QPSK modulation format.

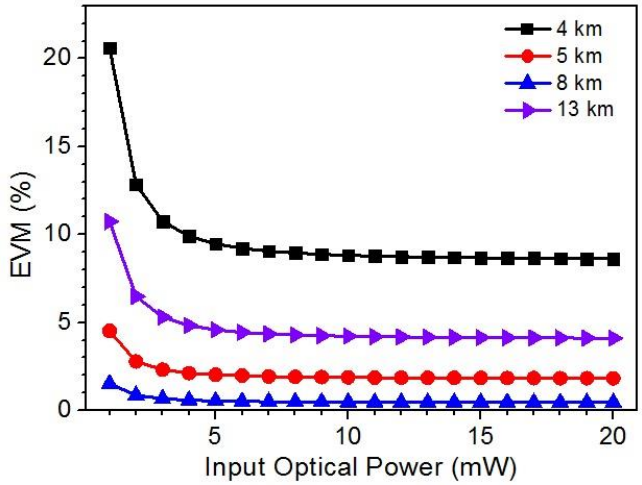

Fig. 4.22: EVM vs. Input Optical Power (data channel) for different link lengths. D=17 ps/nm/km, , α=0.2 dB/km, RF=30 GHz, QPSK modulation format.

From the result of Fig. 4.21 and as EVM is penalised at a low input power, we further simulate cases below 1 mW of power on the data channel. In Fig. 4.23 the optical power of the data channel is swept from 0.1 to 1 mW (i.e. from -10 dBm to 0 dBm) for a RF frequency of 20 GHz. As the optical power is decreased, the signal quality is greatly affected even for link lengths far from the critical case as it the case in Fig. 4.23 (a) for 5 and 20 km while for the critical length and regions around the signal can be greatly attenuated as shown in Fig. 4.23 (b) which can be the reason for this very high EVM value.

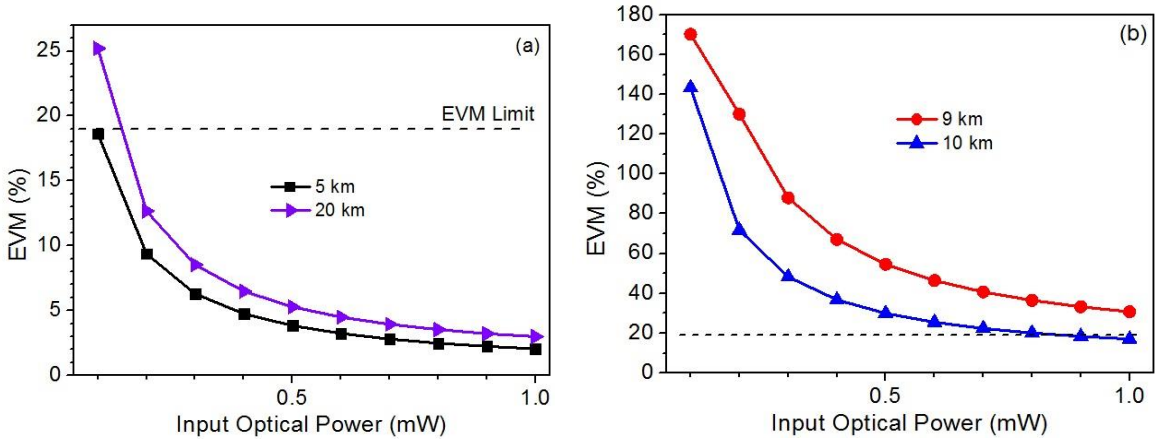

Fig. 4.23: EVM vs. Input Optical Power, D =17 ps/nm/km, α=0.2 dB/km, RF= 20 GHz (a) 5 and 20 km (links far from critical length) (b) 9 and 10 km (around critical length L_1).

As this power is more sensitive near the critical lengths, we further simulate different cases to investigate the effect on non-linear effects especially the Kerr nonlinearity that includes Self Phase Modulation (SPM) and Cross Phase Modulation (XPM) effects. Both SPM and XPM are originate from the refractive index dependence on optical power. They both may gradually degrade the signal quality because of the higher temporal broadening as data is being transmitted throughout the fiber [30-31]. For a RF carrier frequency of 20 GHz and as the data channel optical power increases the impact of non-linear effects start being significant as seen in Fig. 4.24 for 9 km (critical length).

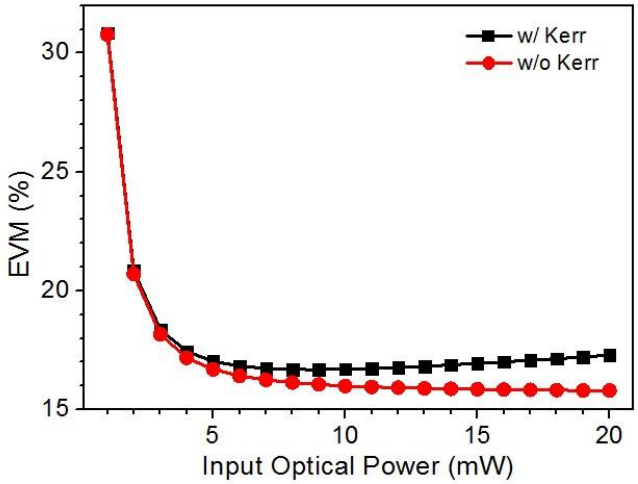

Fig. 4.24: EVM vs. Input Optical Power for L= 9 Km (critical length) with Kerr non-linearity On and OFF. D=17 ps/nm/km, α=0.2 dB/km, RF=20 GHz.

Fig. 4.25 shows a comparison between two data channel optical powers injected into the link for different link lengths and a RF carrier frequency of 20 GHz. As this power increases the impact of Kerr effect is more relevant at the critical length.

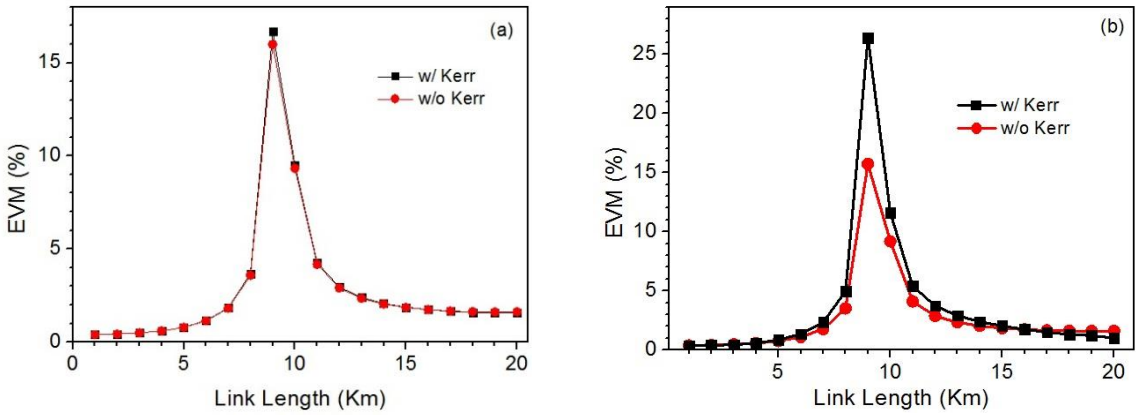

Fig. 4.25: EVM vs. link length with L swept with 1 km, D =17 ps/nm/km, α=0.2 dB/km, RF= 20 GHz. Input optical power (a) 10 mW, (b) 100 mW

As a conclusion, the optical power of data laser is another important parameter that have to be considered especially for distances near the critical length. The non-linear effect like SPM can dominate at higher power levels and longer distances. The impact of these effects is addressed in detail in Chapter five

4.2.3 Impact of temperature on Chromatic Dispersion

Other conditions that can affect the performance of the ARoF link are the environmental conditions, and especially temperature [19]. Many studies have reported that changing the fiber temperature in SMFs may lead to fluctuations in the fiber chromatic dispersion (D) parameter [32,33]. This behavior comes from the linear changing of the zero dispersion wavelength because of the temperature increment being of around 0.025 nm/ºC [32]. To analyze this possible contribution in the ARoF link we performed some simulations focusing on the signal quality impact. Practically, the D values of the fiber can be calculated from the zero dispersion wavelength and dispersion slop at the zero dispersion wavelength as in [33]:

$$D(\lambda) = \frac{S_o}{4}\left(\lambda - \frac{{\lambda_o}^4}{\lambda^3}\right) \tag{4.4}$$

where D (λ) is the fiber chromatic dispersion parameter at the C-band, S_o is the dispersion slope at the zero dispersion wavelength, λ is the wavelength at the C-band and λ_o is the zero dispersion

wavelength, respectively. The dispersion as a function of temperature can be expressed as in [33] by considering that both parameters in equation 4.4 (S_o and λ_o) are temperature dependent:

$$\frac{dD}{dT} = \frac{1}{4}\left(\lambda - \frac{{\lambda_o}^4}{\lambda^3}\right)\frac{dS_o}{dT} - \frac{S_o{\lambda_o}^3}{\lambda^3}\frac{d\lambda_o}{dT} \tag{4.5}$$

where dS_o/dT and $d\lambda_o/dT$ parameters represent the variation of S_o and λ_o with temperature respectively.

We then calculated the chromatic dispersion dependency on temperature for different wavelengths within the C-band for a standard silica SMF, as shown in Fig. 4.26, by using Eqs. (4.3) and (4.4). S_o and λ_o and their variations are taken from [33]. As we can see as the temperature increases, the dispersion parameter is slightly decreased which may have a noticeable impact on ARoF system, as pointed out in previous sections. Moreover, the expected D variations due to temperature represented in Fig. 4.26 are of the same order of magnitude to those studied in section 4.3.1.1 where even small changes of 0.1 ps/nm/km can significantly change the critical length L_1 (transmission distance where the first RF fading occurs) and shift the frequency-length product to higher distances.

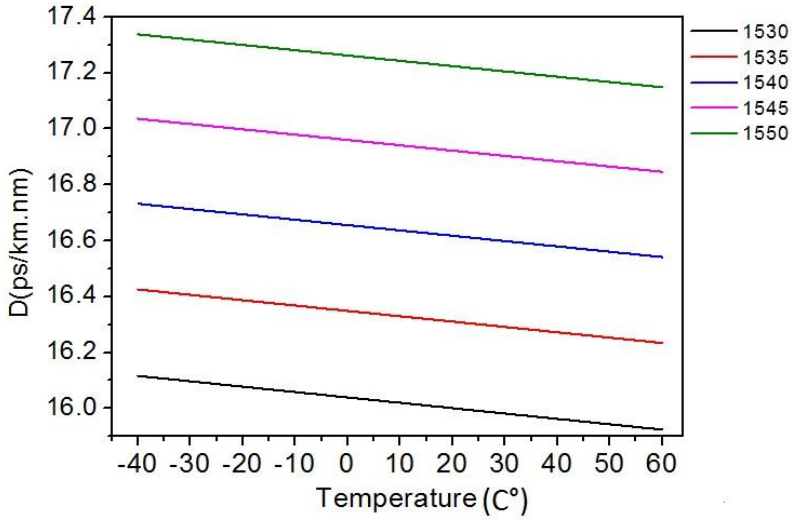

Fig. 4.26: Simulation of chromatic dispersion parameter vs. temperature for different wavelengths within the C-band.

From Fig. 4.26, for example, we conclude that the variation of D of the fiber with respect to temperature (△D/△T) when working at 1550 nm will be around 0.0022 ps/nm/km/C° If we compare this value with the simulation results in Fig. 4.15 and 4.16, 0.05 ps/nm/km D variation can be resulted from a T increment of about 22.5 C°. These D variations can be critical in terms of EVM while working near L_1 as shown in Fig. 4.15 and Fig. 4.16.

4.3 Experiments

In this section we experimentally test 5G NR transmission over SMF to check the tendency and validity of the simulation study presented above. These measurements are performed in collaboration with PhD student J. D. López-Cardona. Different modulation formats are tested and for different links lengths. Firstly, the experimental setup is described in details for wired (over SMF) and wireless transmission. Then we show the experimental results for different cases and compare them with the standard. The EVM and constellation diagrams are used as metrics to investigate data signal quality at different transmission conditions. The schematic diagram of the ARoF system implemented is depicted in Fig. 4.27. A laser diode (LD) at 1532 nm with input optical power of +10.44 dBm generates a continuous wave optical signal externally modulated through a Mach-Zehnder modulator (MZM). The SMW200A Vector Signal Generator (VSG) provides the RF carrier signal modulated with a baseband signal defined in the 5G NR standard. This signal drives the MZM and emulates the 5G user data. 256QAM, 64QAM, 16QAM and QPSK modulation formats with 30 kHz subcarrier spacing and 100 MHz bandwidth channels are tested. Different ARoF-based SMF link lengths (1 km, 5 km, and 10 km) are tested. An Erbium Doped Fiber Amplifier (EDFA) is employed to amplify the data signal meanwhile Amplified Spontaneous Emission (ASE) is filtered out by a bandpass optical filter.

A 99:1 coupler is used for monitoring the data traffic power at reception. The data traffic signal is then detected using a 20 GHz bandwidth high-speed photodiode (PD). A RF power amplifier stage is finally employed to amplify the electrical signal prior to the reception stage where the received signal is directly fed to a Vector Signal Analyzer (VSA) with 20 GHz of bandwidth.

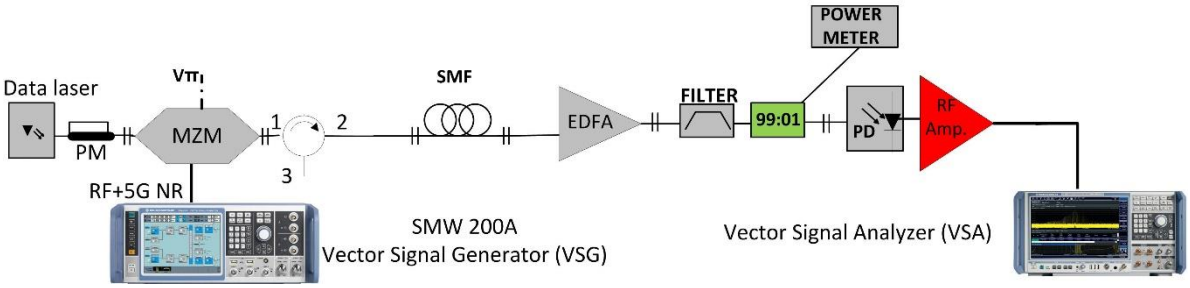

Fig. 4.27: Schematic diagram of the experimental setup implemented to test ARoF over SMF. PM: polarization maintaining fiber.

Metrics such as EVM and constellation diagram are used here to evaluate system performance and compared to the standard [21]. Different carrier frequencies are also considered up to 20 GHz. The different parameters of the setup are set in order to ensure EVM values compliant with standard. The RF input power is set to +10 dBm and data laser power is about +10.44 dBm. The EDFA gain is also set to 24 dB while the RF electrical amplifier gain is about 10 dB.

Set of Fig. 4.28 shows the measured EVM performance of three carrier frequencies, 3, 10 and 20 GHz, for different link lengths and using two modulation formats (QPSK and 16-QAM). As seen for the two lower carrier frequencies (3 and 10 GHz), EVM values are always within the EVM limit defined by the standard with values around 5%-7% for the back to back (B2B) condition and 1, 5 and 10 km-long links. The case is different for the 20 GHz as seen in Fig. 4.28 c where EVM is dramatically degraded at longer link lengths and even exceeding the EVM limit before the 10 km-long case. The significant EVM penalty at a distance of 10 km is consistent with the simulation analysis, using VPI software, carried out in the previous section 4.3.1.1. For 20 GHz of carrier frequency the critical length (L_1) is around 9.4 km according to this simulation analysis. So the fiber link distances around this value show a great penalty in the EVM figure of merit due to the RF power fading because of the chromatic dispersion influence.

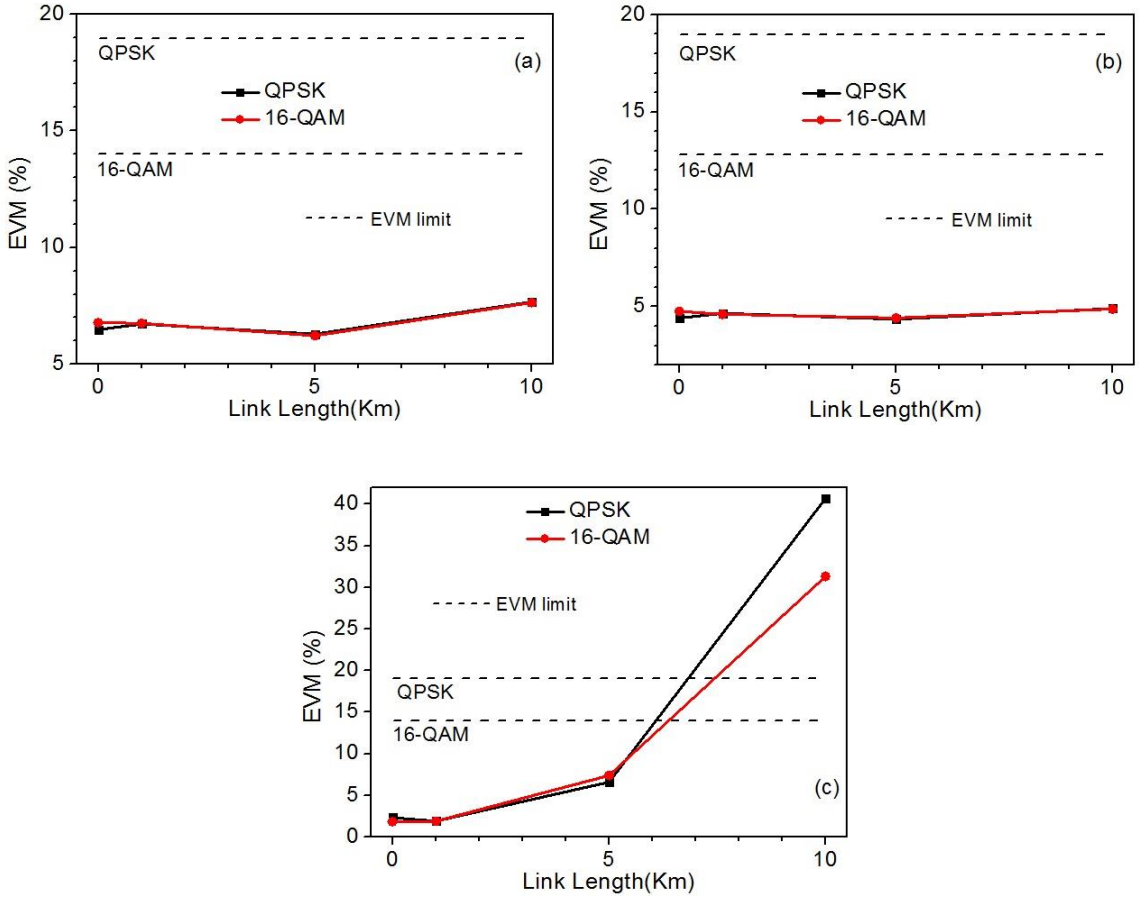

Fig. 4.28: Measured EVM vs. Link length for QPSK and 16-QAM (a) 3 GHz (b) 10 GHz (c) 20 GHz. Dashed lines refer to the EVM limit defined by the standard depending on the modulation format considered.

The constellation diagrams for the measured cases of RF carrier frequency of 20 GHz are shown in Fig. 4.29 for the two modulation formats and for 5 km and 10 km, respectively.

The figures show how the symbols are particularly affected by the RF power fading at 10 km. For QPSK modulation, the measured RF received power is -28.44 dBm at 10 km compared to – 12.1 dBm and – 10 dBm for the 5 km and back-to-back, respectively. For 16-QAM the same behavior is observed with a measured RF received power of -28.95 dBm at 10 km whereas -12.10 dBm and -9.30 dBm for 5 km and back-to-back, respectively.

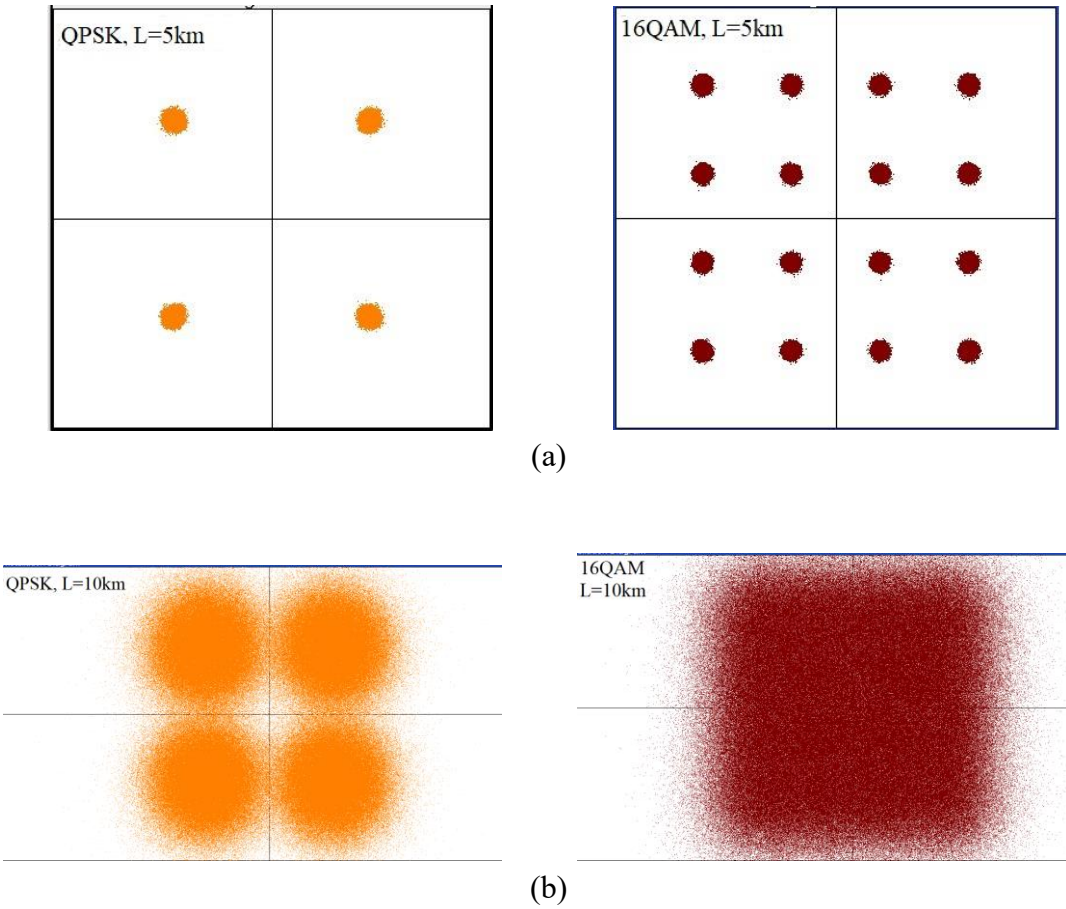

Fig. 4.29: Measured constellation diagram at RF carrier frequency of 20 GHz. (a) 5 km. Left: QPSK, EVM 6.60%. Right: 16-QAM, EVM 7.40%. (b) 10 km. Left: QPSK, EVM 40.67%. Right: 16-QAM, EVM 31.31%.

We then compare both experimental and simulation results by emulating the experimental parameters through new simulations for the 16-QAM modulation format. The linearizer model is not applied here as it is not used in the experiments. Also in the simulation for a better comparison we consider the real distance of SMF spool of 10 km measured by Optical Reflect Time Domain Reflectometer (OTDR) which is about 10.86 km. Results are shown in Fig 4.30. As the chosen experimental link length is close to critical length (see Table 4.2), different D values are simulated. By simulating chromatic dispersion of 15.1 ps/nm/km, the same behaviour is resulted for both experiments and simulations being EVM linearly degrade

up to 10 km, real chromatic dispersion can be around this value. In fact, this value can have some variations depending on experiments conditions or environments, for instance fiber temperature as we discussed.

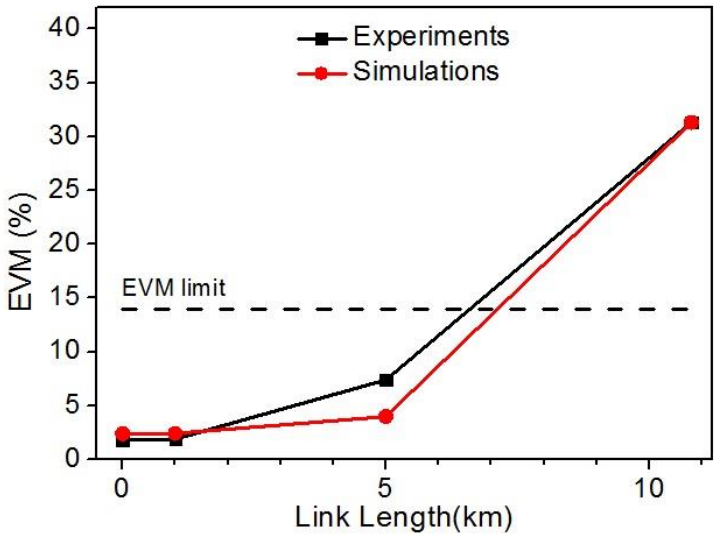

Fig. 4.30: Comparison between experimental and simulation results for the case of 16-QAM, RF 20 GHz by emulating experimental parameters in the simulation and considering chromatic dispersion of 15.1 ps/nm/km.

Additional measurements are done considering more advanced modulation formats (64-QAM and 256-QAM) to further investigate the RF fading effect and EVM behavior. Different carrier frequencies for a 10 km-long fiber link. The main results are summarized in Table 4.3. In all cases, the EVM is kept under the aforementioned EVM limit defined by the 5G standard. Different parameters within the setup are carefully investigated and set to achieve a RoF transmission with acceptable EVM values. As an illustrative example, Fig. 4.31 shows the constellation diagram for 64-QAM and 256-QAM modulation formats for a RF carrier frequency of 15 GHz.

Table 4.3
EVM measured values for RoF transmission over 10 km-long SMF for different carrier frequencies and modulation formats

Frequency (GHz)	EVM%	
	64-QAM	256-QAM
3	3.91	3.25
8	3.62	2.91
15	4.2	3.39

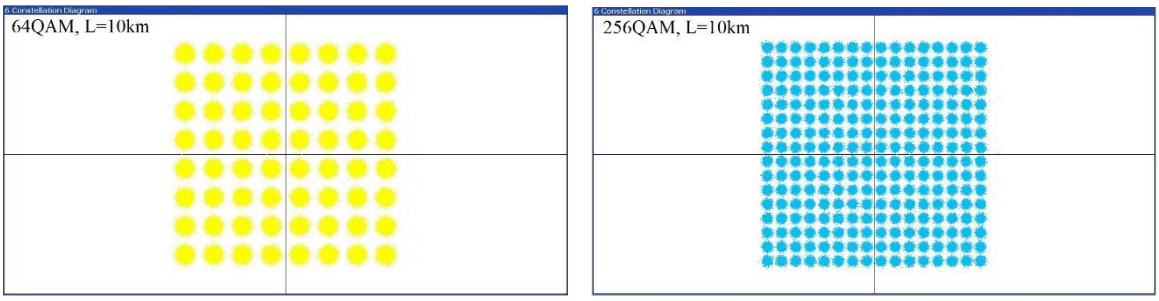

Fig. 4.31: Constellation diagram at RF 15 GHz for 10 km SMF. Left: 64-QAM, EVM 4.2%. Right: 256-QAM, EVM 3.39%.

Moreover, additional experiments are implemented with ARoF based wireless transmission to proof the concept of future 5G signals in a full system. Also to check the feasibility of RF transmission with frequency band higher than sub-6 GHz band.

A 15 GHz ARoF wireless link up to 70 cm with 50 MHz of signal bandwidth is implemented utilizing the same experimental setup shown in Fig. 4.24. The output from the high-speed photodiode is connected to a transmitting horn antenna where the modulated data traffic propagated to a receiving horn antenna, the latter connected to the test equipment (VSA) as shown in Fig. 4.32. The performance is tested for QPSK and 16-QAM modulation formats with an EVM of 10.12% and 9.80% respectively when there is no fiber transmission. After 10 km wired and 70 cm wireless transmission for 15 GHz transmission EVM is kept within the standard with values of 12.40% and 13.21% for QPSK and 16-QAM respectively. Working with this carrier frequency and link length of 10 km no power fading due to D is expected as the critical length is around 17 km, as it is concluded from the previous simulation study (see Fig. 4.10 and Table 4.2). For this reason, experimental EVM values compliant with EVM standard limits are obtained.

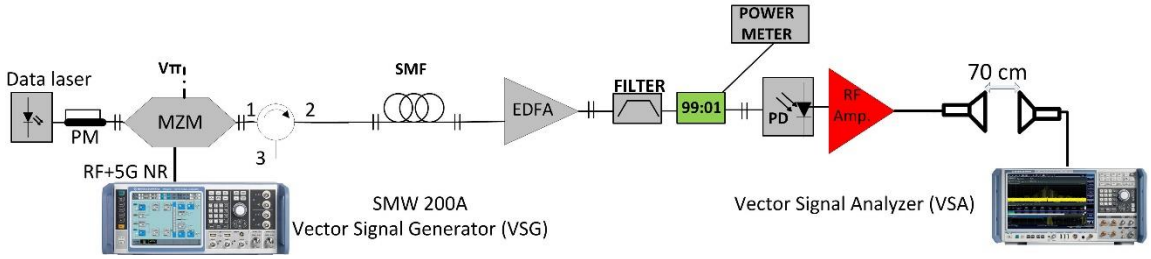

Fig. 4.32: Schematic diagram of the ARoF-based experimental setup with wireless transmission.

Fig. 4.33 shows the experimental setup for the wired and wireless links. Also some of the components used are shown separately. The same setup is used for all link lengths of SMF.

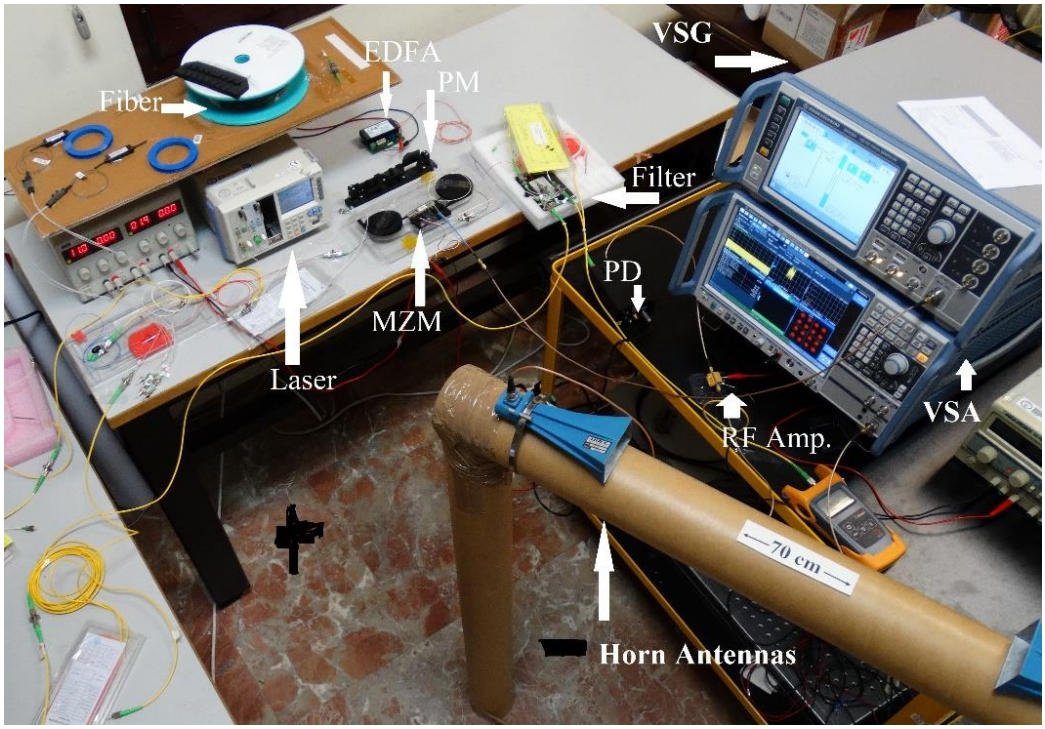

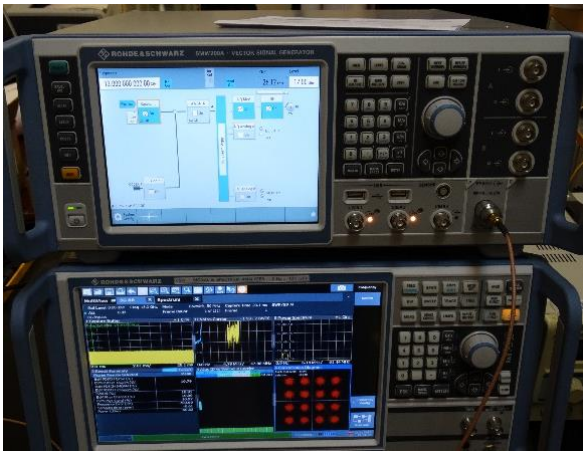

Fig. 4.33: Photo of the experimental setup to show the different components employed.

4.4 Conclusions

In this chapter we address the potential of ARoF transmission in C-RAN for future 5G cellular networks. We propose and characterize the transmission of 5G NR numerology over single mode fibers using ARoF link. Extensive simulation results based on VPI software are presented. The results discuss the different design link aspects such as the fiber length or the RF carrier frequencies suitable for future designing of 5G optical front-haul networks. The results show the importance of considering the impact of fiber impairments, mainly chromatic dispersion when considering 5G mm-wave carrier frequencies and ARoF transmission. For instance, at 30 GHz of carrier frequency the RF power fading due to chromatic dispersion of the fiber is expected to occur at 4 km with periodic notches at 12 km thus leading to EVM values beyond the limits imposed by the 5G standard and meaning an unfeasible high-speed data fiber link design. In special cases, the non-linear effects like Kerr is of importance too. Some of the simulations results are supported by experimental characterization and measurements. Set of experiments are implemented with fiber transmission up to 10 km and wireless transmission up to 70 cm with different RF carrier frequencies up to 20 GHz. It is possible to get experimental EVM values within the standard limits for links up to 10 km and RF carrier frequencies up to 15 GHz and for different modulation formats includes more advanced ones (such as 256-QAM). Different metrics are used to evaluate the performance. The impact of temperature on D of the fiber is briefly studied too. The analysis shows that the increment in temperature can cause D variations. These variations might be of most importance when working with RF frequencies near their critical lengths as we show with the results presented in the chapter. For example, 1 C° increment in temperature can cause D variation of 0.0022 ps/nm/km. We also discuss how these increments in T can affect EVM.

4.5 References

[1] T. Umezawa, P. T. Dat, K. Kashima, A. Kanno, N. Yamamoto, and T. Kawanishi, "100-GHz radio and power over fiber transmission through multicore fiber using optical-to-radio converter," *Journal of Lightwave Technology*, vol. 36, no. 2, pp. 617–623, Jan. 2018.

[2] D. Wake, A. Nkansah, and N. J. Gomes, "Radio over fiber link design for next generation wireless systems," *Journal of Lightwave Technology*, vol. 28, no. 16, pp. 2456–2464, Aug. 15, 2010.

[3] Cisco VNI Forecast: "Cisco Visual Networking Index: Global Mobile Data Traffic Forecast Update, 2017—2022," Cisco Public Information, 2019, Available Online, Accessed on 2020: https://s3.amazonaws.com/media.mediapost.com/uploads/CiscoForecast.pdf

[4] International Telecommunication Union (ITU) - Telecommunication Standardization Sector, Geneva, FG IMT-2020: Report on Standards Gap Analysis, 2016.

[5] K. Kanta et al., "Analog fiber-wireless downlink transmission of IFoF/mmWave over in-field deployed legacy PON infrastructure for 5G front-hauling," *IEEE/OSA Journal of Optical Communications and Networking*, vol. 12, no. 10, pp. D57-D65, October 2020.

[6] K. Tanaka and A. Agata, "Next-generation optical access networks for C-RAN," in *Proc. Optical Fiber Communications Conference and Exhibition (OFC)*, pp. 1-3 Los Angeles, USA, 2015.

[7] C. Tsai, Y. Chi, P. Peng and G. Lin, "Long-reach MMWoF using single-sideband modulated dual-mode VCSEL with 16-QAM OFDM at 8 Gbit/s," in *Proc. Optical Fiber Communications Conference and Exhibition (OFC)*, Los Angeles, CA, pp. 1-3, 2017.

[8] G. Giannoulis et al., "Analog Radio-over-Fiber Solutions for 5G Communications in the Beyond-CPRI Era," in *Proc. 20th International Conference on Transparent Optical Networks (ICTON)*, Bucharest, pp. 1-5, 2018.

[9] H. Kim, "RoF-based Optical Front-haul Technology for 5G and Beyond," in *Proc. Optical Fiber Communications Conference and Exposition (OFC)*, San Diego, CA, pp. 1-3, 2018.

[10] S. Rommel, et al., "Towards a Scaleable 5G Front-haul: Analog Radio-over-Fiber and Space Division Multiplexing," *Journal of Lightwave Technology*, vol. 38, no. 19, pp. 5412-5422, 1 Oct.1, 2020.

[11] Checko, H. L. Christiansen, Y. Yan, L. Scolari, G. Kardaras, M. S. Berger, *et al*., "Cloud RAN for Mobile Networks—A Technology Overview," *IEEE Communications Surveys & Tutorials*, vol. 17, no. 1, pp. 405-426, 2015.

[12] C. Ranaweera, E. Wong, A. Nirmalathas, C. Jayasundara and C. Lim, "5G C-RAN architecture: A comparison of multiple optical front-haul networks," in *Proc. International Conference on Optical Network Design and Modeling (ONDM)*, Budapest, Hungary, 2017.

[13] M. Matsuura and Y. Minamoto, "Optically Powered and Controlled Beam Steering System for Radio-Over-Fiber Networks," *Journal of Lightwave Technology*, vol. 35, no. 4, pp. 979-988, 15 Feb.15, 2017.

[14] G. Raybon et al., "Single carrier high symbol rate transmitter for data rates up to 1.0 Tb/s," in *Proc. Optical Fiber Communications Conference and Exhibition (OFC)*, Anaheim, CA, pp. 1-3, 2016.

[15] I. A. Alimi, A. L. Teixeira and P. P. Monteiro, "Toward an Efficient C-RAN Optical Front-haul for the Future Networks: A Tutorial on Technologies, Requirements, Challenges, and Solutions," *IEEE Communications Surveys & Tutorials*, vol. 20, no. 1, pp. 708-769, 2018.

[16] J. Kani, J. Terada, K. Suzuki and A. Otaka, "Solutions for Future Mobile Front-haul and Access-Network Convergence," *Journal of Lightwave Technology*, vol. 35, no. 3, Feb. 2017, pp. 527–534.

[17] T. Salgals, A. Ostrovskis, A. Ipatovs, V. Bobrovs and S. Spolitis, "Hybrid ARoF-WDM PON Infrastructure for 5G Millimeter-wave Interface and Broadband Internet Service," *Photonics & Electromagnetics Research Symposium - Fall (PIERS - Fall)*, pp. 2161-2168, Xiamen, China, 2019.

[18] J.S. Wey and J. Zhang, "Passive Optical networks for 5G evolution", in *Proc. SPIE Broadband Access Communication Technologies XII 10559*, pp. 105590N, California, United States, 2018.

[19] Nanni , J. Polleux, C. Algani, S. Rusticelli, F. Perini and G.Tartarini, ‘‘VCSEL-Based Radio-over-G-652 Fiber System for Short-/Medium-Range MFH Solutions,’’ *Journal of Lightwave Technology*, vol. 36, no 19, pp. 4430-4437, October 2018.

[20] A. A. Zaidi, R. Baldemair, V. Moles-Cases, N. He, K. Werner and A. Cedergren, "OFDM Numerology Design for 5G New Radio to Support IoT, eMBB, and MBSFN," *IEEE Communications Standards Magazine*, vol. 2, no. 2, pp. 78-83, June 2018.

[21] 3GPP TS 38.104, Rel. 15. 3GPP, March 2018.

Available Online, Accessed on 2020: https://www.etsi.org/deliver/etsi_ts/138100_138199/138104/15.05.00_60/ts_138104v150500p.pdf,

[22] A. A. Zaidi et al, "Waveform and Numerology to Support 5G Services and Requirements," *IEEE Communications Magazine*, vol. 54, no. 11, pp. 90-98, November

2016.

[23] Available Online, Accessed on 2020: https://www.ngmn.org/work-programme/5g-white-paper.html

[24] C. Tsai, Y. Chi, P. Peng and G. Lin, "Long-reach MMWoF using single-sideband modulated dual-mode VCSEL with 16-QAM OFDM at 8 Gbit/s," in *Proc. Optical Fiber Communications Conference and Exhibition (OFC)*, Los Angeles, CA, pp. 1-3, 2017.

[25] H. H. Elwan, J. Poette and B. Cabon, "Simplified Chromatic Dispersion Model Applied to Ultrawide Optical Spectra for 60 GHz Radio-Over-Fiber Systems," *Journal of Lightwave Technology*, vol. 37, no. 19, pp. 5115-5121, 1 Oct.1, 2019.

[26] U. Gliese, S. Norskov and T. N. Nielsen, "Chromatic dispersion in fiber-optic microwave and millimeter-wave links," *IEEE Transactions on Microwave Theory and Techniques,* vol. 44, no. 10, pp. 1716-1724, Oct. 1996.

[27] P. C. Won, W. Zhang and J. A. R. Williams, "Self-Phase Modulation Dependent Dispersion Mitigation in High Power SSB and DSB + Dispersion Compensated Modulated Radio-over-Fiber Links," in *Proc. IEEE MTT-S International Microwave Symposium Digest*, pp. 1947-1950, San Francisco, CA, 2006.

[28] H. Schmuck, "Comparison of optical millimetre-wave concepts with regard to chromatic dispersion," *IET Electronics Letters*, vol. 31, no. 21, pp. 1848-1849, 1995.

[29] H. Li et al., "Real-Time 100-GS/s Sigma-Delta Modulator for All-Digital Radio-Over-Fiber Transmission," *Journal of Lightwave Technology*, vol. 38, no. 2, pp. 386-393, 15 Jan.15, 2020.

[30] Katsumi Takano, Takashi Murakami, Yuki Sawaguchi, and Kiyoshi Nakagawa, "Influence of self-phase modulation effect on waveform degradation and spectral broadening in optical BPSK-SSB fiber transmission," *Optics Express*, vol. 19, pp. 9699-9707, 2011.

[31] Xiaojun Liang and Shiva Kumar, "Analytical modeling of XPM in dispersion-managed coherent fiber-optic systems," *Optics Express,* vol. 22, pp. 10579-10592, 2014.

[32] M. J. Hamp, J. Wright, M. Hubbard, and B. Brimacombe, "Investigation into the temperature dependence of chromatic dispersion in optical fiber," *IEEE photonic Technology Letters.,* vol. 14, no. 11, pp. 1524–1526, Nov. 2002.

[33] P. Andre and A. N. Pinto, "Chromatic dispersion fluctuations in optical fibers due to temperature and its effects in high speed optical communication system,", *Optics communication*, Elsevier 2004.

Chapter 5:

Integration of Power-over-Fiber in Radio-over-Fiber Systems for 5G Cellular Networks

This chapter integrates and analyzes the potential of Power-over-fiber (PoF) in some parts of future 5G cellular solutions based on radio access networks considering currently installed front-haul solutions with single mode fibers. The integration of optically powered communication systems for 5G new radio (NR) data transmission is described. PoF signals up to 2 W are experimentally injected in parallel with the designed Radio over Fiber (RoF) system that was characterized and implemented in **Chapter four**. 256QAM, 64QAM, 16QAM and QPSK data traffic with 100 MHz of bandwidth are transmitted simultaneously with the PoF signal for link lengths ranging from 100 m up to 10 km showing an EVM compliant with 5G NR standard. The utilization of PoF technology to optically powering remote units and Internet-of-Things (IoT) solutions based on RoF links is also discussed. Some examples of low power consumption radio cells, IoT sensors and different RF components are provided. The feeding capability of the designed PoF system is also addressed. The impact of high power levels of PoF signal on data signal quality is analysed in detail by experiments and simulations. Metrics such as EVM, constellation diagrams and RF spectrums are used for this purpose.

5.1 Introduction

Power-over-Fiber (PoF) is now seen as a realistic option to feed some reconfigurable elements in optical access networks with single mode fibers (SMF) [1]. And to optically powering remote radio units (RRUs) through specialty fibers such as double-cladding fibers for high power levels [2] or multicore fibers for high data rates demands in future mobile front-haul with analog RoF (ARoF) [3,4] with space division multiplexing (SDM) capabilities. The reduction of the cell size of RRUs boosted to support the bandwidth demands of RF signals targeted by the upcoming 5G technology will mean a dramatic increment in the number of RRUs installed. Affordable deployments require simplified low power consumption RRUs as those described in [5] that require less than 100 mW. As 5G requirements, and so related equipment, envisage smaller cell coverage to support the RF signals on demand, technology is going towards low power consumption solutions. This scenario opens up new application niches for PoF technology [6] thus allowing dynamic control of RRUs powering based on specific strategies using energy optimization algorithms, driving the required significant reduction of power demands of future 5G-based RRUs. This can solve many economic and environmental consequences due to the rapid growth in the data traffic demand and so in energy consumption due to a massive antenna deployment in mobile networks [7].

The use of passive optical networks (PONs) for wireless data convergence has been investigated and trialed so far even for future 5G optical network deployments [8]. With the recent growth in the deployment of optical access networks, optical fiber is almost ubiquitous and found very close to the customers, exactly where it is required for small-cell access networks that are based on RoF techniques.

On the other hand, and as discussed in **Chapter four,** Analog RoF (ARoF) is a promising candidate for the future 5G mobile front-haul due to its important advantages like low transmission loss and the simplicity required at the RRU, also providing the bandwidth requirements demand by 5G. So that ARoF-based C-RANs can face all challenges addressed by the upcoming 5G technology like high data rates, low latency and energy consumption [9]. Some experiments of analog transmission of 5G NR signals over SMF were reported in [10].
In this scenario, from the point of view of operators, there is a considerable interest in the reuse of the already deployed broadband fiber networks, being SMFs the most popular and widely used mean for these optical fiber-based infrastructures. While introducing remote powering capabilities via optical fiber means, the PoF technique also allows a simple way to transmit optical data and power simultaneously into optical fibers beyond employing a dedicated fiber channel to perform the PoF feature [11].

Moreover, in future 5G networks, envisaging a huge number of RRUs deployed in densely populated areas or events, the coexistence of PoF and data signals over the same single-

channel may lead to important installation savings and simplifying the entire broadband access network. Additionally, it can be cost-effective solution. SMF fiber small core area limits the maximum optical power launched [12] into a single channel in PoF applications, as previously pointed out within **Chapter Three**. And similar considerations apply for any single mode individual core of a multicore fiber (MCF) [13]. However, in future low power consumption femtocells or in energy optimized scenarios using PoF to provide sleep-mode RRU operation as an added-value PoF functionality, those power levels can be enough. The evolution to a broadband access networking architecture compliant with a cost-effective network operation envisions the coexistence of PoF and data traffic signals over the same SMF-based channel. Then the simultaneous injection of high-power laser (HPL) signals for PoF purposes in a fiber channel requires analyzing the impact of the latter on the data traffic signal quality as well as a discussion about the PoF requirements to assure a negligible data traffic penalty.

Hence in this chapter, we propose the use of SMF to implement a C-RAN front-haul architecture connecting the central office (CO) to the remote radio units (RRUs) for future 5G cellular ARoF-based networks together with the possibility of optically powering RRUs or other components in the transmission system. We integrate the potential of the PoF technology on the previously deployed ARoF systems with 5G numerology [14] described in **Chapter four**. We experimentally address the impact on Error Vector Magnitude (EVM) when introducing a PoF signal over SMF for remote feeding purposes on different carrier frequencies of radio data transmission. The EVM performance and evolution for different modulation formats and link lengths for different PoF power levels is analyzed. Safety power levels for coexistence of data and energy with negligible impact are derived. The potential of using PoF technology in RoF systems for future 5G front-haul is also discussed. We analyze by simulations the fiber nonlinearities that can affect the quality of the transmitted 5G signals. The measurements included in this chapter are performed in collaboration with PhD student J. D. López Cardona.

5.2 Integration of Power over Fiber in the Front-haul of Future Mobile Communication

A detailed study about the state of the art of PoF technology being applied to RoF systems is presented in our research group work [13] that is partially related to this PhD work. However, this work presents for the first time to the best of our knowledge the integration of PoF in a ARoF link using standard single mode fibers with 5G NR signals. It also represents a first approach towards SDM solutions based on MCF [13].

A scenario for its implementation in crowded environments with in building connections like commercial malls, metro stations or football stadiums is proposed. As a use case, we consider the football stadium where high connectivity is required for different events that

might be held in such places. Stadiums have been already considered as launching events by the 5G pan-European trials road map [15] where some 5G services are to be tested during the upcoming UEFA Euro 2020 confirmed to take place during 2021. However, some trials have been already performed in some stadiums in Europe. Different services can be provided like virtual reality applications, live sport streaming and other entertainment applications inside, around and in the fans zone of the stadium. For that, we proposed a solution that can integrate medium-range links of mm-wave transmission following 5G requirements. This study may help in the design of future Radio over Fiber systems supporting 5G services in such environments and applications where 10 km-long SMF links connecting the BBUs and the RRUs in a centralized fashion can be quite enough for the expected coverage area and type of scenario. SMF can provide an optimal solution for this type of access network, as the first step to expand the capacity in future 5G front-haul solutions tends to exploit the existing infrastructure based on SMF by adding bundles of SMF fiber.

PoF technology is advantageous as it may help to improve the flexibility and reliability of the system. The use of fiber bundles allows the possibility of considering different PoF scenarios i.e shared or dedicated [13]. Additionally, this can partially solve the problem of the small core area of SMF fibers as aforementioned that limits the maximum energy delivered to the remote side by consider more fibers for feeding purposes. Depending on the final application and the power consumption of the hardware component to be remotely powered, PoF technology can be used isolated or in combination with standard electrical power supplies. PoF can be considered not to fully substitute all the mobile front-haul topology using traditional power sources due to the power consumption demands of current base stations and antenna systems (and related coverage area); but to support the new installations in specific areas as a complement or added-value functionality in future cellular networks. PoF can be utilized in the different services that C-RAN can support as integrating in a centralized way multiple IoT devices with its massive deployment requirements [16]. Different RRUs in the network can transmit and receive information from IoT devices while its processing is done in the BBU after sending back the information via the fiber backbone.

On the other hand, IoT in the near future represents a massive number of low power devices connected to the internet with the need of being frequently updated. The current network standard like LTE cannot support efficiently this technology as it is mainly developed for mobile broadband [17]. For that 5G NR can address all the limitations to enable IoT with good functionality. In compliance with the proposed scenario, IoT smart stadium can be easily integrated with the physical infrastructure of a 5G front-haul based on SMF fiber bundles. Thanks to the current low power IoT ecosystems, PoF can be an option to power wireless IoT sensor networks.

Table 1 gives an example of the small radio cells and smart IoT nodes, and their low power consumption, where PoF can be an optimal solution for powering. It also shows some RF communication components with low power consumption. Current radio dot systems

represent energy and cost effective solutions with ideal network performance [18]. The quantity of Dots required is dependent on coverage and performance criteria and will range from 4,000 to 10,000 square feet per Dot, i.e. from around 370 m^2 to 930 m^2. These small cells can be distributed and installed even under fans seats of the stadium. They can connect multiple IoT sensor nodes distributed in the stadium to monitor different environmental conditions like temperature. Low power vision systems based on IoT nodes can replace the traditional concept of cameras [19] sometimes where high resolution systems are not required or low power consumption schemes are preferred.

Table (5.1):
Small Radio Cells with IoT and RF communication low power devices for the considered scenario of the PoF integration in C-RAN for 5G applications

Category	Device	Function	Consumption
Small Radio Cells	Radio Dot System [18]	Small radio cell for Wi-Fi connectivity	< 200 mW**
IoT Sensors	OV9655 smart camera	Monitor people in specific areas	90 mW
	Vison Sensor [19]	Monitoring Fans activities, Gates entrance, Parking	17.9 µW
	HTS221	Measure Temperature	7.2 µW
	BME280 Sensor	Measure Humidity and Pressure	1.32 mW
RF Component	FGA01	Photodiode	40 mW
	ADL5321	Broadband RF driver Amp. For a variety of applications e.g. cellular infrastructure, defense equipment, instrumentation equipment	122 mW
	LTC6242	Low noise Single-Ended input to different output amplifiers	50 mW
	ADF41020	Microwave PLL synthesizer to implement optical oscillator	94.5 mW

**Depending on the operation mode (explained in the feeding capability section)

5.2.1 Power-over-Fiber Scenarios

This section describes in detail the structure of the proposed optical front-hauling network in our selected use case (football stadium) with the integration of PoF. Different feeding possibilities or architectures are proposed. Fig. 5.1 shows the configuration of the proposed C-RAN network where radio transmission between base band units (BBUs) at CO and variety of RRUs (Radio Dots) is done in a centralized way. The evolution towards centralized topologies for radio access networks conforming the front-haul infrastructure for mobile

networks is assumed for the configuration of the PoF system depicted in Fig. 5.1 thus obtaining a centralized PoF scheme for remote powering purposes. Under this assumption, the PoF source is located at the CO, where the BBU is also located in RoF systems. As we aforementioned, the stadium is taken as a possible representative example but the deployed system can have potential in other areas where 5G is required for mission critical services.

Data and PoF signal are multiplexed at CO and injected in SMF link where currently installed front-haul can be utilized. After SMF transmission, both signals are received at the residential gateway which houses Demux device, data and PoF signals are demultiplexed. Afterwards, data signals are received by different radio dots using SMF in ring topology by exploiting network switches. The residential gateway will also deliver energy to IoT nodes and radio dots in a star topology by employing asymmetric power splitters [20] for energy distribution depending on the power consumption of each device.

However, the solution of optical splitters with different IoT configurations is also optional and can be used separately if PoF is considered to feed IoT sensors in the stadium. However, due to very low power consumption of IoT sensors, the PoF system can still have good functionality even if considering the optical splitter losses.

Focusing on the specific scenario proposed in this chapter, the main idea is not to have a fully optically powered whole stadium coverage by this Radio Dots network but to have this solution in specific areas of the stadium where a better user experience is required. For instance, at premium or VIP areas which depending on the coverage area of single Dots can be enough for this kind of application. These Radio Dots are given within this chapter as an example of real commercial low-power 5G units and where the mid- and long-term market tends with respect to remote units (in terms of power demand). As a first step, these Radio Dots can be installed at specific areas of interest that can be optically powered as we aforementioned.

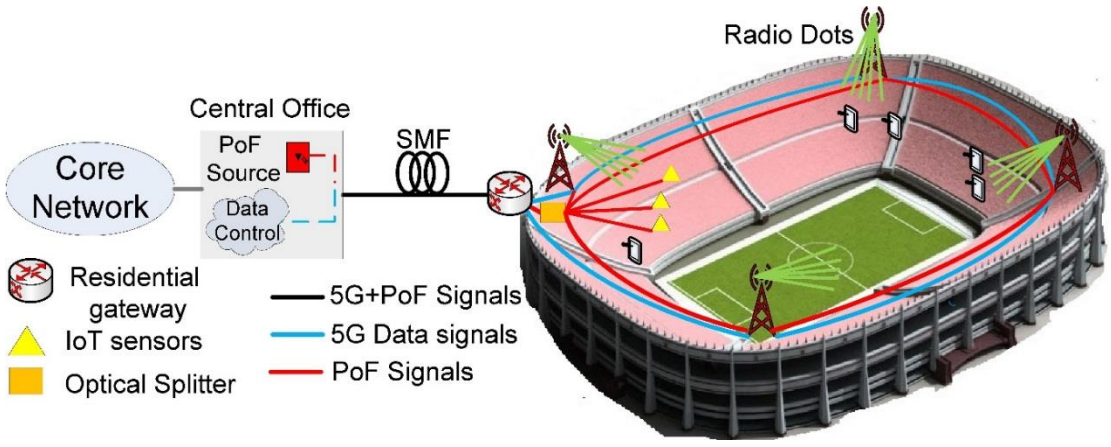

Fig. 5.1: Proposed configuration of SDM-based (SMF bundles) optical front-hauling integrating different optically feeding technologies.

As SMF link will be distributed along the stadium, another powering architecture can be utilized as shown in Fig. 5.2. In this scenario, Remote Nodes (RN) will be at each site of the stadium near the Radio Dots. All the processing for data and PoF signals can be done there. Demux devices can be placed in each RN to separate data from power. Afterwards for the powering, PV cells inside RN can convert the optical power into electrical one and feed the specific Radio Dot and the IoT sensors installed close to it.

The scalability analysis for the proposed PoF system is later analysed in this chapter depending on the experimental results and the delivered energy at the remote site.

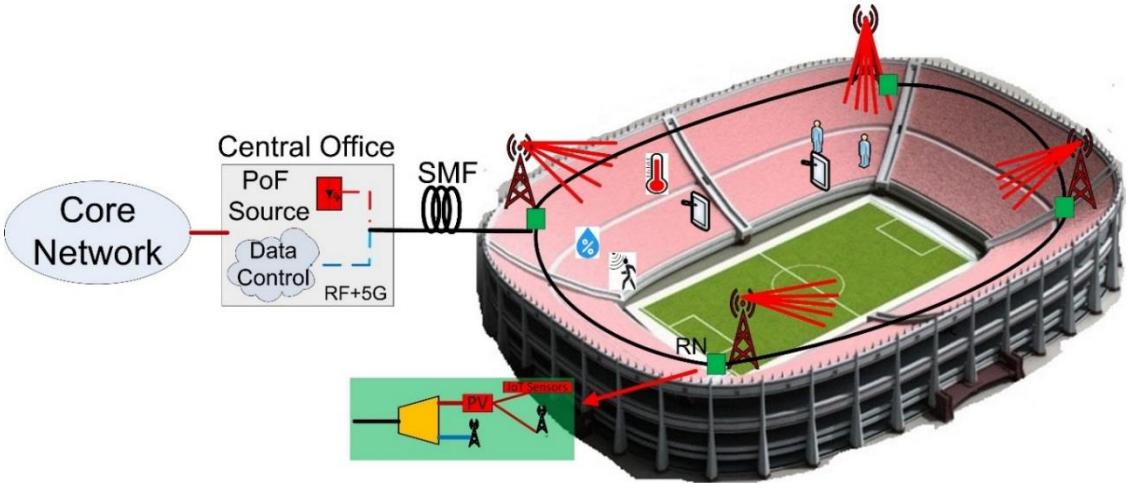

Fig. 5.2: Another possible configuration for SDM-based (SMF bundles) optical front-hauling integrating different optically feeding technologies.

Optically powering such systems can be cost effective and ensure service continuity [21]. The most important aspect in this chapter is to ensure that this technology can be integrated with the infrastructure of the next generation access networks based on RoF and with acceptable penalty (no impact in the ideal case) on the data traffic signal quality. For instance, the proposed system can be integrated within the architecture proposed in [22] where a Fiber-Wireless (Fi-Wi) hybrid approach is considered to support IoT networks. It is based on a network power saving design based on turning into sleep mode some phases of the Optical Network Units (ONUs) in cooperation with the Optical Line Terminals (OLTs) thus bringing additional power economy to the network. Finally, to cope with 5G bandwidth requirements, the targeted and tested frequency bands will be beyond the sub 6 GHz frequency band.

5.3 PoF-RoF System

5.3.1 Experimental testbed

The analog RoF (ARoF) system implemented is depicted in Fig. 5.3, where an inset picture of the experimental setup is included. A laser diode (LD) at 1532 nm generate a continuous wave externally modulated through a Mach-Zehnder modulator (MZM). The SMW200A

Vector Signal Generator (VSA) provide the RF carrier signal modulated with a baseband signal defined in the 5G NR standard. This signal drives the MZM and emulates the 5G user data. 256QAM, 64QAM, 16QAM and QPSK modulation formats with 30 kHz subcarrier spacing and 100 MHz bandwidth channels are tested. The modulated optical carrier (data traffic) is then multiplexed with the HPL PoF signal at 1480 nm (PoF power delivery purposes). The HPL source linewidth is 2 nm. This PoF source is tested for secure continuous operation for at least 5 hours in SMF. This duration can over-span a typical game/match/sport duration which fits with the proposed scenario.

High-power handling multiplexer (MUX) and demultiplexer (DEMUX) devices are used to combine and separate both the PoF and data traffic signals to be transmitted and received. The insertion losses for both Mux and Demux are < 1 dB. Different ARoF-based SMF link lengths (100 m, 5 km, and 10 km) are tested. An Erbium Doped Fiber Amplifier (EDFA) is employed if data signal needs amplification to get the required EVM meanwhile Amplified Spontaneous Emission (ASE) is filtered out by a bandpass optical filter. A 99:1 coupler is used for monitoring the data traffic power at reception. The data traffic signal is then detected using a 20 GHz high-speed photodiode (PD). A RF power amplifier stage is finally employed to amplify the electrical signal prior to the reception stage where two methods are used to detect and analyze 5G transmission performance. In the first one, the signal is directly connected to a vector spectrum analyzer (VSA) with 20 GHz of bandwidth. In the second, a mixer and a local oscillator (LO) are added for down-converting the information signal frequency and receive it within the oscilloscope bandwidth of 2 GHz. In the latter configuration, the EDFA is not employed

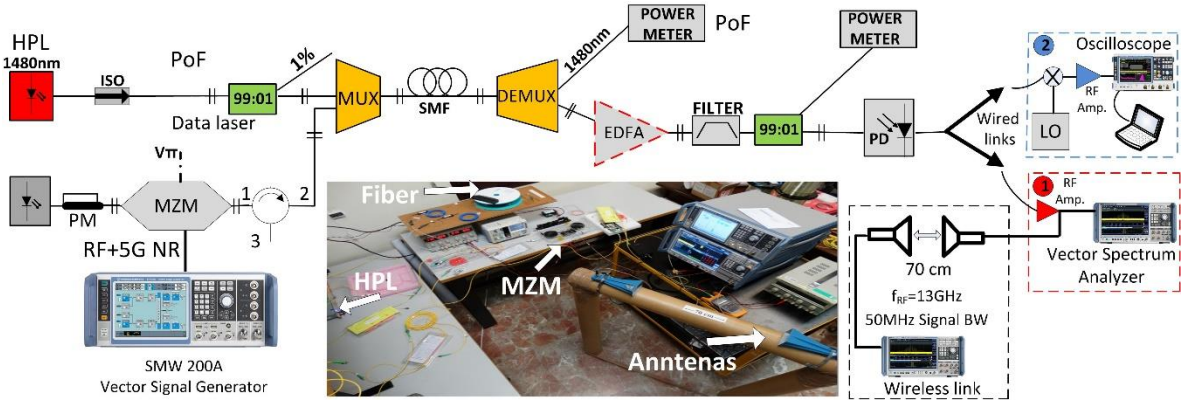

Fig 5.3: Experimental setup for the evaluation of the RoF transmission of 5G NR signals with the coexistence of PoF signals with photo.

The highest link length experimentally tested is 10 km that can be enough to deploy the main scenario proposed in section 5.2. Depending on the simulation results discussed in **Chapter Four**, different RF carrier frequencies up to 20 GHz are launched and experimentally tested. This can help to ensure the difference between working with radio transmission at distances near the critical length (L_1) and distances far from it.

5.3.2 Experimental results

The quality of the data traffic signal is evaluated through the EVM figure of merit. The measured values are compared with the EVM requirements for downlink transmission signals from base stations provided within the 5G NR standard [14]. Fig. 5.4 shows the EVM results for different modulation formats, for an input RF power (P_{RF_IN}) of +12 dBm, a RF frequency carrier of 13 GHz and two link lengths (100 m and 5 km), using the wired set-up reported on Fig. 5.3 (i.e. without the wireless link). Those experimental results show no relevant impact on the system performance for PoF injected power levels below 0.5 W, as EVM keeps under the limits allowed by the 5G NR standard (dashed lines), for both link lengths. This performance is also verified for all HPL powers tests (up to 2W of HPL) for a 100 m-long link (see Fig. 5.4.(a)). Meanwhile at 5 km, the EVM measurements showed a degradation beyond 0.5 W, especially for a 1 W optical power output from the HPL, although the measured values still follow the standard with the exception of the 256QAM modulation test . Due to Mux and other conector/adapter losses, the injected power at fiber input is around 0.82 W and 1.62 W for HPL input power levels of 1 W and 2W respectively. For those two measurements EDFA is employed with constant power mode. We measured data traffic signal power at the reception stage (before PD) to be – 4.566 dBm and – 4.616 dBm for 100 m and 5 km respectively, when HPL is OFF. However, when different power levels from PoF source are injected to the system there are only small variations of received data traffic power (0.01 dB).

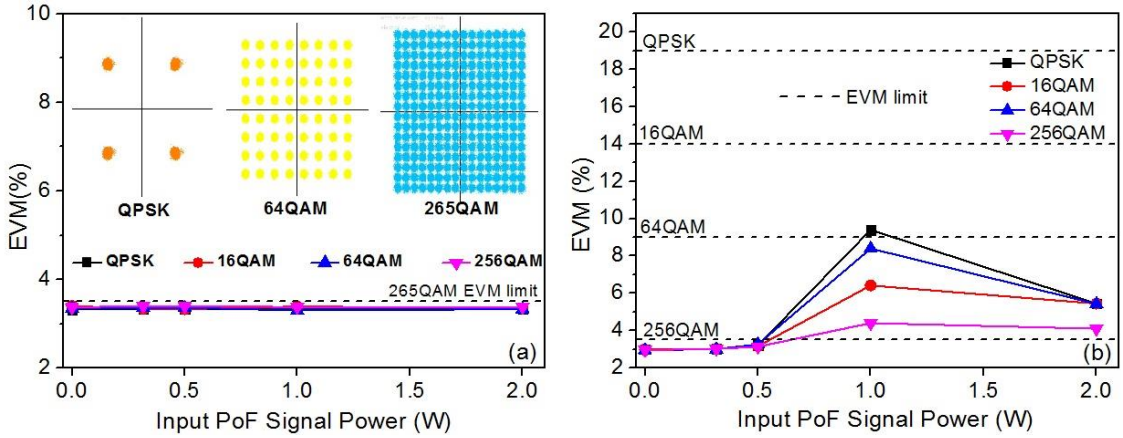

Fig. 5.4: EVM measurements vs input PoF signal of power levels (0, 0.3, 0.5, 1, 2) W. P_{RF_IN}=+12 dBm, f_{RF}=13 GHz. Link length range: (a) 100 m, (b) 5 km.

Fig. 5.5 shows that up to a 0.5 W PoF input signal for a link length of 10 km, there is a negligible impact for the two cases we chose (16-QAM signal at RF 17 GHz, QPSK signal at RF 20 GHz). However, at 1 W of HPL output power the EVM is significantly degraded, being especially dramatic as the resulting EVM exceeds the limit value for the case of 16QAM modulation format. The SMF spool used in the measurements of Fig. 5.5 is exactly 10 km (measured by Optical Time Domain Reflectometer) in order to test the performance

with the higher carrier frequency available from VSA (20 GHz) with longer distances. EVM shows much better performance when HPL is OFF compared with the spool of 10.8 km as we show in **Chapter Four** (Fig. 4.30) as the critical lengths for both 17 GHz and 20 GHz are around 11 km and 13 km respectively for a chromatic dispersion value of 15 ps/nm/km (which is the expected value at 1532 nm). This confirms the importance of considering the critical length for the different carrier frequncies as we discussed in **Chapter Four**. EDFA is not employed for the measurements shown in this figure (Fig. 5.5).

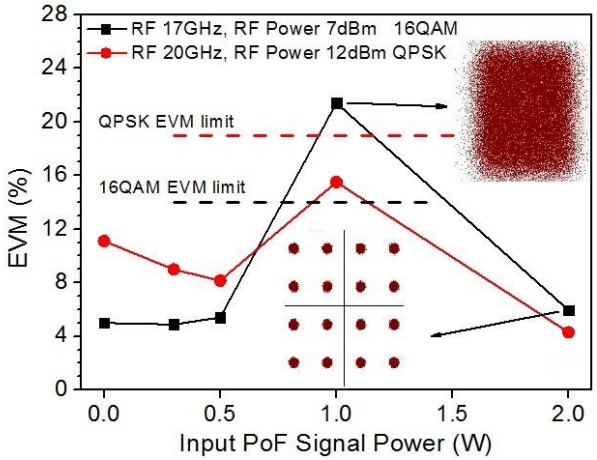

Fig. 5.5: EVM measurements vs input PoF signal, 10 km SMF, Black curve: RF 17 GHz, RF Power 7 dBm, Red curve: RF 20 Ghz, RF Power 14 dBm.

Furthermore, a 13 GHz ARoF wireless link up to 70 cm with 50 MHz of signal bandwidth and with 16-QAM modulation formats is later implemented utilizing the same experimental setup. The output from the high-speed photodiode is connected to a transmitting horn antenna where the modulated data traffic propagated to a receiving horn antenna, the latter connected to the test equipment. The EVM performance of the received signal is then evaluated for different fiber link lengths with simultaneous PoF signal injection as shown in Fig. 5.6. The EDFA is employed with the wireless setup measurements.

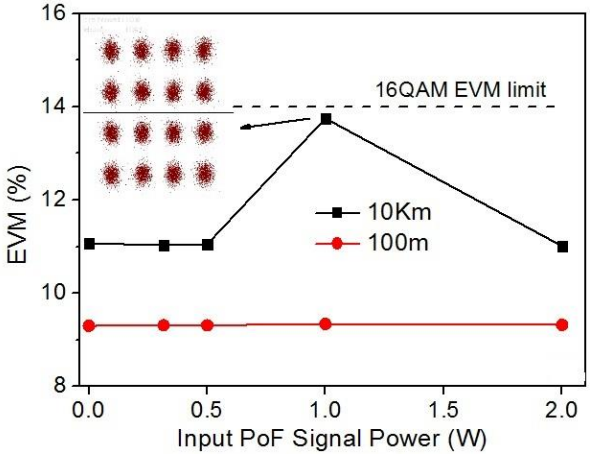

Fig. 5.6: EVM measurements vs input PoF signal for 16QAM EVM after a 70 cm-long ARoF wireless transmission in coexistence with PoF for different injected powers and fiber link lengths P_{RF_IN} = +12 dBm, f_{RF}=13 GHz.

Comparing 16QAM results obtained from both Fig 5.4(b) and those from Fig. 5.6, the EVM degradation for longer link lengths under the same test conditions is also observed due to the power attenuation, in accordance with the results provided in [23] when using a filter to perform single mode operation at 850 nm. As aforementioned, for the last measurements of wireless transmission we select the RF frequency at 13 GHz as it is the highest one that EVM complies with the standard for all link lengths when no PoF signal is applied.

More cases are tested and for higher advanced modulation formats (64-QAM and 256 QAM) as shown in Fig. 5.7. The highest RF frequencies that can achieve an EVM within or close to the EVM standard values are chosen. The same EVM behavior of the other modulation format is obtained with EVM being improved, when HPL input level is 2 W for both measured cases (64-QAM with RF 16 GHz and 256-QAM with RF 13 GHz). The received optical powers for 256-QAM modulation format are – 5.097 dBm and – 4.997 dBm for the case of HPL OFF and 2 W respectively, while for 64-QAM they are -5.066 dBm and – 4.997 dBm respectively. For the other cases of injected HPL levels, the received power is almost the same. This power levels are obtained with an EDFA in constant output power operation mode.
However, for the 256-QAM modulation format, EVM is improved but its value keeps out of the standard limit for higher HPL input levels (1 and 2 W). For 64-QAM EVM is improved for HPL input of 2 W and its value is almost the same as the standard value. A system optimization could improve the EVM results and this could be the case for all other formats.

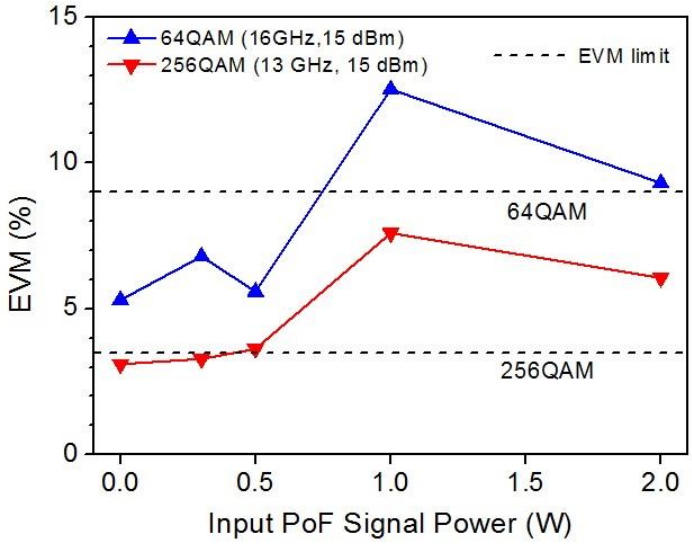

Fig. 5.7: EVM measurements vs input PoF signal of power levels (0, 0.3, 0.5, 1, 2) W for 64QAM and 256QAM for 10 km transmission distance.

As we can see, in some points the EVM is out of the standard when the PoF signal is applied, especially for the 10 km link length with RF of 13 GHz or even higher. In the following

measurements, we address the EVM for different carrier frequencies less than 13 GHz in the 10 km link length for these advanced modulation formats. We select the HPL level at 2 W as it is the one that provides the maximum energy at the remote site and also due to the improvement of the EVM value as compared with 1 W input HPL level. This improvement at 2 W versus 1 W is discussed in the next subsection.

Fig. 5.8 shows the results for two modulation formats, the RF power is chosen as the minimum one to keep EVM within the standard thus being set to+ 7.5 dBm while the RF carrier frequencies are varied from 3 to 11 GHz. As we can see in Fig. 5.8 a and b for 16QAM and 64QAM modulations, respectively, the EVM is kept under the limit for the different carrier frequencies with the highest HPL level applied; especially for the case of 64-QAM. EDFA is employed here too and the received optical power is fixed with small variation.

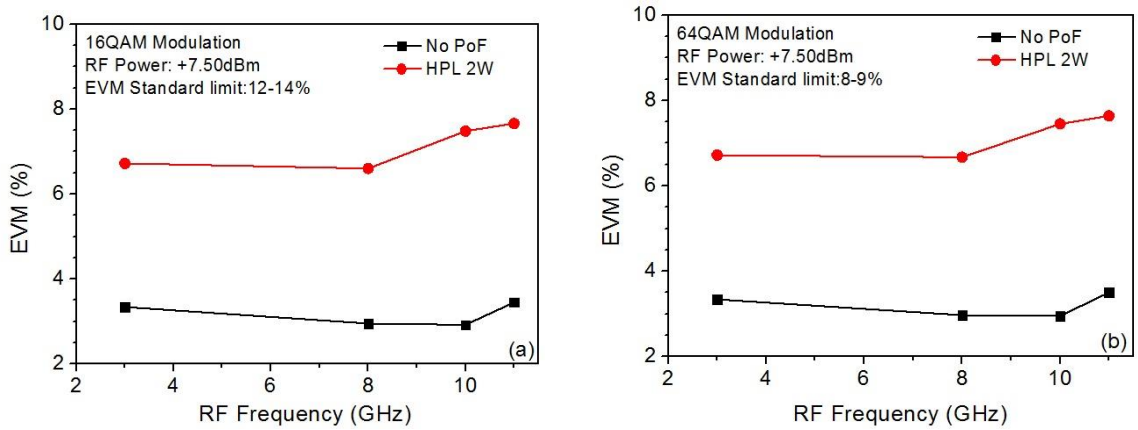

Fig. 5.8: EVM vs. RF carrier frequency for 10 km link length with the coexistence of PoF level of 2W with RF power of 7.5 dBm: (a) 16QAM (b) 64QAM.

In all the measurements reported and for link distances of units of km, the EVM shows negligible impact for PoF signals up to 0.5 W while significantly degraded within the range from 1 W to 2 W. However, it is worth mentioning that beyond 1 W HPL output power (up to 2W) EVM results show a slight improvement. Thus, the PoF signal may additionally contribute to enhance the data traffic signal quality or mitigate some data traffic impairments that are present in optical communication systems. The effect of the RF power and carrier frequency and the type of the modulation format is clearly seen too. In the next section, we explain in detail by further experiments and simulations the reason of this behavior.

5.4 Experimental EVM Performance Discussion

5.4.1 Experimental verification

In this section, we discuss in detail the performance of the implemented RoF link and its EVM figure of merit behaviour in coexistence with the injected PoF signal, especially for longer distances links. As a general trend the EVM suffers a noticeable (negligible or not)

penalty when a PoF signal is injected into the system compared to the HPL OFF status. The main reasons are related to HPL source or PoF channel characteristics. This HPL has a wide spectrum with an optical output spectrum not only at 1480nm, which is the wavelength of interest for PoF purposes, but also with some small additional signals around the C-band, i.e. data transmission band, thus adding extra noise to the communication signal being the EVM consequently degraded. Moreover, the HPL presents some instabilities around 1 W.

Fig. 5.9 shows the HPL spectrum and the experimental setup for measuring it. HPL output signal of + 25 dBm is fed to the optical spectrum analyser (OSA) by using a 99:1 splitter and a filter in order not to damage the OSA (with a maximum input power of 100 mW).

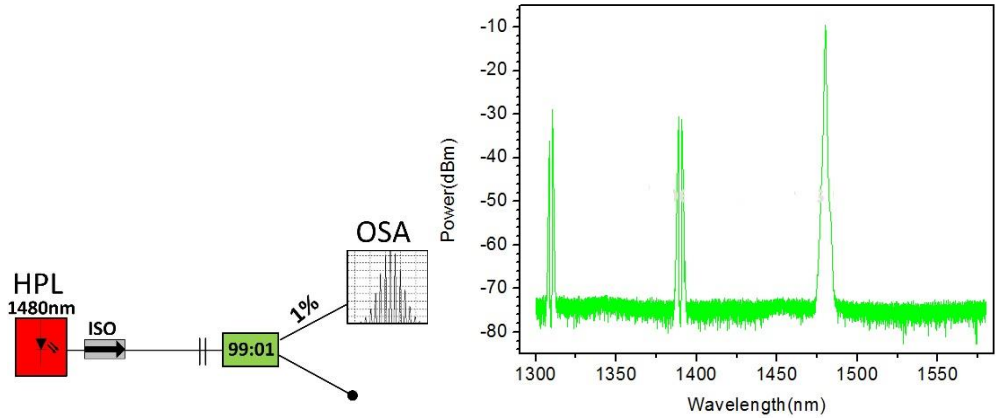

Fig.5.9: Schematic of the setup for measuring HPL spectrum. HPL spectrum at +25 dBm output power.

We also measure the temporal response of the HPL output power to check any HPL instabilities with the experimental setup shown in Fig. 5.10. The optical coupler and Variable Optical Attenuator (VOA) attenuate the output power level from HPL that reaches the photo-detector. The photo-detector output is connected to the oscilloscope.

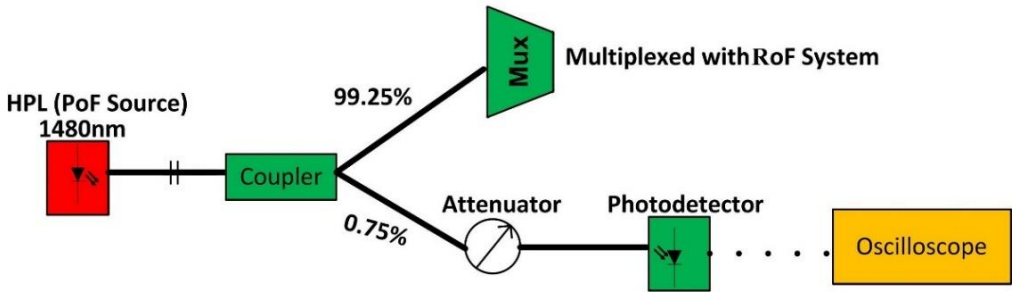

Fig.5.10: schematic diagram of HPL stability measurements.

We measure the average value and noise fluctuations of HPL output at different power levels. For example, we show in Fig. 5.11 the average voltage (DC coupling value) and noise fluctuations (AC coupling values) for three different output power levels from HPL. The noise fluctuations at 1W is higher compared to other power levels which is an additional reason for the EVM degradation at this specific power.

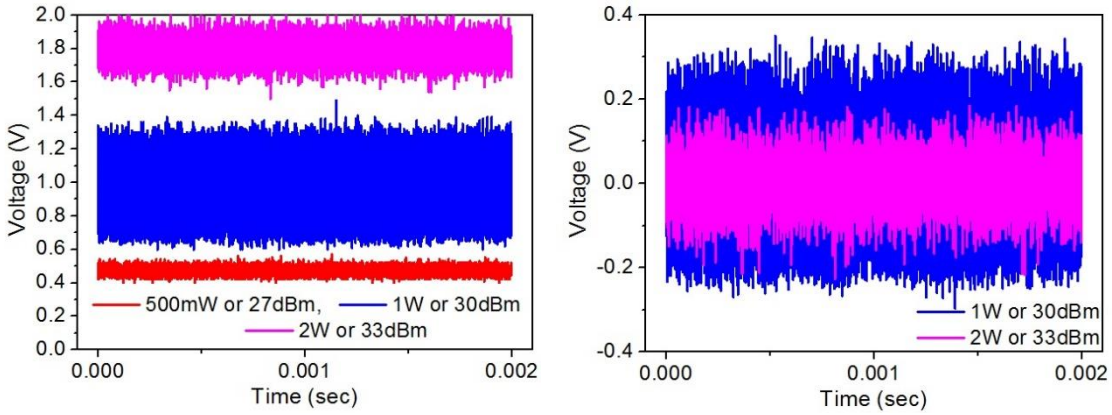

Fig. 5.11: Average DC coupling values for different output optical power of HPL source. Right: Noise fluctuations for different HPL power levels (AC coupling).

However, additional measurements are carried out to measure the temporal response and stability for the received data signal after propagation through the fiber. We measure for different links lengths and with different HPL powers to see if this noise directly affects the signal quality. In Fig. 5.12 (a-c) we show the average value and standard deviation (SD) for the case of 100 m, 5 km and 10 km respectively. In all cases, we use RF carrier frequency of 17 GHz, RF power of +7dBm and 16QAM modulation format. In these measurements, the baseband signal bandwidth is 5 MHz.

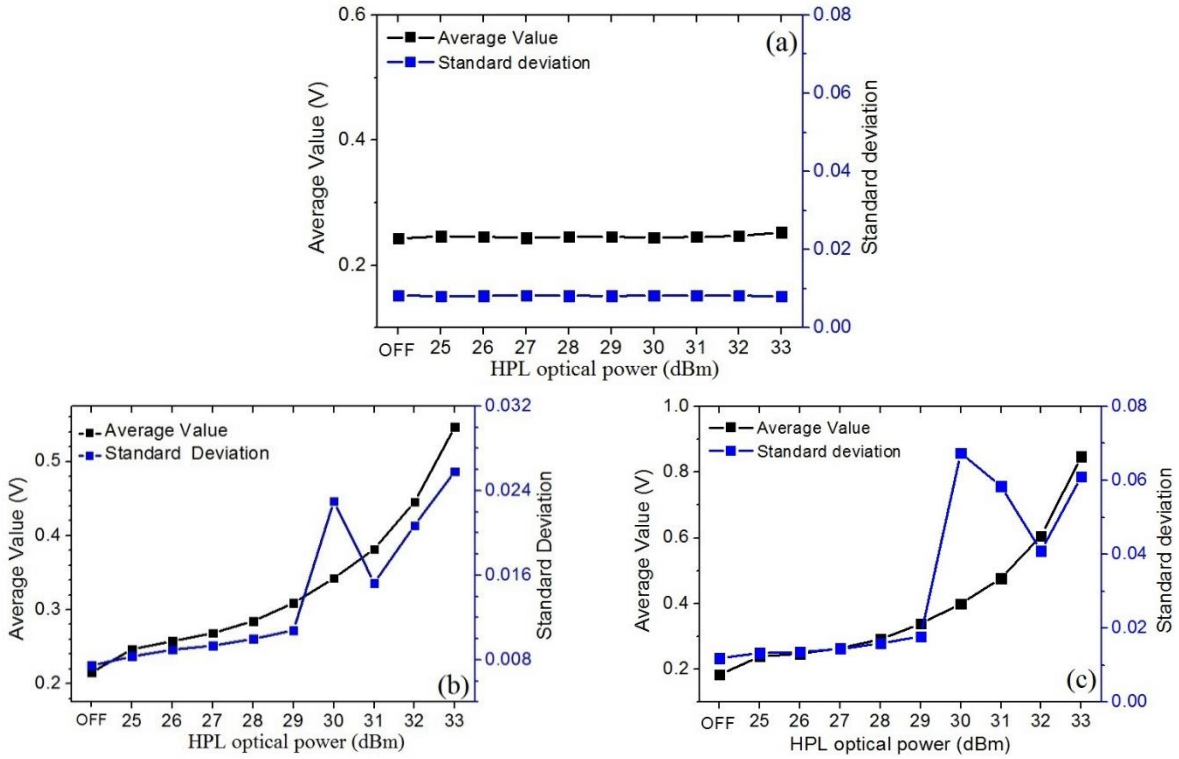

Fig.5.12: Average DC values and SD for the data signal at reception stage after fiber transmission for different HPL optical powers (a) 100 m (b) 5 km (c) 10 km.

It can be clearly seen from the above fig. 5.12 that firstly, for 100 m there is no impact due to HPL noise fluctuations at 1 W; as SD is almost the same for all cases. From the average values, we conclude that there is no power transfer from HPL to data signal due to fiber nonlinearities. This is in accordance with the EVM behavior shown in the chapter for 100 m. For 5 km and 10 km, the performance is different as we can see higher SD at 1 W (or +30 dBm) in the case of 10 km and at 2 W (or +33 dBm) in the case of 5 km. This increment in the average value for 5 km and 10 km is due to power transfer from HPL signal at 1480 nm to data signal at 1532 nm due to Stimulated Raman Scattering (SRS) that is explained later in this chapter.

For 10 km, we show in Fig. 5.13 the electrical spectrums for the noise fluctuations at 1 W and 2 W. We can see that a bit more noise fluctuations are transferred at 2 W output optical power from HPL.

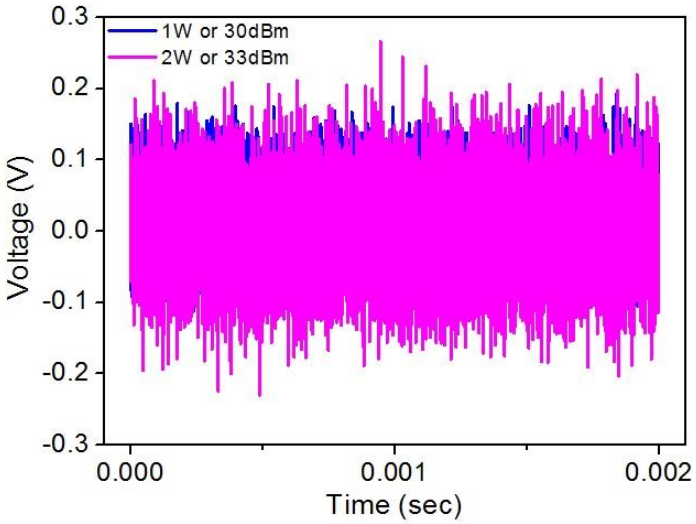

Fig.5.13: Noise fluctuations for received data signal at 10 km for HPL of 1 W and 2W.

From that, we conclude that additional factors apart from those reported in previous chapters, need to be considered to explain the EVM behavior, especially when working with long distances and governed by the fiber non-linearities.

The transmission of high-power levels in the small core area of a SMF can give rise for different nonlinear effects, being a dominant EVM degradation cause. For that, we identify here some effects that can have the most significant impact like SRS and Kerr nonlinearity; SBS can be neglected due to the linewidth of our HPL. SRS effect in optical fibers has been widely discussed in the literature [24]. For a specific threshold power and an effective transmission distance [13], the input power transfers from higher to smaller frequencies as a result of the frequency shift which can be around 13.2 THz due to SRS. Depending on the HPL wavelength (1480 nm) and data channel (1532 nm) as well as the high HPL power levels

used in the proposed setup, SRS can have great impact as it can increase the optical power of data channel. This increased power may induce Self Phase Modulation (SPM) that may arise from the fiber refractive index (n) dependence on the optical power and consequently, the effective refractive index (n^o) is given as [25]:

$$n^o = n_o + n_2 \frac{P_o}{A_{eff}} \tag{5.1}$$

where n_o is the linear refractive index, n_2 is the non-linear index coefficient, P_o is the optical power and A_{eff} is the effective area of the fiber . In silica fiber n_2=2.6 10^{-16} cm^2/W, corresponding to the non-linear refractive index coefficient. The effective refractive index is power dependent and increases with the optical power.

When SPM arises, the propagation constant (β) becomes power dependent and is given as:

$$\beta^\circ = \beta + \gamma P_o \tag{5.2}$$

where γ, the non-linear coefficient is given by:

$$\gamma = \frac{2\pi n_2}{A_{eff}\,\lambda} \tag{5.3}$$

where λ is the wavelength of the laser data source.

In RoF links with double-side band modulation, the recovered RF power strongly depends on the incident optical power under non-linear transmission. The relationship between chromatic dispersion induced power fading and the fiber non-linear effects that may arise from these higher optical power levels (i.e SPM) become of great importance [25]. SPM causes a phase shift in communication systems that can degrade EVM and it can be expressed as [26]:

$$\phi_{\mathrm{NL}}(z,T) = -\frac{1-exp(-\alpha z)}{\alpha}\,\frac{2\pi}{\lambda}\,n_2|A(0,T)|^2 \tag{5.4}$$

where α is the fiber attenuation parameter, z is the transmission distance, and $|A(0,T)|^2$ is the field envelope at fiber input.

The frequency chirping generated from SPM has negative sign as shown in Eq. (5.4) which is increased as the transmission distance increases. As the chromatic dispersion induced phase shift has an opposite impact with respect to the SPM induced phase shift counterpart, then SPM can partially mitigate the dispersion effect in microwave optical systems [26]. From our experimental results, we can see that HPL higher power levels enhance the resulting EVM value as it is very sensitive to the phase change induced by SPM resulted from the HPL injection.

On the other hand, Cross Phase modulation (XPM) phenomena has to be taken into account too. XPM can cause similar broadening to the signal as SPM as it originates from intensity dependence of refractive index as in the case of SPM [27]. The only difference is that SPM contribution mainly depends on the power level of the data signal itself while for the case of XPM the phase of the data signal can be directly affected if another signal is propagated along the fiber (which is PoF signal in our case). XPM impact also increases as the power of the other transmitted signal increases.

As a result, the interaction between all SPM, XPM and D have to be carefully studied. Increasing the transmission distance or working in a region near to the critical length increases the impact as we show in **Chapter Four**, even without PoF simultaneous transmission.

For supporting the above analysis, we develop some additional measurements on LEAF™ fibers and compare them with standard SMF. LEAF™ is one of the most optimized non-zero dispersion shifted fibers (NZDSF) mainly deployed for long haul and metro networks. This fiber shows a different non-linear behavior compared to SMF due to its large effective area and different dispersion profile. From the data sheet, the main parameters for LEAF™ are as follows: its dispersion parameter is around 4 ps/nm/km at 1530-1560 nm with an attenuation of $\alpha \leq 0.22$ dB/km and an effective core area of 72 μm^2. Those parameters for standard SMF-28 are 17 ps/nm/km at 1550 nm, attenuation $\leq$ 0.18 dB/km and 80 μm^2, respectively. However, LEAF™ fiber shows another trade-off between chromatic dispersion and fiber non-linearities compared to other NZDSFs. One disadvantage compared to other NZDSFs is its large chromatic dispersion slope (0.11 ps/nm^2/km) while for others NZDSFs it is around 0.07 ps/nm^2/km [28].

The results for the same test conditions of simultaneous PoF and RoF transmission over a 5 km-long link for LEAF™ fiber are shown in Fig. 5.14. They are performed for different modulation formats with a RF frequency of 13 GHz and RF power of 12 dBm. The EVM behavior for LEAF™ fiber is different to that with SMF for the same conditions and PoF levels. In Fig. 5.14, the EVM degrades linearly when increasing the injected PoF power levels.

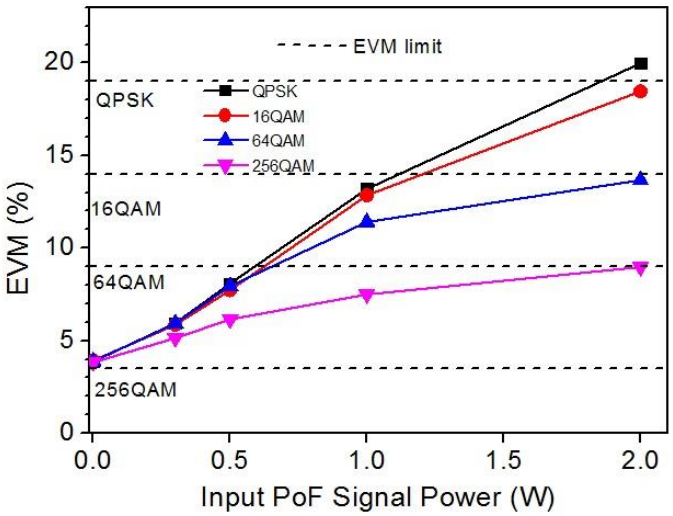

Fig.5.14: EVM measurements vs input PoF signal of power levels (0, 0.3, 0.5, 1, 2) W. P_{RF_IN}=+12 dBm, f_{RF}=13 GHz. Link length 5 km for LEAF^{TM} fiber.

For a better comparison, we plot EVM for 64-QAM measurements for both fibers (SMF and LEAF^{TM}) extracted from figures (5.4 b and 5.14), see Fig. 5.15. The EVM values for both fibers increase as HPL level increases up to 1 W. However, the large effective area of the LEAF^{TM} fiber reduces the SRS effect that implies a reduction of the SPM phase-shift contribution, thus not leading to a dispersion-induced power penalty compensation so the degradation slope is higher. This large effective area in comparison to other NZDSF is due to the fact that the core of LEAF^{TM} fiber does not confine light perfectly due to its specific refractive index profile [28]. So that the transmitted power is distributed over a large area and thus decreases the peak power in the core. Apart from that, the transmission over LEAF^{TM} leads to the generation of higher nonlinear interaction noise [29] due to its lower chromatic dispersion and higher nonlinear coefficient. This low level of chromatic dispersion leads to make XPM to induce more nonlinear phase noise compared to SMF [30]. We show, in Fig. 5.16, the constellation diagram for the two cases (HPL OFF and HPL 2 W) of 64QAM RoF transmission over LEAF^{TM} included in Fig. 5.14. It is clearly seen how the symbols are distracted when HPL input power is set to 2 W.

For the SMF case, higher HPL levels tend to compensate for the frequency chirping due to chromatic dispersion thus leading to a EVM enhancement as seen at 2 W of HPL output power, in comparison with the measured EVM at 1 W of HPL. The temporal broadening of signals that might result from both SPM and XPM at higher PoF levels and its interaction with that resulted from chromatic dispersion (D) of the fiber might result in this EVM improvement at 2 W. However, there is small difference in EVM for 1 W and 2 W HPL power levels in the case of 5 km compare to 10 km for the SMF. In this case, fiber laser instabilities are the responsible in combination with the fact that both Kerr non-linearities

(SPM and XPM) and D are more dominant for higher link lengths or when working with carrier frequencies close to critical one.

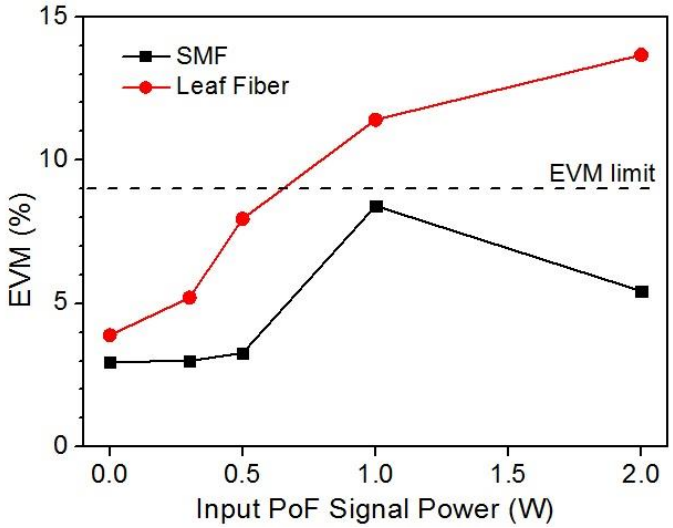

Fig. 5.15: EVM measurements vs input PoF signal of power levels (0, 0.3, 0.5, 1, 2) W P_{RF_IN}=+12 dBm, f_{RF}=13 GHz., 64QAM modulation format. Link length of 5 km for both SMF and for LEAF™ fibers.

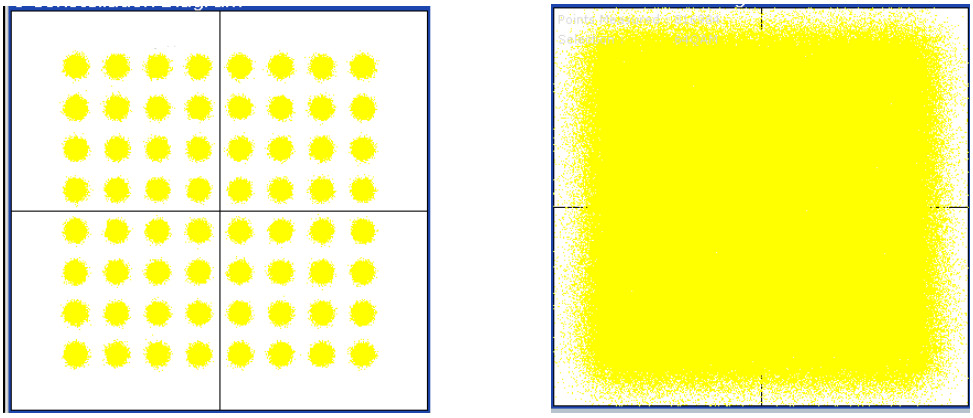

Fig. 5.16: Experimental constellations diagram for 64QAM signal after 5 km transmission of LEAF™ fiber. P_{RF_IN}=+12 dBm, f_{RF}=13 GHz. Left: HPL OFF, Right: HPL 2 W.

5.4.2 Simulations verification for the EVM experimental performance

A set of simulations based on VPI software tool are performed to further investigate the HPL impact on the EVM performance. We analyse different cases for different modulation formats and RF carrier frequencies. We simulate both experimental cases shown in Fig. 5.5 for 10 km transmission distance.

Firstly, we simulate the experimental cases with RF carrier frequency of 17 GHz, RF power of +7 dBm, and 16QAM modulation format (see Fig. 5.5). All Kerr related non-linear effects (SPM and XPM), either in parallel or independently are considered. Meanwhile Raman is always considered. We perform simulation steps of 0.1 W for investigating the impact. Fig. 5.17 show the results.

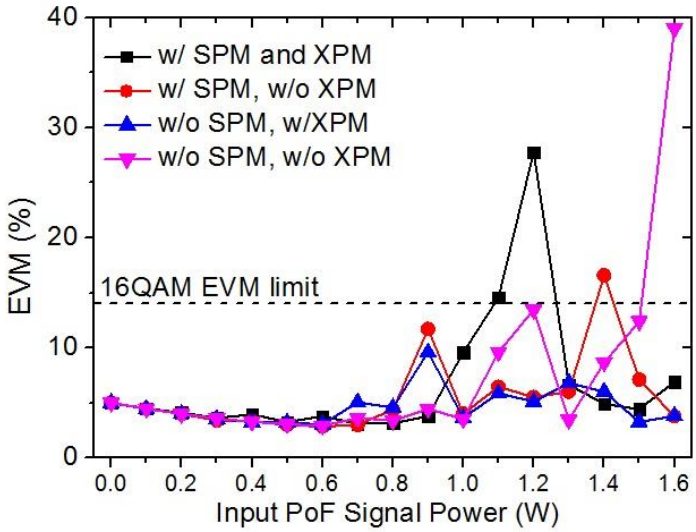

Fig. 5.17: Simulation results of EVM vs input PoF signal for 10 Km SMF, RF 17 GHz, 16-QAM and D=15 ps/nm/km.

From Fig. 5.17, EVM shows the same experimental behavior (see Fig. 5.5) of either degradation or improvement at specific HPL levels. When considering all effects (black curve), EVM value is kept under the standard up to 1.2 W. However, it starts to degrade at 1W of PoF power from 3.13% in the 0.8 W case to 9.57%, which is the case in the experimental results. EVM keeps degrading being 1.2 W HPL level the worst EVM case (27.78%) which is also close to the worst EVM value in the experimental part (22.5%).

For a deep investigation about the reason of EVM being so large at some specific cases, we simulate the recovered RF spectrum with different PoF signal power levels around 1 W. The simulation results are shown below in Fig. 5.18. It is clearly shown that EVM is degraded

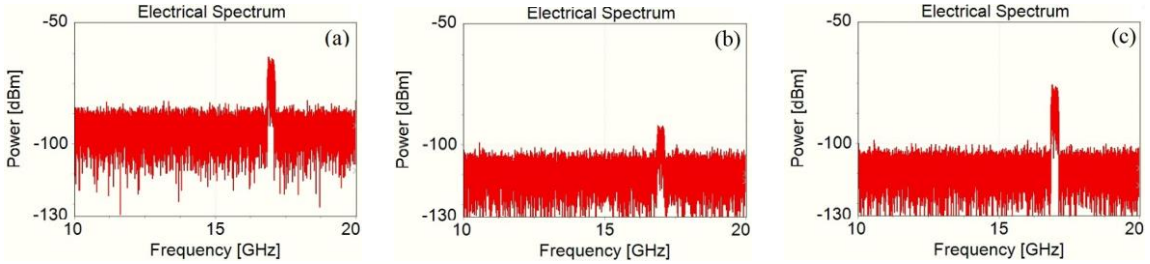

Fig. 5.18: Electrical spectrums of recovered RF signal when all fiber non-linear effects are considered (black curve of Fig. 5.17) for different PoF signal level levels. (a) 1 W (b) 1.2 W (c) 1.4 W.

because the received RF power is faded for HPL levels slightly beyond 1W. Please notice the dramatic case for HPL equals to 1.2W.
The simulated constellation diagrams, shown below in Fig. 5.19, reveal how symbols are distorted in the 1.2 W case compared to the other cases when HPL is increased to 1.4 W.

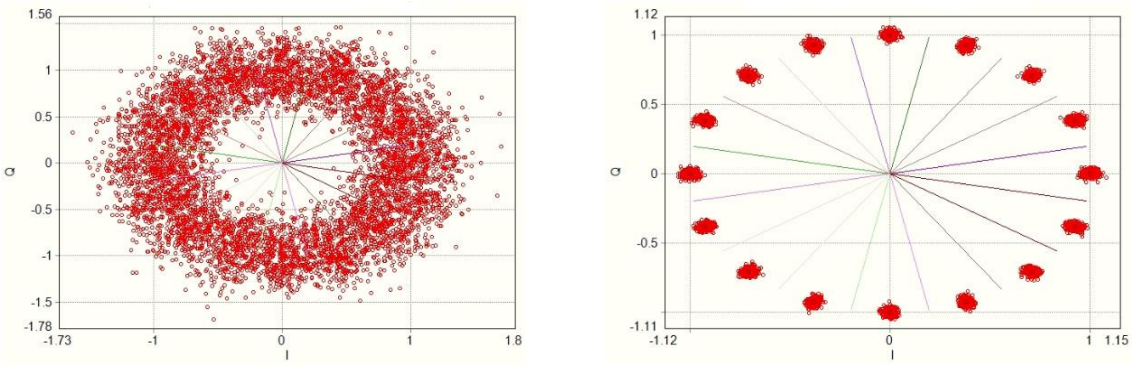

Fig. 5. 19: Constellation diagrams related to EVM measurements when all fiber non-linear effects are considered (black curve of Fig. 5.17) for different PoF levels, Left: 1.2 W and Right: 1.4 W.

In Fig. 5.20, we simulate the recovered RF signal in the time domain for two cases, HPL OFF and HPL 1.2 W that is the worst EVM case as shown previously in Fig. 5.17. The results show how the signal magnitude is degraded which might be due to RF power fading and also the variation of the signal phase with time which also proves the phase noise that might be generated due to the interaction between the D, SPM and XPM.

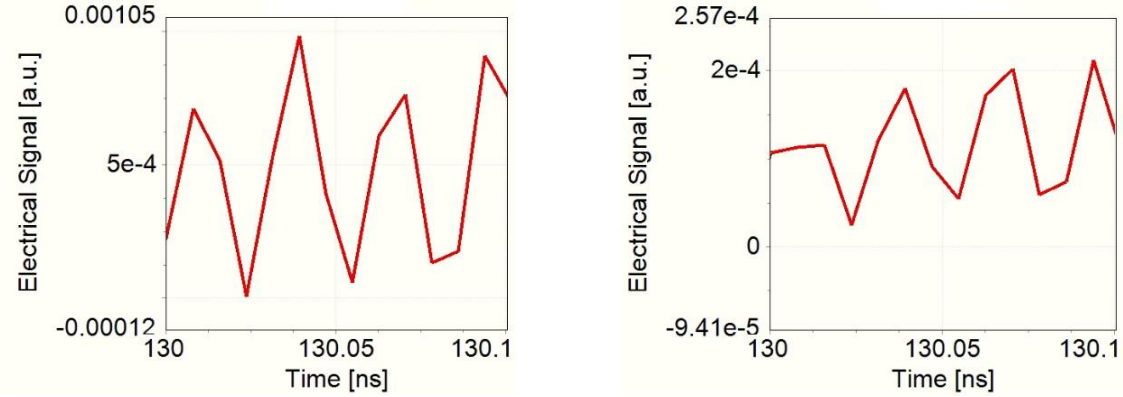

Fig. 5.20: Electrical spectrums of recovered RF signal when all fiber non-linear effects are considered (black curve of Fig. 5.17) for different PoF signal levels. Left: HPL OFF, Right HPL 1.2 W (worst EVM case).

As a summary, Fig. 5.17 shows that after 1 W of PoF signal power, EVM performance is strongly dependent on the interaction between fiber D, SPM and XPM. For example, when only SPM is activated, the notch in the EVM shifts to 1.4 W with a lower EVM value (red

curve, Fig. 5.17), which differs from the first case (black curve) when both SPM and XPM are considered. Increasing the transmission distance or working in a region near to the critical length increases the impact of both XPM and SPM. Using the expressions and simulation results in **Chapter Four** about the critical length (L_1), we see that L_1 for 20 GHz is 9.5 km meanwhile for 17 GHz is 13 km. The larger experimental EVM values at 1 W for 10 km versus 5 km comes from the fact that L_1 is closer to 10 km than 5 km for both RF frequencies.

To see how the D influences the behaviour of the system, different parameters are simulated for the same conditions. The results are shown in Figure 5.21, with SPM and XPM activated. These values are chosen as the SMF dispersion at 1532 nm, the wavelength used in our experiments, can be around 15 ps/nm/km as we discussed in **Chapter Four**. Our simulation results confirm that as in 15 ps/nm/km, the experimental and simulation results are best match. In the simulation of Fig. 5.17, the dispersion parameter is set to 15 ps/nm/km.

As a conclusion, the interaction between all D, SPM and XPM effects have to be carefully considered in high PoF systems (≥ 1 W) integrated with RoF systems.

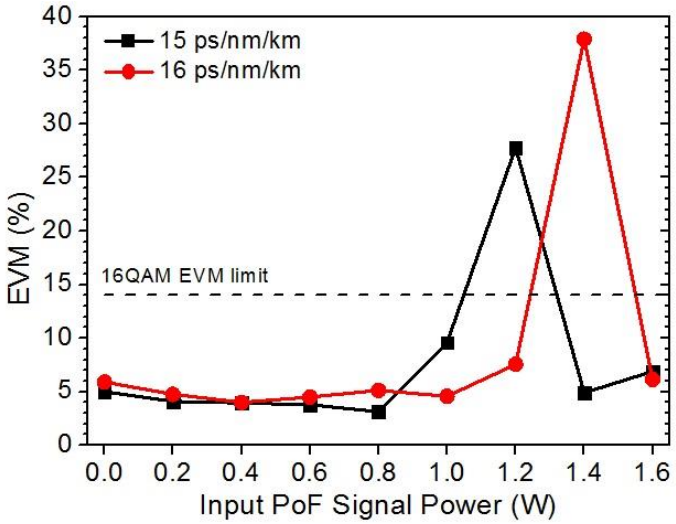

Fig. 5.21: Simulations of EVM vs input PoF signal. f_{RF}=17 GHz., 16QAM modulation format, 10 km-long SMF link. All non-linear effects considered (Raman, XPM and SPM) for different D coefficients.

More simulations are performed for other experimental cases of Fig. 5.5. RF signal at 20 GHz with QPSK modulation is simulated for 10 km of SMF link. RF power is set to +14 dBm while laser data is set to 9 mW in order to get EVM value within the standard when HPL is OFF. After sweeping the HPL input power levels up to 1.6 W with steps of 0.1 W, the EVM experimental performance match the simulations but with a fiber dispersion of 14 ps/nm/km as shown in Fig. 5.22. The highest EVM degradation occurs with PoF level of 0.9 W that is also close to the experimental value. To investigate the highest value of EVM, further simulations are performed with PoF power variations of 0.025 W around 0.9 W as

shown in the inset in Fig. 5.22. As when working near the critical length, it is also important to notice that with PoF powers close to the critical one (the one that leads to the highest EVM degradation) the small power variations can greatly affect the radio transmission performance. All Kerr and Raman effects are activated in these simulations.

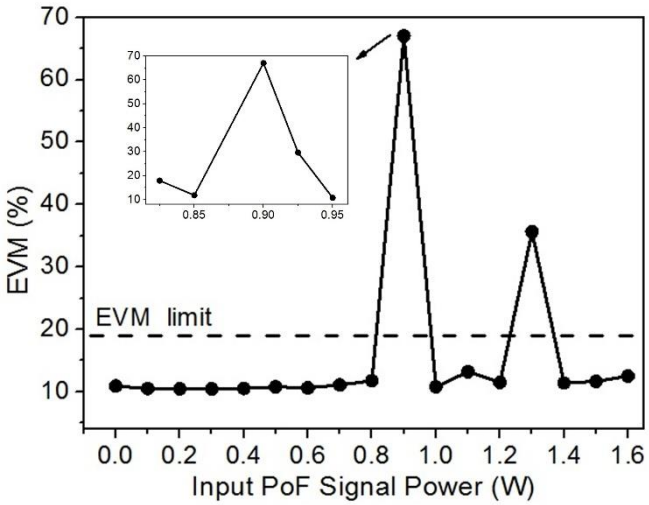

Fig. 5.22: Simulations of EVM vs input PoF signal for 10 km SMF, RF 20 GHz, QPSK and D=14 ps/nm/km.

Apart from the fact that the interaction between chromatic dispersion and fiber non-linearities can be the main reason behind this improvement or degradation of EVM at specific HPL levels; these high HPL levels may also slightly increase the fiber temperature. Those temperature variations may change the fiber dispersion as discussed in **Chapter Four** so the temperature due to HPL could also have its impact on the EVM performance of the system. However, this issue is out of the scope of this work. As a result, choosing HPL levels and checking their instabilities are critical design parameters for ARoF links and must be carefully selected, especially for injected power levels greater than 1 W.

5.5 Feeding Capability and Scalability Analysis

After the energy levels delivered at the remote site, one of the important design parameters of any PoF system is the efficiency of the photovoltaic cell (PV). The selection of any PV cell should look for a matching with HPL wavelength and fiber attenuation. Although at 1480 nm, the currently available PV cells have low efficiency around 26% [31, 32], the fiber attenuation is around 0.2 dB/km so being an optimal solution for longer distances. Our previous work [13], and as we discussed in **Chapter Three,** also showed that high power levels can be delivered with no power degradation due to nonlinear effects like SRS or SBS. In our experiments, we measure the HPL level that can be delivered at the end of the link (demux output, see Fig. 5.3). The highest HPL output (when HPL input is 2 W) is about 870 mW (+29.4 dBm) to be delivered at the PV cell input with a transmission distance of 10 km

as shown in Fig. 5.23. These power levels are measured for the case of 16-QAM modulation format with RF frequency of 17 GHz and for 10 km link length (see Fig. 5.5).

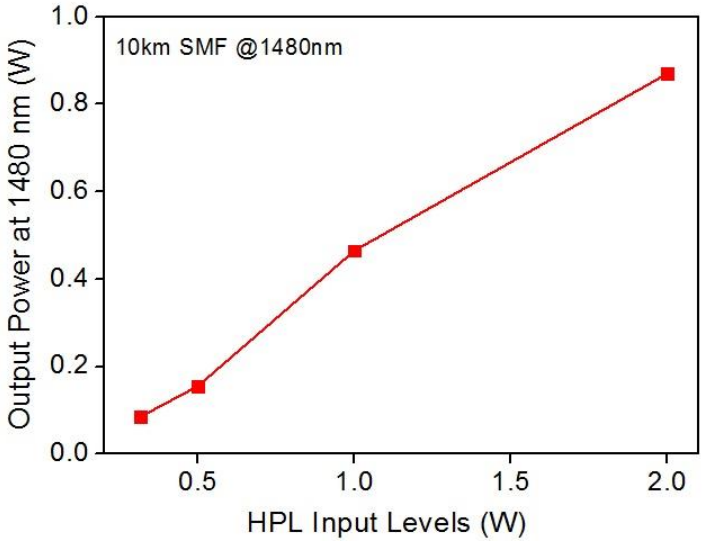

Fig. 5.23: HPL 1480 nm Output vs. Input levels for 10km SMF. Input levels: at HPL device input, Output levels: after demultiplexing. The measurement is done for the case of RF 17 GHz, 16-QAM modulation (see fig. 5.5)

If we consider 26% PV cell efficiency [12], then the electrical power (P_{elec}) at the remote site will be 226.2 mW**.** This power level can drive apart from radio cells, different electronic components or systems as the ones proposed in [5, 11]. For example, the module in [5] is an essential component in the system for RF conversion. The total electrical power provided by PoF was 80 mW by using 4 cores out of 7 cores of MCF. In [11], there are different remote unit types for different reaching distances (short-, medium- and long-) where each remote unit contains a VCSEL, a photodiode and three amplifiers. The required electrical powers to drive these devices for the short-, medium- and long- remote unit configuration were 103, 158 and 221 mW, respectively. The last case uses 1 km of SMF. The optical powering capability of our system, 226.2 mW of electrical power, provides energy enough to feed those systems even for a longer distance of 10 km. On the other hand, at shorter distances (i.e in case of 100 m) this optical power can be increased up to 1350 mW and hence achieve electrical powers of 350 mW. Being able to feed also some of the low power consumption RF components listed in Table 5.1.

Moreover, this power is enough to feed sensor networks in IoT applications like the one in [33] where a low power real time IoT system is used to monitor the structural health of a football stadium, in compliance with the main scenario proposed in section 5.2. Also in [22] where PoF is proposed in a power saving scheme for C-RAN integrated IoT networks. The feeding capability can be even increased by using SMF bundles or other powering scheme (dedicated scenario) by saving mux/demux losses or other possible losses from fiber

nonlinearity due to data/power simultaneous transmission [13]. As 5G front-haul architectures solutions propose the use of MCFs for ARoF and PoF technologies [3, 34-35], so it can integrate the system described in section 5.3; where different cores can be used for energy and/or data as shown in Fig. 5.24 [35] which can represent a dedicated core scenario. In [4], we show different MCFs design configurations that can help to increase the delivered energy. Some experimental results also provided in that work for 4-MCF show no penalty in the signal quality due to PoF transmission. Different types of MCFs can be used to integrate flexible C-RAN with high bandwidth and optical powering capability. For example, as the one proposed in [36] (7-MCF), which has relatively large effective area ($75\mu m^2$) compared with other MCFs, as proposed in [13] which can reduce losses in PoF channel due to non-linear effects from the conclusions discussed in **Chapter Three.**

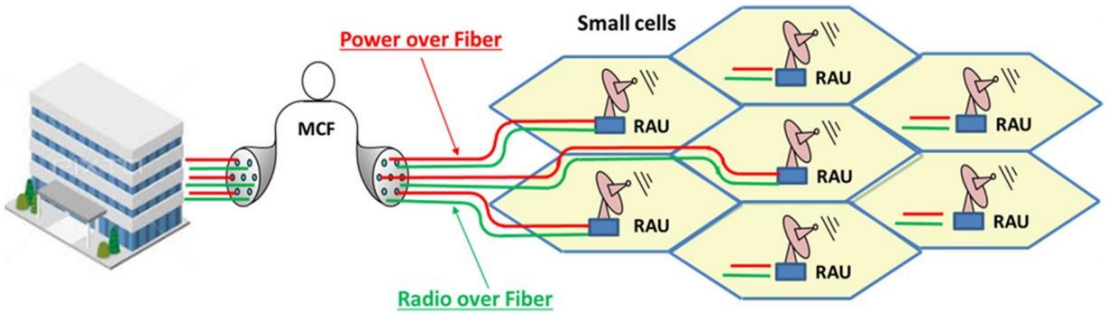

Fig. 5.24: Schematic diagram for PoF and RoF transmission over MCF © 2018 [35].

However, and in accordance with high bandwidth demands by the upcoming 5G technology which requires the installation of a large number of antennas or cells, not only low power remote antenna units are required but also the implementation of additional techniques such as turning some cells on sleep mode [37] to improve the system efficiency. This can open the door to integrate PoF in such systems.

Some analysis is performed to show the scalability of the experimentally tested PoF-RoF system as shown in Table 5.2 and for 10 km link length. For this purpose, N is the number of remote nodes that can be optically feed by the PoF system to determine the system scalability. We consider 3 types of nodes depending on the type of elements that they can feed. The number of each type of nodes are N_A, N_B and N_C. N_A nodes consume 100 mW for powering the small radio cells proposed in section 5.3. About the power consumption, these low power coordinated small radio cells can be powered with different powering levels depending on the operation mode as shown in [38]. Power consumptions for each Radio Dot unit range from as low as 100 mW to around 1 W, depending if they are either single/dual band, number of MIMO channels and the full duplexing type (Frequency Division Duplex (FDD) / Time Division Duplex (TDD)). So that for our calculation we consider the lowest

power consumption case when each Radio Dot can consume as low as 100 mW for both uplink and downlink transmission being working in FDD mode. N_B nodes consume 100 mW for powering different RF communication devices like PD and/or amplifiers, transmitters etc, as those described in Table 5.1 and finally N_C nodes demand 1 mW that can be enough to power multiple low power consumption IoT sensors with the required control units. From the measured value of 870 mW optical power, the P_{elec} after PV cell conversion is of 226.2 mW. This power can feed 1 radio cell so N_A is equal to 1, N_B is 1 too where it can feed two PD or one amplifier for example or any other components that consume power within this range while N_C is 26. As we discuss above one possibility to increase feeding capability is by using SMF fiber bundles. The number of the fibers can be flexible and depend on the specific design requirements.

In Table 5.2, we show how the use of 10 SMF, i.e. a SMF fiber bundle of 10 fibers, can greatly increase the feeding capability as N_A and N_B are both increased from 1 to 10 and N_C to 260. We further show the use of MCF as the one previously described in this section with the same power levels. It is clearly seen how using MCF can increase the system scalability as with 1 MCF N_A and N_B both can be increased from 1 to 7 while N_C from 26 to 58. On the other hand, the use of a dedicated scenario can save some power. In the table, we consider the use of the dedicated scenario for the implemented system. In the calculations for the dedicated scenario, we save Mux/Demux losses that can be around 2 dB. This can increase P_{elec} from 226.2 mW to 358.90 mW when using 1 SMF and in turn increase the number of the optically feed nodes. All the results are considering the parallel powering for the different nodes. The number of each remote node can be increased by consider powering it separately. This can be decided depending on the final application and system requirements.

Table 5.2
Scalability analysis to show feeding capability of the system for different scenarios considering shared and dedicated schemes, the use of single or bundle SMF and also the use of 7-MCF for 10 km

	Fiber	Power (mW)	No. of Powered Nodes		
			N_A	N_B	N_C
Shared Scenario	1 SMF	226.2	1	1	26
	10 SMF	2262	10	10	260
	1 MCF [36]	1583.4	7	7	183
Dedicated Scenario	1 SMF	358.9	2	1	58
	10 SMF	3589	23	10	289

5.6 Conclusions

The chapter addresses the integration of PoF in the next generation radio access networks. The possibility to exploit the currently existing infrastructure based on SMF is discussed. The design of power by light systems that can integrate low power consumption RRUs or IoT wireless sensor network is described. The chapter also presents a use case to show the potential of 5G new access technology with optically powered systems in crowded environments. The impact of power-over-fiber (PoF) signals on radio-over-fiber (RoF) transmission for different modulation formats compliant with 5G New Radio (NR) standard is experimentally analyzed and a detailed simulation analysis is done. SMF ARoF links with different modulation formats are implemented, spanning link lengths from 100 m up to 10 km, with simultaneous PoF signal injection with a maximum of 2 W at the HPL output power. For a 100 m-long link no significant EVM penalty is observed for the different PoF signal levels injected. For 5 km and 10 km link lengths we measure that 5G NR signals over different RF carriers can coexist with injected PoF signals up to 0.5 W with negligible EVM penalty. Beyond 0.5 W of PoF power injection values, EVM results show a significant degradation due to fiber instabilities and non-linear effects. However, for PoF power values greater than 1 W (at HPL output) the EVM results are enhanced for standard SMF.

The experimental EVM behavior with the different HPL power levels is analyzed too. EVM enhancement at higher PoF levels can be an interesting feature that needs more consideration in the future. However, we show that SPM resulted from the amplified data signal due to Raman interaction with PoF signal can partially compensate for the chromatic dispersion that in turn enhance EVM. Another Kerr effect, namely XPM can have its impact too and induce phase noise to the system especially at higher PoF levels. The interaction between the chromatic dispersion of the fiber and its non-linearity can be the main reason for this EVM behavior as we show by simulations and also by comparing SMF with other types of fibers that show different trade-off between the chromatic dispersion and non-liner effects.

A total optical power of 870 mW at the remote site is successfully delivered with EVM values in compliance with 5G requirements and for 10 km of transmission distance. The scalability analysis of the feeding power shows the capability of the proposed system to power low-power consumption small radio cells, electronic components in communication systems and IoT sensor networks. The chapter provides different examples for these cells, devices and IoT sensors that consume power within the range of the energy delivered within this work. Apart from that, we show that PoF can be applied to improve data signal quality utilizing fiber nonlinearity with HPL high power levels.

5.7 References

[1] Y. Bi, S. Shen, J. Jin, K. Wang, and L. G. Kazovsky, ‘‘Remotely powered and reconfigured quasi-passive reconfigurable nodes for optical access networks,’’ *Journal of Electrical and Computer Engineering*, vol. 2016, Art. no. 2938415, Jan. 2016.

[2] M. Matsuura and J. Sato, “Bidirectional radio-over-fiber systems using double-clad fibers for optically powered remote antenna units,” *IEEE Photonic Journal*, vol. 7, no. 1, pp. 1–9, Feb. 2015.

[3] G. Otero *et al*., "SDN-Based Multi-Core Power-Over-Fiber (PoF) System for 5G Front-haul: Towards PoF Pooling," *in Proc*. of *European Conference on Optical Communication (ECOC)*, pp. 1-3, Rome, 2018.

[4] C. Vázquez, D. S. Montero, F. M. A. Al-Zubaidi and J. D. López-Cardona, "Experiments on Shared- and Dedicated- Power over Fiber Scenarios in Multi-core Fibers," *in Proc. of European Conference on Networks and Communications (EuCNC)*, pp. 412-415, Valencia, Spain, 2019.

[5] T. Umezawa *et al*., "Multi-Core Based 94-GHz Radio and Power over Fiber Transmission Using 100-GHz Analog Photoreceiver," in *Proc. 42nd European Conference on Optical Communication (ECOC)*, pp. 1-3, Dusseldorf, Germany, 2016.

[6] C. Vázquez et al., “Integration of power over fiber on RoF systems in different scenarios,” *in Proc. of SPIE (Broadband Access Communication Technologies*), p. 101280E, 2017.

[7] J. Wu, Y. Zhang, M. Zukerman, and E. K.-N. Yung, ‘‘Energy-efficient base-stations sleep-mode techniques in green cellular networks: A survey,’’ *IEEE Communication. Surveys Tutorials,* vol. 17, no. 2, pp. 803–826, 2015.

[8] J.S. Wey and J. Zhang, ‘‘Passive Optical Networks for 5G evolution” in *Proc. SPIE Broadband Access Communication Technologies* XII 10559, p. 105590N, 2018.

[9] C. Ranaweera, E. Wong, A. Nirmalathas, C. Jayasundara and C. Lim, "5G C-RAN with Optical Front-haul: An Analysis From a Deployment Perspective," *Journal of Lightwave Technology*, vol. 36, no. 11, pp. 2059-2068, 1 June, 2018.

[10] D. Konstantinou et al., "Analog Radio Over Fiber Front-haul for High Bandwidth 5G Millimeter-Wave Carrier Aggregated OFDM," *in Proc. 21st International Conference on Transparent Optical Networks (ICTON)*, Angers, France, pp. 1-4, 2019.

[11] D. Wake et al., "Optically Powered Remote Units for Radio-Over-Fiber Systems," *Journal of Lightwave Technology*, vol. 26, no. 15, pp. 2484-2491, Aug.1, 2008.

[12] J. D. López-Cardona, C. Vázquez, D. S. Montero and P. C. Lallana, "Remote Optical Powering Using Fiber Optics in Hazardous Environments," *Journal of Lightwave Technology*, vol. 36, no. 3, pp. 748-754, 2018.

[13] C. Vázquez *et al*., "Multicore Fiber Scenarios Supporting Power Over Fiber in Radio Over Fiber Systems," *IEEE Access*, vol. 7, pp. 158409-158418, 2019.

[14] 3GPP TS 38.104, Rel. 15. 3GPP, (Mar 2018).

[15] 5G PAN-EUROPEAN TRIALS ROADMAP VERSION 2.0. Available Online, Accessed on 2020:

https://5g-ppp.eu/wp-content/uploads/2017/05/5GInfraPPP_TrialsWG_Roadmap_Version2.0.pdf

[16] M. Fiorani et al., "Modeling energy performance of C-RAN with optical transport in 5G network scenarios," *IEEE/OSA Journal of Optical Communications and Networking*, vol. 8, no. 11, pp. B21-B34, Nov. 2016.

[17] G. A. Akpakwu, B. J. Silva, G. P. Hancke and A. M. Abu-Mahfouz, "A Survey on 5G Networks for the Internet of Things: Communication Technologies and Challenges," *IEEE Access*, vol. 6, pp. 3619-3647, 2018.

[18] Available Online, Accessed on 2020: https://www.ericsson.com/en/networks/offerings/5g/5g-supreme-indoor-coverage..

[19] M. Rusci et al., "An Event-Driven Ultra-Low-Power Smart Visual Sensor," *IEEE Sensors Journal*, vol. 16, no. 13, pp. 5344-5353, 2016.

[20] J. D. López-Cardona, D. Sánchez Montero and C. Vázquez, "Smart Remote Nodes Fed by Power Over Fiber in Internet of Things Applications," *IEEE Sensors Journal*, vol. 19, no. 17, pp. 7328-7334, 2019.

[21] F. M. A. Al-Zubaidi, D. S. Montero and C. Vázquez, "SI-POF Supporting Power-over-Fiber in Multi-Gbit/s Transmission for In-Home Networks," *Journal of Lightwave Technology*, vol. 39, no.1, pp. 112-121, 2020.

[22] K. Miyanabe et al., "An Internet of Things Traffic-Based Power Saving Scheme in Cloud-Radio Access Network," *IEEE Internet of Things Journal*, vol. 6, no. 2, pp. 3087-3096, April 2019.

[23] J. Nanni, J. Polleux, C. Algani, S. Rusticelli, F. Perini and G. Tartarini, "VCSEL-Based Radio-Over-G652 Fiber System for Short-/Medium-Range MFH Solutions," *Journal of Lightwave Technology*, vol. 36, no. 19, pp. 4430-4437, 2018.

[24] J. Bromage, "Raman amplification for fiber communications systems," *Journal of Lightwave Technology*, vol. 22, no. 1, pp. 79-93, Jan. 2004.

[25] P. C. Won, W. Zhang and J. A. R. Williams, "Self-Phase Modulation Dependent Dispersion Mitigation in High Power SSB and DSB + Dispersion Compensated Modulated Radio-over-Fiber Links," in *Proc. IEEE MTT-S International Microwave Symposium Digest*, pp. 1947-1950, San Francisco, CA, 2006.

[26] F. Ramos, J. Marti, V. Polo and J. M. Fuster, "On the use of fiber-induced self-phase modulation to reduce chromatic dispersion effects in microwave/millimeter-wave optical systems," *IEEE Photonics Technology Letters*, vol. 10, no. 10, pp. 1473-1475, 1998.

[27] Xiaojun Liang and Shiva Kumar, "Analytical modeling of XPM in dispersion-managed coherent fiber-optic systems," *Optics Express,* no. 22, pp. 10579-10592, 2014.

[28] R. Ramaswami, K. Sivarajan and G. Sasak, "Optical Networks: Practical Perspectives," pp. 96-97 Edition 3, Nov. 2009.

[29] Junhe Zhou, Yuheng Wang, and Yunwang Zhang, "Blind back-propagation method for fiber nonlinearity compensation with low computational complexity and high performance," *Optics Express*, no. 28, pp. 11424-11438, 2020.

[30] A. Tan and E. Pincemin, "Performance Comparison of Duobinary and DQPSK Modulation Formats for Mixed 10/40-Gb/s WDM Transmission on SMF and LEAF^{TM} Fibers," in *Proc. of Lasers and Electro-Optics/Quantum Electronics and Laser Science Conference and Photonic Applications Systems Technologies*, OSA Technical Digest Series (CD) (Optical Society of America), paper CMH2, 2007.

[31] M.Dumke, G.Heiserich,S.Franke,L.Schulz,andL.Overmeyer,"Power transmission by optical fibers for component inherent communication," *Journal of Systemic Cybernetics and Informatics*, vol. 8, no. 1, pp. 55–60, 2010.

[32] X. Xu et al., "Optically powered communication system with distributed amplifiers," *Journal of Lightwave Technology*, vol. 28, no. 21, pp. 3062–3069, Nov. 2010.

[33] D. Phanish et al., "A wireless sensor network for monitoring the structural health of a football stadium," in *Proc. of IEEE World Forum on Internet of Things (WF-IoT)*, pp. 471-477, Milan, 2015.

[34] R. Muñoz et al, ''Experimental demonstration of advanced service management in SDN/NFV front-haul networks deploying ARoF and PoF,'' *in Proc. European Conference on Optical Communication* (ECOC), Dublin, Republic of Ireland, pp. 459–463, 2019.

[35] T. Umezawa, P. T. Dat, K. Kashima, A. Kanno, N. Yamamoto and T. Kawanishi, "100-GHz Radio and Power Over Fiber Transmission Through Multicore Fiber Using Optical-to-Radio Converter," *Journal of Lightwave Technology*, vol. 36, no. 2, pp. 617-623, 2018.

[36] B. Zhu, T. F. Taunay, M. Fishteyn, X. Liu, S. Chandraskekhar, M. F. Yan, J. M. Fini, E. M. Monberg, and F. V. Dimarcello, "112-Tb/s space-division multiplexed DWDM transmission with 14-b/s/Hz aggregate spectral efficiency over a 76.8-km seven-core fiber," *Optics Express*, vol. 19, no. 17, pp. 16665–16671, Aug. 2011.

[37] J. Zuo, J. Zhang, C. Yuen, W. Jiang and W. Luo, "Energy Efficient User Association for Cloud Radio Access Networks," *IEEE Access*, vol. 4, pp. 2429-2438, 2016.

[38] Available Online, Accessed 2021: https://mediabank.ericsson.net/deployedFiles/ericsson.com/Taking%20the%20next%20step%20in%20the%20indoor%20revolution.pdf

Chapter 6:

Conclusions and Future Works

6.1. CONCLUSION

In this research work, different studies towards high bandwidth systems supporting 5G services have been proposed. The studies present data transmission networks based on plastic (SI-POF) and silica optical fibers to integrated full coverage from the service provider through the access network based on silica fibers to the final user within home networks scenarios based on plastic optical fibers. We integrate the potential of the Power over Fiber technology in the different designed data transmission networks. We analyze the impact of Power over Fiber on the transmission quality and discuss the different powering scenarios.

The two main conclusions of the work presented here can be described as follows:
First, the feasibility of SI-POF to provide high bandwidth connectivity in parallel with optical feeding capability to integrate smart homes with different 5G services such as Internet of Things has been demonstrated.

Second, the possibility of utilizing currently installed front-haul solutions over SMF to transmit 5G New Radio signals over tens of kilometers with data signal quality following 5G standard requirements has been also proved. And this is in parallel with delivering hundreds of mW of electrical energy for feeding purposes.

We summarize the research contributions on the development of these networks designs as follows:

- A Multi Gbit/s data transmission system based SI-POF has been presented. Real time link at 1 Gbit/s over 10 m SI-POF with BER of 1×10^{-10} is implemented with different energy delivery schemes based on Power over Fiber technology for in-home scenarios. Detailed analysis of Power over Fiber impact on data signal quality is presented. The designed system discusses for the first time to the best of our knowledge the integration of smart home networks supported by Multi Gbit/s data transmission and optical powering capabilities over plastic optical fibers. Several mW of optical power are experimentally delivered at the remote site. The work shows the potential of this power to integrate IoT based sensor networks to support smart home automation. The designed system outperforms the state of the art in terms of transmission efficiency and power per bit figures of merit.

- Extensive simulation studies supported by experimental validation to address the energy delivery efficiency in different powering architectures considering different types of fibers. The limitation due to fiber nonlinearities is studied in detail to address power limits. The impact of transmitting high power levels from Power over Fiber source on the data signal quality in the shared scenario is deeply studied in different systems configurations. The results within this part can be useful to decide Power over Fiber source characteristics, power levels and prober fiber parameters.

- Developed Analog Radio over Fiber links following 5G New Radio numerology to support future radio access networks. The results including experiments and series of simulations address the design parameters for specific Radio over Fiber links.

- The integration of Power over Fiber in the designed Radio over Fiber links and to study the impact on the transmission quality for the different power levels in detail.

- Different powering scenarios are presented to discuss the potential of Power over Fiber in future radio access networks. These include optically powering small radio access units and Internet of Things devices.

The work presents different examples of low power consumption devices including small radio cells and wireless sensors that can open the door to utilize Power over Fiber technology as the powering source. Different use cases and scalability analysis are presented throughout different chapters.

As a conclusion, the research outcomes add simulations and experiments in two novel Power over Fiber systems to the state of the art. The first one is by integrating the Power over Fiber in home network based SI-POF which represent **Chapter two** in this work. The second system is by developing optically powered Radio over Fiber systems following 5G standard in SMF. This part is covered by **Chapter four** and **Chapter five**. The designed parameters and power limits for Power over Fiber source (high power lasers) that can be utilized in such systems is covered by **Chapter three**.

6.2. Future Work

Finally, some issues related to the presented research work can represent open lines of future research as following:

- Increase the optical feeding capability inside home networks based SI-POF by using high output power LD sources. From that the long term stability of the SI-POF would be an interesting topic. These high power levels may increase fiber temperature that can cause aging problems specially when applying to the blue channel.
- Additional research on the EVM improvement at higher Power over Fiber levels in Single Mode Fiber that can help to decide the Radio over Fiber system design parameters more accurately. Apart from powering purposes, this can open the door

for Power over Fiber to be used for improving data signal quality in parallel with powering purposes.

- Other conditions that can affect the performance of the Radio over Fiber link are the environmental conditions, and especially the temperature. The HPL power levels used in the experiments may increase the fiber temperature. Some studies have reported that changing the fiber temperature in Single Mode Fibers may lead to fluctuations in the fiber chromatic dispersion parameter that is a very important design parameter as we show in this work. Additional research on the fiber temperature and its effect on data signal quality by changing the chromatic dispersion of the fiber will be an interesting topic to be considered in the future.

- More studies about the resulted optical crosstalk in Multi-Core Fibers due to Power over Fiber transmission in such fibers and its impact on the data signal quality in the shared powering scenario.